

MODAL INTERACTIONS IN SHELL DYNAMICS

by

Raouf A. Raouf

Dissertation submitted to the Faculty of the
Virginia Polytechnic Institute and State University
in partial fulfillment of the requirements for the degree of
Doctor of Philosophy
in
Engineering Mechanics

APPROVED:

Ali H. Nayfeh, Chairman

Dean T. Mook

Scott L. Hendricks

Eric R. Johnson

Saad A. Ragab

March, 1989

Blacksburg, Virginia

MODAL INTERACTIONS IN SHELL DYNAMICS

by

Raouf A. Raouf

Ali H. Nayfeh, Chairman

Engineering Mechanics

(ABSTRACT)

A numerical-perturbation approach is used to study modal interactions in the dynamic response of infinitely long circular cylindrical shells to an external harmonic excitation. The excitation frequency is near the linear natural frequency of the breathing mode (i.e., primary resonance of the breathing mode) and the linear natural frequency of the breathing mode is approximately twice that of a flexural mode (i.e., two-to-one internal or autoparametric resonance). The method of multiple-time scales is used to derive a set of autonomous first-order nonlinear differential equations that describe the modulation of the amplitudes and phases of the interacting modes. The same approach is used to study the axisymmetric dynamic response of spherical shells to a radial harmonic excitation having a frequency near one of the linear natural frequencies of a flexural mode (i.e., primary resonance of a flexural mode) and in the presence of a two-to-one internal resonance between the excited mode and a lower flexural mode. The modulation equations derived for infinitely long circular cylindrical shells and for axisymmetric spherical shells are scaled to the same form and their fixed points, periodic solutions, and chaotic solutions are studied as the amplitude or the frequency of excitation varies. As the excitation amplitude varies, the fixed-point solutions of the modulation equations exhibit the jump and saturation phenomena. They also undergo supercritical and subcritical Hopf bifurcations as the frequency or the amplitude of excitation varies.

Between the two Hopf-bifurcation frequencies, the fixed-point solutions are unstable and limit cycles exist. Some limit cycles experience symmetry-breaking (pitchfork) bifurcation followed by an infinite cascade of period-doubling bifurcations culminating in chaos. Other limit cycles lose stability through cyclic-fold bifurcations causing a transition to chaos.

The same procedure is used to study the nonlinear dynamic response of infinitely long circular cylindrical shells to a subharmonic excitation of order one-half of the breathing mode in the presence of a two-to-one internal resonance. The force-response curves exhibit saturation, jumps, and Hopf bifurcations. They also show that the shell does not respond until a certain threshold level of excitation is exceeded. The frequency-response curves exhibit jumps and pitchfork and Hopf bifurcations. For certain parameters and excitation frequencies between the Hopf-bifurcation values, limit-cycle solutions of the modulation equations are found. As the excitation frequency changes, the limit cycles deform and lose their stability through either pitchfork or cyclic-fold (saddle-node) bifurcations. Some of these saddle-node bifurcations cause a transition to chaos. The pitchfork bifurcations break the symmetry of the limit cycles. Period-three motions are observed over a narrow range of excitation frequencies.

Lastly, a computerized symbolic manipulator is used to analyze the dynamic response of an infinitely long circular cylindrical shell to radial harmonic excitations. The excitation frequency is near the linear natural frequency of a flexural mode (i.e., primary resonance of a flexural mode). Due to the complete circular symmetry of the shell, each natural frequency corresponds to two orthogonal mode shapes. The mode with the same spatial variation as the excitation is called the driven mode and the other mode is called the companion mode. Modal interactions between the driven mode and the companion mode are studied. The steady-state response of the

shell can involve either the driven mode alone (single-mode response) or both the driven and companion modes (two-mode response). The frequency-response curve exhibits jumps and Hopf bifurcations. Between the Hopf-bifurcation frequencies, the modulation equations exhibit multiple limit-cycle solutions. As the excitation frequency varies, these limit cycles go through either saddle-node collisions or incomplete sequences of period-doubling bifurcations. Some of the saddle-node bifurcations result in the birth of limit cycles and some result in transition to chaos.

To my parents

Acknowledgements

The author wishes to express his gratitude to Professor Ali H. Nayfeh for serving as his major advisor. His valuable advice, continuous support and guidance were essential to the completion of this work. Thanks are also due to the committee members: Professor Dean Mook, Professor Scott Hendricks, Professor Saad Ragab and Professor Eric Johnson. Their comments were essential in bringing this work into its final shape. The author also thanks _____ for many stimulating discussions, and for his assistance in developing the computer programs and _____ for his help in typing parts of this manuscript. Last but not least, the author wishes to thank his wife _____ for her support and understanding during the completion of this work.

Thanks are also due to the National Science Foundation for supporting this research under Grant No. MSM-852-1748 and the Air Force Office of Scientific Research for supporting this research under Grant No. AFOSR-86-0090.

Table of Contents

LITERATURE SURVEY	1
1.1 Dynamics of Shell Structures	1
1.2 Dynamics of Various Physical Systems	6
BASIC CONCEPTS IN NONLINEAR DYNAMICS	14
2.1 Attractors	15
2.2 Fixed-Points (Constant Solutions)	16
2.2.1 Stability of fixed-point solutions	16
2.2.2 Bifurcation of fixed-point solutions	17
2.3 Limit Cycles (Closed Orbits)	19
2.3.1 Detection of closed orbits	19
2.3.2 Stability of closed orbits	24
2.3.3 Bifurcation of closed orbits	27
2.4 Poincare' Sections	28
2.5 Lyapunov Exponents and Lyapunov Dimension	29
EQUATIONS OF MOTION	31

3.1 Preliminaries from the Theory of Surfaces	32
3.2 Equations of Motion of Infinitely Long Circular Cylindrical Shells	36
3.3 Equations for the Axisymmetric Motion of Closed Spherical Shells	41
CASES INVOLVING TWO-TO-ONE INTERNAL RESONANCE	47
4.1 Primary Resonance	48
4.1.1 Primary resonance of the breathing mode of an infinitely long circular cylindrical shell	48
4.1.2 Primary resonance of a flexural mode of a closed spherical shell	55
4.1.3 Numerical results	67
4.2 Subharmonic Resonance of the Breathing Mode of Cylindrical Shells	85
4.2.1 Numerical results	89
MODAL INTERACTION BETWEEN THE DRIVEN AND COMPANION MODES IN INFINITELY LONG CYLINDRICAL SHELLS	106
5.1 Perturbation Solution	108
5.2 Numerical Simulation	114
5.3 Comparison with Maewal (1981, 1986)	125
CONCLUSIONS AND RECOMMENDATIONS	131
6.1 Conclusions	131
6.2 Dynamics of Cylindrical and Spherical Shells	132
6.2.1 Primary-Resonant Excitation of Cylindrical and Spherical Shells with Two-To-One Internal Resonances	133
6.2.2 Subharmonic-Resonant Excitation of Cylindrical Shells with Two-To-One Internal Resonance	134
6.2.3 Primary-Resonant Excitation of Cylindrical Shells with One-To-One Internal Resonance	135

6.2.4 Routes to Chotic Motions	136
6.3 Recommendations for Future Research	137
REFERENCES	138
CONSTANTS FOR EQUATIONS (5.13) AND (5.14)	153
CONSTANTS FOR EQUATIONS (5.19) AND (5.20)	154
Vita	157

List of Illustrations

Figure 2.1. Generic bifurcation patterns 20

Figure 3.1. Generic surface with surface-oriented coordinate system 34

Figure 3.2. Kinematics of deformation for a cylindrical shell 38

Figure 3.3. Kinematics of deformation for a spherical shell 43

Figure 4.1. A typical Force Response curve for cylindrical shells under primary-resonant excitation 70

Figure 4.2. A typical Force Response curve for cylindrical shells under primary-resonant excitations 72

Figure 4.3. Frequency response curve for cylindrical shells under primary-resonant excitations 73

Figure 4.4. A schematic bifurcation diagram for cylindrical shells between the Hopf bifurcation frequencies 75

Figure 4.5. Symmetry-breaking and first sequence of period-doubling bifurcations 76

Figure 4.6. Time histories and two-dimensional projections of the Poincare' section 77

Figure 4.7. Time history and fast Fourier transform of a chaotic attractor 78

Figure 4.8. Two-dimensional projection of the Poincare' section for a chaotic attractor 79

Figure 4.9. An unstable limit cycle separating two stable ones 80

Figure 4.10. Limit-cycle solutions 82

Figure 4.11. Time history and fast Fourier transform of a chaotic attractor 83

Figure 4.12. Two-dimensional projection of the Poincare' section for a chaotic attractor 84

Figure 4.13. A typical Force Response curve for a subharmonically excited cylindrical shell	90
Figure 4.14. A typical Force Response curve for a subharmonically excited cylindrical shell	91
Figure 4.15. Frequency response curve for a subharmonically excited cylindrical shell	92
Figure 4.16. Schematic for the behavior of a subharmonically excited shell between the Hopf bifurcation frequencies	95
Figure 4.17. Limit cycle I	96
Figure 4.18. Deformation of attractor X as a function of excitation frequency	97
Figure 4.19. Floquet multipliers for limit cycle X around the symmetry-breaking frequency	98
Figure 4.20. Limit cycles IX and X	100
Figure 4.21. Limit cycle III (unstable)	101
Figure 4.22. Limit cycle II	102
Figure 4.23. Chaotic attractor VII	104
Figure 4.24. Limit cycle XII (period three motion)	105
Figure 5.1. Frequency-response curves for $F = -6.4$	116
Figure 5.2. Frequency-response curves for the companion mode	118
Figure 5.3. A schematic bifurcation diagram for the orbits of the modulation equations	119
Figure 5.4. A two-dimensional projection of attractors 1 and 2 at $\sigma = 14.0$	122
Figure 5.5. A two-dimensional projection of the period-doubled attractors 3 and 4 at $\sigma = 12.40$	123
Figure 5.6. A two-dimensional projection of attractors 5 and 6 at $\sigma = 13.3$	124
Figure 5.7. A two-dimensional projection of the chaotic attractor at $\sigma = 10.0$..	127
Figure 5.8. Power spectral density for q_1 at $\sigma = 10.0$	128
Figure 5.9. Different two-dimensional projections of the Poincare' section of the chaotic attractor	129
Figure 5.10. A two-dimensional projection of attractors 9 and 10 at $\sigma = -65.0$..	130

CHAPTER 1

LITERATURE SURVEY

1.1 Dynamics of Shell Structures

In 1821, Sophie Germaine (who in 1815 won the French Academy of Science award for deriving the equations of motion of plates) presented a simplified equation of motion for a cylindrical shell (Soedel, 1981). Her equation reduces to the correct plate equation but when reduced to the equation of motion of a ring a sign mistake is passed on. Other than this sign mistake, her equation is identical to the ring equation given by Euler in 1766. In 1874, Aron derived a set of five equations of motion for a cylindrical shell. His equations were complicated because of his reluctance to simplify them. He, however, showed that they reduce to the plate equations when the curvature terms are ignored. In 1882, Rayleigh proposed what came to be one of the most popular assumptions in the theory of shells; namely, the inextensionality assumption. He proposed that the contribution of the extensional

strain energy to the total strain energy of the shell can be neglected. This assumption was later reputed by Love in 1888 who argued that for a sufficiently thin shell, the extensional terms are predominant over the flexural terms because the extensional terms are proportional to the thickness-to-radius ratio whereas the flexural terms are proportional to the cube of that ratio. Love was the first to present a useful shell theory; in addition to the small strains and small thickness-to-radius ratios, Love used the approximations previously used by Kirchhoff in thin plate analysis. Although he gave the solution procedure for the calculation of the natural frequencies of a finite cylindrical shell, it was not until the 1930's that numerical results started to appear. Among the first were those of Flugge (1960) who calculated the natural frequencies of a cylindrical shell and Forsberg (1964) who calculated the natural frequencies of a spherical shell.

Nonlinear theories of shells were first derived for special geometries. Donnell (1933, 1938) and Mushtari (1938) proposed , independently, one of the most widely used simplifications in the theory of shells. They neglected the contribution of the in-plane displacements to the bending strain energy but not the membrane energy, and also neglected the in-plane inertia and out-of-plane shear. They used these assumptions to derive the equations of motion for circular cylindrical shells. Vlasov (1951) generalized their approach to shells of any geometry and noted that these assumptions are particularly good for shallow shells. This became known as the shallow shell theory or the Donnell-Mushtari-Vlasov equations. Some of the nonlinear theories for shells were derived by Reissner (1950, 1963), Novozhilov (1953), Sanders (1959, 1963), Leonard (1961), Naghdi and Nordgren (1963), Koiter (1966), Budiansky (1968), Marlowe and Flugge (1968), Simmonds and Danielson (1972), Simmonds (1979), Pietraszkiewicz and Szwabowicz (1981), Schmidt (1984, 1985), and Libai and Simmonds (1988). The main differences among these theories

are the approximations used in the derivation of the kinematic relationships. Naghdi (1963) pointed out that many of the proposed theories of shells maintain some inconsistencies. Koiter and Simmonds (1972) discussed the problem of obtaining estimates of error bounds in the theory of shells.

The methods of solution of the resulting nonlinear equations of motion for shell structures can be broadly classified into three types: purely numerical methods (e.g., Stricklin, Martinez, Tillerson, Hong, and Haisler, 1971; and Mente, 1973), purely analytical methods such as perturbation methods (e.g., Maewal 1978, and Simmonds 1979), and a combination of analytical and numerical methods in which the partial-differential equations are discretized into a set of temporal nonlinear ordinary-differential equations (Nayfeh and Mook, 1979; Nayfeh, 1988a). A popular approach is the Galerkin procedure in which the assumed spatial modes are used as weighting functions to minimize the residual over the spatial domain. A common practice is to truncate these equations to a finite number of modes and integrate the remaining equations numerically in the time domain. Mente (1973) studied the nonlinear response of cylindrical shells by integrating up to fifteen circumferential harmonics and three axial harmonics. Many researchers, however, retained only one mode, thereby missing the important phenomenon of modal interactions. Although single-mode analyses can provide some insight into the problem of nonlinear dynamics, the interesting behavior results from modal interactions, see Nayfeh and Mook (1979) for a comprehensive literature review. Such a phenomenon may occur when the linear natural frequencies of some modes are commensurate or nearly commensurate. Because of the central importance of this concept to nonlinear dynamics, we choose to organize this review according to internal resonance conditions.

Shells with Two-To-One Internal Resonances

The first studies of modal interactions in the response of shells were initiated by Mclvor (1962, 1966), Goodier and Mclvor (1964), Mclvor and Sonstegard (1966), and Mclvor and Lovell (1968). They analyzed the responses of cylindrical and spherical shells to radial and nearly radial impulses, taking into account the coupling of a breathing mode and a flexural mode when their frequencies are in the ratio of two-to-one. They transformed their equations into a Mathieu-type equation and studied its stability regions. They numerically integrated the governing equations of motion and found that the energy is continuously exchanged between the resonant modes. A similar approach was used by Bieniek, Fan, and Lackman (1966) to study the symmetric response of cylindrical shells. Yasuda and Kushida (1984) studied theoretically and experimentally the axisymmetric response of shallow spherical shells. They studied the case of primary resonance of a higher flexural mode in the presence and absence of a two-to-one internal resonance. They analyzed the stability of periodic solutions and verified their analysis experimentally. Their theoretical analysis showed regions of almost periodic motions for some values of the excitation frequency. They experimentally observed periodic responses of the shell but did not report any experimental observations of almost periodic motions. Raouf (1986) and Nayfeh and Raouf (1987) used the method of multiple-time scales to study the forced nonlinear response of infinitely long circular cylindrical shells to primary resonant excitations of the breathing mode and a flexural mode in the presence of a two-to-one internal resonance. They showed that the response exhibits the jump phenomenon. They also showed that above a certain threshold of excitation the amplitude of the excited mode saturates and spills over the extra input energy into the coupled flexural mode, which responds nonlinearly. They showed that the

response can exhibit a Hopf bifurcation, resulting in amplitude- and phase-modulated motions.

Shells with One-To-One Internal Resonances

Evensen (1966) studied the one-to-one internal resonance in the inextensional forced flexural response of thin circular rings. He showed that the response involves either a single or two coupled bending modes. He reported experimental observations of regions in the frequency-response curve where nonsteady vibrations were found. He verified his results by analog-computer simulations. Chen and Babcock (1975) used the Lindsdet-Poincare' technique (Nayfeh 1973,1981) to study the nonlinear response of finite cylindrical shells to harmonic excitations. They studied the driven and companion modes and their interaction. They reported experimental observations of "nonstationary" responses "in which the amplitude drifts from one value to another". Maewal (1986a) studied the modal interaction between the driven and companion modes of axisymmetric shells. He used the method of multiple-time scales to derive a set of evolution equations for the amplitudes of the modes. He noted that these equations have the same form as those derived earlier by Miles (1984a, 1984b) for internally resonant surface waves in a circular cylinder. He numerically integrated these evolution equations and showed that for certain ranges of the excitation frequency, the response is chaotically modulated. Maganty and Bickford (1987) used the method of multiple-time scales to study the nonlinear free vibrations of circular rings in the presence of one-to-one internal resonances between an in-plane mode and out-of-plane mode. They found a continuous exchange of energy between the coupled modes. Later in 1988, they studied the forced response of the same system to a harmonic in-plane or out-of-plane excitation.

They showed that for certain values of the excitation frequencies, an in-plane excitation can produce non-planar oscillations and vice versa.

1.2 Dynamics of Various Physical Systems

Experimental and theoretical investigations into the nonlinear responses of different structural and mechanical systems show that most of the nonlinear behavior of shells is also present in those systems. Nayfeh and Mook (1979) presented a comprehensive literature survey of the nonlinear oscillations of physical systems. They studied the nonlinear dynamics of discrete single-degree-of-freedom systems, multi-degrees-of-freedom systems, and continuous systems. They introduced the concept of modal interaction, which allows the reduction of a continuous system to a finite-degrees-of-freedom system. Holmes and Moon (1983) published a review article that contains examples of physical systems which display chaotic dynamics. Their examples included experimental studies of the oscillations of postbuckled beams around their buckled positions; nonlinear circuits examined by Ueda (1979); magnetomechanical devices, such as rotating disks in a magnetic field (Robbins, 1977) and torsional oscillations of a compass needle in an oscillating or rotating magnetic field (Croquette and Pointou, 1981); feedback control systems; and chemical reactions, such as the reaction-diffusion system (Rossler, 1976). Moon (1987) presented a survey of mathematical models and physical experimentations which exhibit chaotic vibrations. It also presented a variety of theoretical and experimental tools to study chaos. Nayfeh (1988a) presented several examples of physical systems

that exhibit complicated nonlinear responses, such as saturation, jumps, period-multiplying bifurcations, and chaos. He advocated a numerical-perturbation approach for analyzing these problems. His examples included cylindrical shells, experiments with two-beam frames, surface waves in cylindrical containers, subharmonic instability of two-dimensional boundary layers on flat plates, and three-dimensional propagation of sound in partially choked ducts.

Most of the existing studies of nonlinear dynamics deal with either single-degree-of-freedom or two-degree-of-freedom systems. One main difference between the two systems is that a large level of excitation is needed to cause chaotic motions in the former, whereas chaos can occur in the latter at low levels of excitation. The number of degrees of freedom of a dynamical system is dictated by physical and mathematical considerations. The distinction is obvious in the case of discreteized systems, such as particle dynamics, but is not as obvious in the case of a continuous system, such as a beam or a shell. A continuous system has infinite degrees of freedom because it possesses infinite number of modes. Depending on the approximation scheme used to study such a system, only a finite number of these modes is considered in the analysis. The number of studied modes is the number of degrees of freedom of the system.

Single-degree-of-freedom systems with nonlinear characteristics are the simplest nonlinear systems and thus the most extensively studied. For example, Nayfeh and Khdeir (1986a, 1986b) studied the nonlinear rolling of ships in regular beam seas. They modeled the ship as a single-degree-of-freedom system and demonstrated that its response undergoes a cascade of period-doubling bifurcations culminating in chaos. Dowell and Pezeshki (1986) investigated the nonlinear single-mode response of buckled beams. They showed that the single-mode response undergoes a sequence of period-doubling bifurcations culminating in

chaos. They compared their results with the experimental results of Moon (1980) and reported good agreement in general. Zavodney and Nayfeh (1988) studied the response of a single-degree-of-freedom system with quadratic and cubic nonlinearities to a fundamental parametric resonance. They presented a second-order perturbation solution and verified its results by using analog- and digital- computer simulations. They showed that this system exhibits period-multiplying and -demultiplying bifurcations as well as chaotic motions.

Single-degree-of-freedom models gave an insight into the nonlinear characteristics of dynamical systems, but, by design, they overlooked the important phenomenon of modal interactions. To study this phenomenon, it was imperative that systems with at least two degrees of freedom be studied. Following is a review of studies in two-degrees-of-freedom systems:

Systems with Two-To-One Internal Resonances

Sethna (1965) studied the vibrations of two-degree-of-freedom systems with quadratic nonlinearities. He showed that these systems exhibit amplitude-modulated motions with large modulation periods. Nayfeh, Mook and, Marshall (1973) and Mook, Marshall, and Nayfeh (1974) investigated the coupling between the pitch (heave) and roll modes of a ship. They modeled their system as two coupled oscillators with quadratic nonlinearities. They studied the cases of primary and secondary resonances when the linear natural frequency of the pitch mode is approximately twice that of the roll mode (i.e., $\omega_2 \approx 2\omega_1$). They showed that when the excitation frequency is near ω_2 , the response exhibits the saturation phenomenon. Furthermore, they showed that when the excitation frequency is near ω_1 , there exist conditions under which stable steady-state responses of the ship are not periodic, but rather amplitude- and phase-modulated motions. Nayfeh (1988b) studied the

nonlinear coupling between the pitch and roll modes of a ship in a regular sea when the pitch frequency is approximately twice the roll frequency. He showed that in the case when the encounter frequency is near the roll frequency (i.e., primary resonance of the pitch mode), the system exhibits the saturation phenomenon for a level of excitation above a certain threshold. He also demonstrated the existence of Hopf bifurcations. He showed that Hopf bifurcations also exist when the encounter frequency is near the roll frequency (i.e., primary resonance of the roll mode). In both cases, Hopf bifurcation leads to amplitude- and phase-modulated combined roll and pitch motions. Hatwal, Mallik and Ghosh (1983a, 1983b) studied forced nonlinear oscillations of a two-degree-of-freedom system in the presence of two-to-one autoparametric resonance. They showed that the response of such a system exhibits both periodic and chaotic motions. They advocated the use of statistical analysis to study the chaotic responses.

Nayfeh and Zavodney (1986) studied the response of two-degree-of-freedom systems with quadratic nonlinearities to combination parametric resonances. They presented a perturbation solution which predicted periodic solutions and amplitude- and phase-modulated motions and numerically verified their results. They also showed that the limit-cycle solutions experience period-doubling bifurcations. Streit, Bajaj, and Krousgrill (1988) studied the same system. They found Hopf bifurcations resulting in limit-cycle solutions. These limit cycles go through a cascade of period-doubling bifurcations culminating in chaos.

Haddow, Barr, and Mook (1984) presented experimental verifications of the saturation phenomenon in a simple experimental set up consisting of two beams and two concentrated masses. Nayfeh and Zavodney (1988) reported experimental observations of amplitude- and phase-modulated oscillations in a two-degree-of-freedom mechanical model having quadratic nonlinearities and linear

natural frequencies in the ratio of two-to-one. The lower mode was externally excited by a near-resonant harmonic excitation. They showed a qualitative agreement with the results of a second-order perturbation solution. Nayfeh, Balachandran, Colbert, and Nayfeh (1988) conducted experiments on a structure consisting of two light-weight beams and two concentrated masses and reported periodically and chaotically modulated motions. They reported what seems to be a cascade of period-doubling bifurcations resulting in chaos.

Miles (1985) studied a parametrically excited double pendulum in the presence of two-to-one internal resonance conditions when the lower mode is excited by a principle parametric resonance. He showed that two types of motion are possible: a rigid-body translation or coupled oscillations of the pendulum superimposed on these translations. He concluded that there are no Hopf bifurcations. Consequently no periodically-modulated or chaotic motions appear possible. Nayfeh (1987a) studied the same problem and found that the response exhibits a Hopf bifurcation leading to amplitude- and phase-modulated motions. Furthermore, he showed that with the proper choice of the system parameters, the periodic motion of the averaged equations goes through period-doubling bifurcations leading to chaos. He also studied the case when the lower mode is excited by a principal parametric resonance and showed that the averaged equations exhibit Hopf bifurcation.

Holmes (1986) used Melnikov method to study two-to-one internal resonances in vertically excited surface waves. He showed that the model has transverse homoclinic orbits, Smale horseshoe, and thus chaotic orbits. Miles (1984c) studied the perfectly tuned two-to-one internal resonance in surface waves when the lower mode is excited by a principal parametric resonance. He found no Hopf bifurcations and concluded that there are no limit-cycle or chaotic solutions for the modulation equations. Nayfeh (1987b) studied the nonlinear response of the free surface of a

liquid in a cylindrical container to a harmonic vertical oscillation in the presence of a two-to-one autoparametric resonance. He relaxed Miles' perfectly tuned condition and showed that when the lower mode is excited with a principal parametric resonance, the set of evolution equations that describe the modulation of amplitudes and phases of the resonating modes have four possible solutions: a trivial motion, a limit cycle involving the resonating modes, an amplitude- and phase- modulated sinusoid, and a chaotically modulated sinusoid. Gu and Sethna (1987) studied surface waves in vertically excited rectangular containers when the frequencies of two modes are in the ratio of two-to-one. They found periodic, almost periodic, and chaotic wave motions.

Systems With One-To-One Internal Resonances

Miles (1984d) studied the the one-to-one internal resonance between planar and nonplanar motions of spherical pendulums. He showed that a resonating planar motion of the base might excite the nonplanar motion, resulting in a cascade of period-doubling bifurcations and chaos.

Maewal (1986b) showed that elastic beams with symmetric cross-sections can exhibit a coupling between their in-plane and out-of-plane modes, and that a resonant transverse excitation can induce out-of-plane responses. He also showed that the beam may exhibit a chaotically modulated response for certain values of the excitation frequency. Nayfeh and Pai (1989) studied the one-to-one internal resonance between the in-plane and out-of-plane motions of beams. They used the method of multiple-time scales to derive a set of modulation equations for the evolution of the amplitudes and phases of the in-plane and out-of-plane modes. They found that as the frequency of excitation varies, the fixed points of the modulation

equations lose stability through Hopf bifurcation and modulated motions result. They also found regions of chaotic responses.

Miles (1984a, 1984b) studied the one-to-one internal resonance between orthogonal surface-wave modes in a circular cylinder in the case of free and forced oscillations. He concluded that exciting one of these modes may excite the other and the response may be periodically or chaotically modulated. He also showed that this modal coupling does not exist above certain values of damping and depth-to-radius ratios. Feng and Sethna (1989) studied symmetry-breaking bifurcations of surface waves in nearly square containers subjected to vertical oscillations and in the presence of one-to-one internal resonance conditions. They showed that the system may exhibit periodic, quasi-periodic, or chaotic solutions. Ciliberto and Gollub (1985) conducted experimental investigations into one-to-one internal resonances in surface waves. They examined the case in which the excitation frequency and amplitude are near the intersection of the instability boundary between two degenerate modes and found that they can compete with each other to produce either periodic or chaotic motion. They used the experimental data to reconstruct the attractors in the phase space and calculate their dimensions and Lyapunov exponents. They found that the chaotic attractors have fractal dimensions and at least one positive Lyapunov exponent. Simonelli and Gollub (1989) experimentally studied wave mode interactions in square and near square containers. They detected multiple attractors and repellers and studied the involved bifurcations.

Miles (1984e) studied the nonplanar motion of stretched strings. He found two points of Hopf bifurcation and suggested the possibility of strange attractors. He did not investigate limit cycles or chaotic attractors. Johnson and Bajaj (1989) studied the one-to-one internal resonance between the planar and nonplanar responses of strings. They found two branches of periodic solutions between the Hopf bifurcation

frequencies. One branch goes through an incomplete sequence of period-doubling bifurcations followed by period-halving bifurcations. The other branch is created by a saddle-node collision and goes through a cascade of period-doubling bifurcations culminating in chaos.

CHAPTER 2

BASIC CONCEPTS IN NONLINEAR DYNAMICS

The current work is concerned with modal interactions in the nonlinear response of infinitely long cylindrical shells and closed spherical shells to different external and internal (autoparametric) resonance conditions. The method of multiple-time scales is used to construct an asymptotically valid expansion for the displacement fields. This method yields a set of autonomous nonlinear ordinary-differential equations for the evolution of the amplitudes and phases of the interacting modes. Fixed-point solutions of these equations represent periodic oscillations of the shell, whereas limit-cycle solutions correspond to amplitude- and phase-modulated oscillations of the shell. These equations have the general form

$$\frac{d\vec{X}}{dt} = \vec{F}(\vec{X}; r) \quad (2.1)$$

where $t \in [t_0, \infty)$, $\vec{F}(\vec{X}; r): \mathbb{R}^n \times \mathbb{R} \rightarrow \mathbb{R}^n$ is a smooth nonlinear vector field, and r is a control (or bifurcation) parameter of the system. The value of the solution $\vec{X}(t)$ of (2.1)

at time t with the initial conditions $\bar{X}_0 = \{x_1, \dots, x_n\}$ is the flow $\bar{\Phi}_t(x_1, \dots, x_n, t)$. In our study, we focus attention on the asymptotic nature of the solutions for large times (i.e., steady-state solutions).

In the following sections we present some basic definitions and concepts from the theory of dynamical systems associated with the solutions of nonlinear autonomous ordinary-differential equations. The references of this chapter include those of Hale (1963), Urabe (1967), Hirsch and Smale (1974), Chua and Lin (1975), Marsden and McCracken (1976), Nayfeh and Mook (1979), Iooss and Joseph (1980), Hassard, Kazarinoff, and Wan (1981), Mees (1981), Chow and Hale (1982), Vanderbauwhede (1982), Lichtenberg and Lieberman (1983), Haken (1983), Guckenheimer and Holmes (1983), Berge', Pomeau and Vidal (1984), Thompson and Stewart (1986), Jordan and Smith (1987), Bedford and Swift (1988), and other published articles referenced within the text.

2.1 Attractors

Given a flow $\bar{\Phi}_t$ on \mathbb{R}^n and a point $x \in \mathbb{R}^n$, the ω limit set of x is defined as

$$\omega(x) = \{y \in \mathbb{R}^n : \exists \{t_n\}, t_n \rightarrow \infty, \bar{\Phi}_{t_n}(x) \rightarrow y\} \quad (2.2)$$

In other words, the ω limit set of x is the set of all points y with the following property: there is an increasing sequence $\{t_n\} \subset \mathbb{R}$ such that $t_n \rightarrow \infty$ and $\bar{\Phi}_{t_n}(x) \rightarrow y$. An α limit set is defined similarly for $t_n \rightarrow -\infty$.

A set $\mathcal{A} \subseteq \mathbb{R}^n$ is said to be an *attractor* of a flow $\bar{\Phi}_t$ on \mathbb{R}^n if \mathcal{A} has an open neighborhood \mathcal{R} such that

$$\forall x \in \mathcal{R}, \bar{\Phi}_{[0, \infty)}(x) \subseteq \mathcal{R} \text{ and } \omega(x) \subseteq \mathcal{J} \quad (2.3)$$

We say \mathcal{J} attracts \mathcal{R} . The largest such \mathcal{R} is called the *basin of attraction* of \mathcal{J} . A repeller is defined similarly with $\bar{\Phi}_{(-\infty, 0]}(x)$ and $\alpha(x)$.

2.2 Fixed-Points (Constant Solutions)

The point $P(\bar{X}_E)$ in the phase space is a *fixed-point solution*¹ of the vector equation (2.1) if

$$\bar{F}(\bar{X}_E; r) = \bar{0} \quad (2.4)$$

2.2.1 Stability of fixed-point solutions

The stability of a fixed-point solution $P(\bar{X}_E)$ is determined by perturbing the flow in the phase space around it and studying the evolution of this perturbation with time.

We let

$$\bar{X} = \bar{X}_E + \bar{\delta} \quad (2.5)$$

Thus equation (2.1) becomes

¹ Also called *equilibrium point*.

$$\frac{d\vec{X}_E}{dt} + \frac{d\vec{\delta}}{dt} = \vec{F}(\vec{X}_E + \vec{\delta}; r) = \vec{F}(\vec{X}_E; r) + [G(\vec{X}_E; r)]\vec{\delta} + \dots \quad (2.6)$$

where $[G] = \vec{\nabla}\vec{F}$ is the Jacobi matrix of the system. We use the vector equation (2.4) and retain the first-order terms in equation (2.6) to get

$$\frac{d\vec{\delta}}{dt} = [G(\vec{X}_E; r)]\vec{\delta} \quad (2.7)$$

The variational vector equation (2.7) constitutes a system of n linear ordinary-differential equations with constant coefficients. They possess solutions proportional to $\exp(\lambda t)$ where λ is an eigenvalue of $[G]$. Thus, for the fixed point $P(\vec{X}_E)$ to be a stable solution of (2.1), the disturbance $\vec{\delta}$ must decay as $t \rightarrow \infty$. The condition for stability is thus

$$\text{Re}(\lambda_i) < 0 \quad \text{for } i = 1, 2, \dots, n \quad (2.8)$$

A system with $\text{Re}(\lambda_i) = 0$ while all other $\text{Re}(\lambda_i) < 0$ is called *neutrally stable*. A fixed point which is neither stable nor neutrally stable is *unstable*.²

2.2.2 Bifurcation of fixed-point solutions

The bifurcation analysis is concerned with the study of the behavior of the flow $\vec{\Phi}_t(\vec{x})$ of system (2.1) as the control parameter r varies. The critical values of r where a sudden qualitative change of the behavior of the flow occurs is called a *bifurcation*

² We do not distinguish between *unstable* and *nonstable* solutions.

point. The fixed-point solutions of the flows studied in this work experience three types of bifurcations; namely, saddle-node, pitchfork, and Hopf bifurcations.

1. Saddle-node bifurcation

This bifurcation is associated with a real eigenvalue crossing the imaginary axis toward the right half of the complex plane, this is usually associated with the jump phenomenon where a stable and an unstable fixed point collide and annihilate each other. Figure 2.1a shows the generic bifurcation pattern for a saddle-node bifurcation.

2. Pitchfork bifurcation

This bifurcation is usually associated with symmetric systems. The system (2.1) is said to be symmetric if it is invariant under the action of a group of linear transformations of \mathbb{R}^n (called a group of symmetries of equation (2.1)). Let γ be a linear transformation of \mathbb{R}^n , equation (2.1) is said to have a group of symmetries S if for all $\gamma \in S$

$$\gamma [\vec{F}(\vec{X}; r)] = \vec{F} (\gamma[\vec{X}]; r) \quad (2.9)$$

As in the saddle-node bifurcation, the pitchfork bifurcation is associated with an eigenvalue of $[G]$ crossing the imaginary axis along the real axis toward the right half of the complex plane. There are two types of pitchfork bifurcations: supercritical pitchfork bifurcation (fig. 2.1b) and subcritical pitchfork bifurcation (also called reversed pitchfork bifurcation) (fig. 2.1c).

3. Hopf bifurcation

This is associated with two complex conjugate eigenvalues of $[G]$ crossing the imaginary axis into the right half of the complex plane with a nonzero speed. This results in branches of periodic solutions bifurcating at the bifurcation point. It

could be either supercritical or subcritical (fig. 2.1d,e). Supercritical Hopf bifurcation is associated with the flow decaying along some eigendirections and a small amplitude closed orbit being born in the manifold locally normal to these directions. A subcritical Hopf bifurcation on the other hand is associated with large-amplitude closed orbits around the Hopf-bifurcation point.

2.3 Limit Cycles (Closed Orbits)

The following theorems are due to Urabe (1967):

Theorem

Let $\vec{X} = \vec{\phi}(t)$ be any solution of (2.1) such that $\vec{\phi}(\tau_1) = \vec{\phi}(\tau_2)$ for $\tau_1 \neq \tau_2$, then the function $\vec{\phi}(t)$ is periodic in t with the period $\tau_2 - \tau_1$.

Theorem

The orbit Γ represented by the solution $\vec{X} = \vec{\phi}(t)$ is closed if and only if $\vec{X} = \vec{\phi}(t)$ is a nonconstant periodic solution.

2.3.1 Detection of closed orbits

To detect periodic orbits of (2.1) one can numerically integrate these equations for a long time until all the transient response decays, a computationally expensive

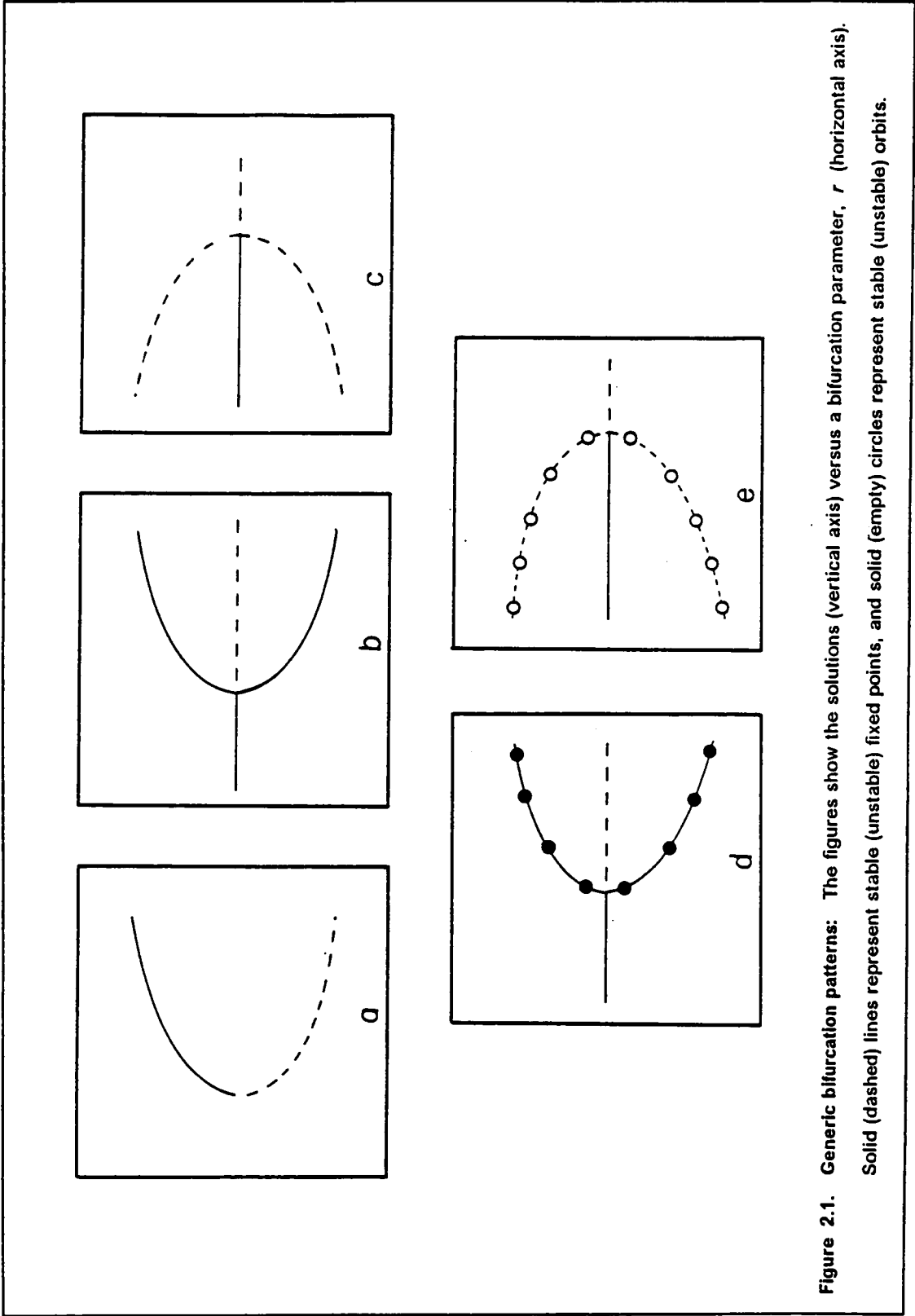


Figure 2.1. Generic bifurcation patterns: The figures show the solutions (vertical axis) versus a bifurcation parameter, r (horizontal axis). Solid (dashed) lines represent stable (unstable) fixed points, and solid (empty) circles represent stable (unstable) orbits.

approach. An algorithm originally proposed by Aprille and Trick (1972) is designed to eliminate the long-time integration process and yield a set of initial conditions on the orbit Γ and its period so that one can construct the orbit by integrating with these initial conditions for one period. We follow Aprill and Trick (1972) and Chua and Lin (1975) in describing this algorithm.

We first transform the initial-value problem into a boundary-value problem with periodic boundary conditions, that is;

$$\begin{aligned}\frac{d\vec{X}}{dt} &= \vec{F}(\vec{X}; r) \\ \vec{X}(0) &= \vec{X}(T)\end{aligned}\tag{2.10}$$

Equations (2.10) can be integrated into

$$\vec{X}(t, \vec{X}_0) = \int_0^t \vec{F}(\vec{X}(t); r) dt + \vec{X}_0\tag{2.11}$$

which upon evaluation at $t = T$ yields

$$\vec{E}(T, \vec{X}_0) \equiv \vec{X}(T, \vec{X}_0) - \vec{X}_0 = \int_0^T \vec{F}(\vec{X}(t); r) dt\tag{2.12}$$

Hence, the periodicity condition becomes

$$\vec{H}(\vec{X}_0, T) = \vec{X}_0 - \vec{E}(T, \vec{X}_0) = \vec{0}\tag{2.13}$$

The problem now is to solve the system of n equations given by (2.13) for $n+1$ unknowns; namely, \vec{X}_0 and T . Aprille and Trick suggest an iteration scheme to solve

(2.13). They fix one of the unknowns and perform a Newton-Raphson iteration on the remaining ones. They give a criterion for choosing the variable to be fixed and prove the convergence of the scheme in the neighborhood of the orbit (step 2 below). The algorithm is listed below:

Step 1

For a given initial state $\vec{X}_0^{(j)}$ and $T^{(j)}$ calculate $\vec{X}^{(j)}$ by integrating (2.1).

Step 2

Select an integer $k \leq n$ such that

$$| \vec{F}_k(\vec{X}^{(j)}(T^{(j)}, \vec{X}_0^{(j)})) | \geq | F_m(\vec{X}^{(j)}(T^{(j)}, \vec{X}_0^{(j)})) | \quad (2.14)$$

$$m = 1, 2, \dots, k-1, k+1, \dots, n$$

where $| \cdot |$ indicates the absolute value.

Step 3

Define the solution vector

$$\vec{v} = [X_{01}, X_{02}, \dots, X_{0k-1}, T, X_{0k+1}, \dots, X_{0n}]^T \quad (2.15)$$

where the superscript T indicates the transpose.

Step 4

Use the Newton-Raphson iteration formula to compute $\vec{v}^{(j+1)}$ from

$$\vec{v}^{(j+1)} = \vec{v}^{(j)} - [I(-k) - E'(T^{(j)}, \vec{X}_0^{(j)})]^{-1} H^{(j)}(\vec{v}^{(j)}) \quad (2.16)$$

where $I(-k)$ denotes the identity matrix with a zero k^{th} element. This is necessary since the k^{th} element in \vec{v} is T and not X_{0k} . The matrix $E'(T, X_0^{(j)}) \equiv \partial \vec{E} / \partial \vec{v}$ is given by

$$[E']_{l,j} = \frac{\partial \vec{X}_l(T, \vec{X}_0)}{\partial X_{0j}}, \quad \text{for } j \neq k \quad (2.17)$$

$$[E']_{l,k} = \frac{\partial X_l(T, \vec{X}_0)}{\partial T} = F_l(\vec{X}(T, \vec{X}_0)) \quad \text{for } l = 1, 2, \dots, n \quad (2.18)$$

where equation (2.17) is evaluated using a combination of integration and finite-difference schemes.

Step 5

Return to step 1 unless $\| \vec{v}^{(j)} - \vec{v}^{(j+1)} \| < \delta$ and $\| X^{(j)} - X_0^{(j)} \| < \varepsilon$ where δ and ε are preassigned error tolerances and $\| \|$ indicates the Euclidian norm.

Step 6

Stop.

This algorithm proved efficient in reducing the computation time but is sensitive to the initial guesses and the step size of the integration. Using different step sizes, we found that the algorithm sometimes landed on different orbits for the same bifurcation parameter.

2.3.2 Stability of closed orbits

The local stability of a closed orbit is determined by disturbing the orbit and studying the evolution of the disturbance with time. Let Γ be a closed orbit of (2.1) represented by $\vec{X} = \vec{\phi}(t) = \vec{\phi}(t + T)$ then

$$\frac{d\vec{\phi}(t)}{dt} = \vec{F}(\vec{\phi}(t); r) \quad (2.19)$$

The local behavior of the flow around Γ is governed by

$$\frac{d\vec{\xi}}{dt} = \left[G(\vec{\phi}(t); r) \right] \vec{\xi} \quad (2.20)$$

The vector equation (2.20) constitutes a set of n linear ordinary-differential equations with periodic coefficients of period T . Floquet theory is used to study the stability of the solutions of these equations. Let $\vec{\xi}(t)$ be an n -dimensional solution vector of (2.20) then it can be shown that $\vec{\xi}(t + T)$ is also a solution. The uniqueness theorem assures that equations (2.20) have only n linearly independent solutions and that all other solutions can be written as a linear combination of these fundamental solutions, thus

$$\vec{\xi}(t + T) = [A] \vec{\xi}(t) \quad (2.21)$$

where $[A]$ is a matrix with constant coefficients called the *monodromy matrix* and its eigenvalues are called the *Floquet multipliers*. Next we introduce the following linear transformation:

$$\vec{\chi}(t) = [P] \vec{\xi}(t) \quad (2.22)$$

where $[P]$ is a nonsingular constant matrix, or

$$\vec{\xi}(t) = [P]^{-1} \vec{\chi}(t) \quad (2.23)$$

where the superscript -1 indicates the inverse of the matrix. Thus (2.21) becomes

$$[P]^{-1} \vec{\chi}(t+T) = [A] [P]^{-1} \vec{\chi}(t)$$

or

$$\vec{\chi}(t+T) = [P] [A] [P]^{-1} \vec{\chi}(t) \quad (2.24)$$

which can be rewritten as

$$\vec{\chi}(t+T) = [B] \vec{\chi}(t) \quad (2.25)$$

where $[B]$ is a Jordan canonical form.

We consider the case of diagonal $[B]$. If the eigenvalues of $[A]$ are distinct, then $[P]$ can be chosen so that $[B]$ is diagonal with the eigenvalue λ_i , $i = 1, \dots, n$ as its (i, i) element. Thus, the individual elements in system (2.25) are given as

$$\chi_i(t+T) = \lambda_i \chi_i(t) \quad (2.26)$$

Consequently,

$$\chi_i(t+nT) = \lambda_i^n \chi_i(t) \quad (2.27)$$

which implies that the orbit is stable if the moduli of all the Floquet multipliers λ_i are less than unity. Since equation (2.19) is autonomous, $\vec{\xi} = \frac{d\phi(t)}{dt} = \frac{d\phi(t+T)}{dt}$ is a solution of (2.20). This implies that one of the Floquet multipliers for equation (2.20)

is always +1. To show that $d\bar{\phi}(t)/dt$ is a solution to (2.20), we use equation (2.19), the chain rule to evaluate $\frac{d}{dt} \frac{d\bar{\phi}}{dt}$, and obtain

$$\frac{d}{dt} \frac{d\bar{\phi}(t)}{dt} = \frac{d}{dt} \left\{ F(\bar{\phi}(t); r) \right\} = \left[G(\bar{\phi}(t); r) \right] \frac{d\bar{\phi}(t)}{dt} \quad (2.28)$$

Equation (2.28) is the same as equation (2.20) with $\bar{\chi}$ replaced by $d\bar{\phi}(t)/dt$. Consequently, $d\bar{\phi}(t)/dt$ is a solution of equation (2.20).

Next, we multiply equation (2.26) by $\exp(-\gamma_i t - \gamma_i T)$, where γ_i is an arbitrary constant to be determined later, and obtain

$$\chi_i(t+T) e^{-\gamma_i(t+T)} = \lambda_i e^{-\gamma_i T} \chi_i(t) e^{-\gamma_i t} \quad (2.29)$$

We now choose

$$\gamma_i = \frac{1}{T} \ln \lambda_i \quad (2.30)$$

Thus equation (2.29) becomes

$$\chi_i(t+T) e^{-\gamma_i(t+T)} = \chi_i(t) e^{-\gamma_i t} = \eta_i(t) \quad (2.31)$$

Hence, $\chi_i(t) \exp(-\gamma_i t)$ is periodic with period T , and χ_i has the normal or *Floquet form* $\chi_i(t) = \exp(\gamma_i t) \eta_i(t)$, $\eta_i(t+T) = \eta_i(t)$. The constants γ_i are called the *characteristic exponents*. They also determine the stability of closed orbits; an orbit is stable if all $\text{Re}(\gamma_i) < 0$ and unstable if at least one $\text{Re}(\gamma_i) > 0$.

These stability conditions also apply for the cases of repeated eigenvalues of [A] (see Nayfeh and Mook, 1979, pp. 279-283).

2.3.3 Bifurcation of closed orbits

As the parameter of the system r changes, the orbital behavior of (2.1) might suddenly change at some critical bifurcation point $r = r_c$. The bifurcation of a closed orbit is always associated with a Floquet multiplier leaving the unit circle in the complex plane. The orbits of the systems studied hereafter suffer three types of bifurcations: symmetry-breaking bifurcation, cyclic-fold bifurcation, and period-doubling bifurcation.

1. Symmetry-breaking bifurcation

This bifurcation is associated with a Floquet multiplier leaving the unit circle in the complex plane through $+1$. Because of this bifurcation, a symmetric orbit loses stability to an asymmetric one. The existence of a symmetry transformation in the system suggests that asymmetric orbits exist in pairs. The unstable symmetric orbit continues to exist after this bifurcation occurs.

2. Cyclic-fold bifurcation

This bifurcation is also associated with a Floquet multiplier leaving the unit circle in the complex plane through $+1$. It differs from the symmetry-breaking bifurcation in that the unstable orbit ceases to exist after this bifurcation occurs. This bifurcation usually indicates the collision of a stable orbit with an unstable orbit and, as a result of this collision, the involved orbits annihilate each other and the flow jumps out of the vicinity of the collision.

3. Period-doubling bifurcation

This bifurcation is associated with a Floquet multiplier leaving the unit circle through -1. In this case, a stable orbit of period T loses stability to another stable orbit of period $2T$. The unstable orbit continues to exist after the bifurcation occurs. In our study, a cascade of period-doubling bifurcations culminates in chaos. This, however, does not always have to be the case; there are reported cases of finite number of period-doubling bifurcations followed by undoublings or by other bifurcations.

2.4 Poincare' Sections

The phase portraits of a complex multi-dimensional dynamic system usually get too complicated and are not easy to analyze. One way of condensing the phase space information is to use a *Poincare' section*.

Let Σ be a section in the phase space such that the phase trajectories cut it transversely. Σ divides the phase space into two regions: Σ^+ and Σ^- . The set of all the points $\subset \Sigma$ where the flow pierces Σ from, say, Σ^+ to Σ^- (or in the other direction) is called a *one-sided Poincare' map*. The simplification introduced by using a Poincare' map is obvious: a closed orbit of period T is represented as a closed curve in the phase portrait but as a finite number of points on the Poincare' section, an orbit of period $2T$ leaves twice as many points on the Poincare' section and so on. Another advantage of using a Poincare' map rather than a phase portrait appears when a symmetry-breaking bifurcation occurs. While such a bifurcation might be confused with a period-doubling bifurcation in the phase portrait, the number of

points it leaves on the section does not double after the bifurcation, thus clearing the confusion.

2.5 Lyapunov Exponents and Lyapunov Dimension

The existence of different kinds of attractors (fixed points, closed orbits, or chaotic attractors) makes it necessary to seek a criterion to distinguish among the different attractors, such a criterion is provided by the Lyapunov exponents. The concept of Lyapunov's exponents is a generalization of the eigenvalues of a fixed point and the characteristic exponents for a closed orbit. It simply tests the behavior of the flow in the neighborhood of a trajectory \vec{X}_0 .

Assume that the system (2.1) has an attractor γ given by \vec{X}_0 . Let

$$\vec{X} = \vec{X}_0 + \delta\vec{X} \quad (2.32)$$

and

$$\frac{d\delta\vec{X}}{dt} = [G(\vec{X}_0; r)] \delta\vec{X} \quad (2.33)$$

The vector equation (2.33) is a set of n linear ordinary-differential equations with variable coefficients. The *Lyapunov exponents* are defined as

$$\lambda = \lim_{t \rightarrow \infty} \frac{1}{t} \ln |\delta\vec{X}| \quad (2.34)$$

Thus an n -dimensional system has n Lyapunov exponents.

Theorem (Haken, 1983)

If $\bar{X}(t)$ is a trajectory which remains in a bounded region and if it does not terminate at a fixed point, at least one of its Lyapunov exponents vanishes.

Another useful quantity that can be used to distinguish among the attractors is the *Lyapunov dimension* d_f . The relationship between the Lyapunov exponents and the Lyapunov dimension is given by Frederickson et al. (1983) as

$$d_f = j + \sum_{i=k}^j \frac{\lambda_k}{|\lambda_{j+1}|} \quad (2.35)$$

where the λ_i are ordered such that $\lambda_n > \lambda_{n-1} > \dots > \lambda_2 > \lambda_1$ and j is defined as

$$\sum_{k=1}^j \lambda_k > 0, \quad \sum_{k=1}^{j+1} \lambda_k < 0, \quad (2.36)$$

For a stable fixed point all the Lyapunov exponents are negative; for a stable limit cycle one of the exponents is zero and the rest are negative; and for a chaotic attractor, one of the Lyapunov exponents is positive and the Lyapunov dimension is fractal.³

³ Strictly speaking; the fractal Lyapunov dimension indicates a *strange attractor* and not a *chaotic attractor*. It is typically the case that strange attractors are also chaotic but this is not always so (Grebogi et. al., 1984).

CHAPTER 3

EQUATIONS OF MOTION

In this chapter we derive the equations of motion for the dynamic response of infinitely long circular cylindrical shells under harmonic radial loads and the equations describing the axisymmetric, torsionless dynamic response of closed spherical shells. The shells are assumed to be thin, linearly elastic, and in a state of plane strain. The nonlinearity is due to the kinematic relationships (i.e., geometric nonlinearity). The usual Love-Kirchhoff's assumptions are used: straight lines normal to the middle surface before deformation remain straight and normal to it after and during deformation. This implies that the transverse shear deformations are negligible, which is equivalent to assuming an infinite shear rigidity in the body of the shell. The thickness h of the shell is unchanged, and the transverse stresses are negligible. We also assume that the ratio $(\frac{h^2}{a^2})$ is small, where a is the radius of the undeformed shell.

3.1 Preliminaries from the Theory of Surfaces

The theory of shells is based on the assumptions that one can reduce the three-dimensional equations of the theory of elasticity into two-dimensional equations. In other words, we assume that the behavior of a three-dimensional continua (the shell) can be represented by that of a two-dimensional surface (the shell's reference surface). This establishes a strong connection between the theory of shells and the theory of surfaces. In this section we discuss concepts from the theory of surfaces which relate to our study of shells.

To present the theory of surfaces in an elegant manner, we choose to use tensor calculus. In what follows a superscripted quantity indicates a *contravariant tensor* and a subscripted quantity indicates a *covariant tensor*. The Greek indices can assume the values 1 or 2, and the Latin indices have a range of values from 1 to 3. The summation convention is used unless the index is between two parentheses (). In what follows, we deal with two sets of coordinate systems; namely, the three-dimensional Cartesian coordinates

$$z^i = (z^1, z^2, z^3) \quad , i = 1, 2, 3 \quad (3.1)$$

for the surrounding space in which ε_i is the unit vector along the i^{th} coordinate axis and the curvilinear coordinates

$$u^\alpha = (u^1, u^2) \quad , \quad \alpha = 1, 2 \quad (3.2)$$

of the surface. A surface is the locus of a point whose coordinates are functions of two independent parameters. Thus the equations of a surface are of the form

$$z^l = z^l(u^\alpha) \quad (3.3)$$

The tangent vectors S_α to the surface at any point are (fig. 3.1)

$$S_\alpha = \frac{\partial z^l}{\partial u^\alpha} \varepsilon_l \quad (3.4)$$

The metric of the surface is defined as

$$a_{\alpha\beta} = S_\alpha \cdot S_\beta = \frac{\partial z^l}{\partial u^\alpha} \frac{\partial z^p}{\partial u^\beta} \varepsilon_l \varepsilon_p \quad (3.5)$$

and $a = \det(a_{\alpha\beta})$. The normal \vec{N} to the surface is

$$\vec{N} = \vec{S}_1 \times \vec{S}_2 \quad (3.6)$$

it can be shown that the unit normal \vec{n} is

$$\vec{n} = \frac{\vec{N}}{|\vec{N}|} = \frac{\vec{S}_1 \times \vec{S}_2}{\sqrt{a}} \quad (3.7)$$

The curvature tensor $b_{\alpha\beta}$ is defined as

$$b_{\alpha\beta} = \vec{n} \cdot \frac{\partial S_\alpha}{\partial u^\beta} \quad (3.8)$$

The first fundamental form of a surface relates the length of a line element (ds) on the surface to the metric of the surface as

$$ds^2 = a_{\alpha\beta} du^\alpha du^\beta \quad (3.9)$$

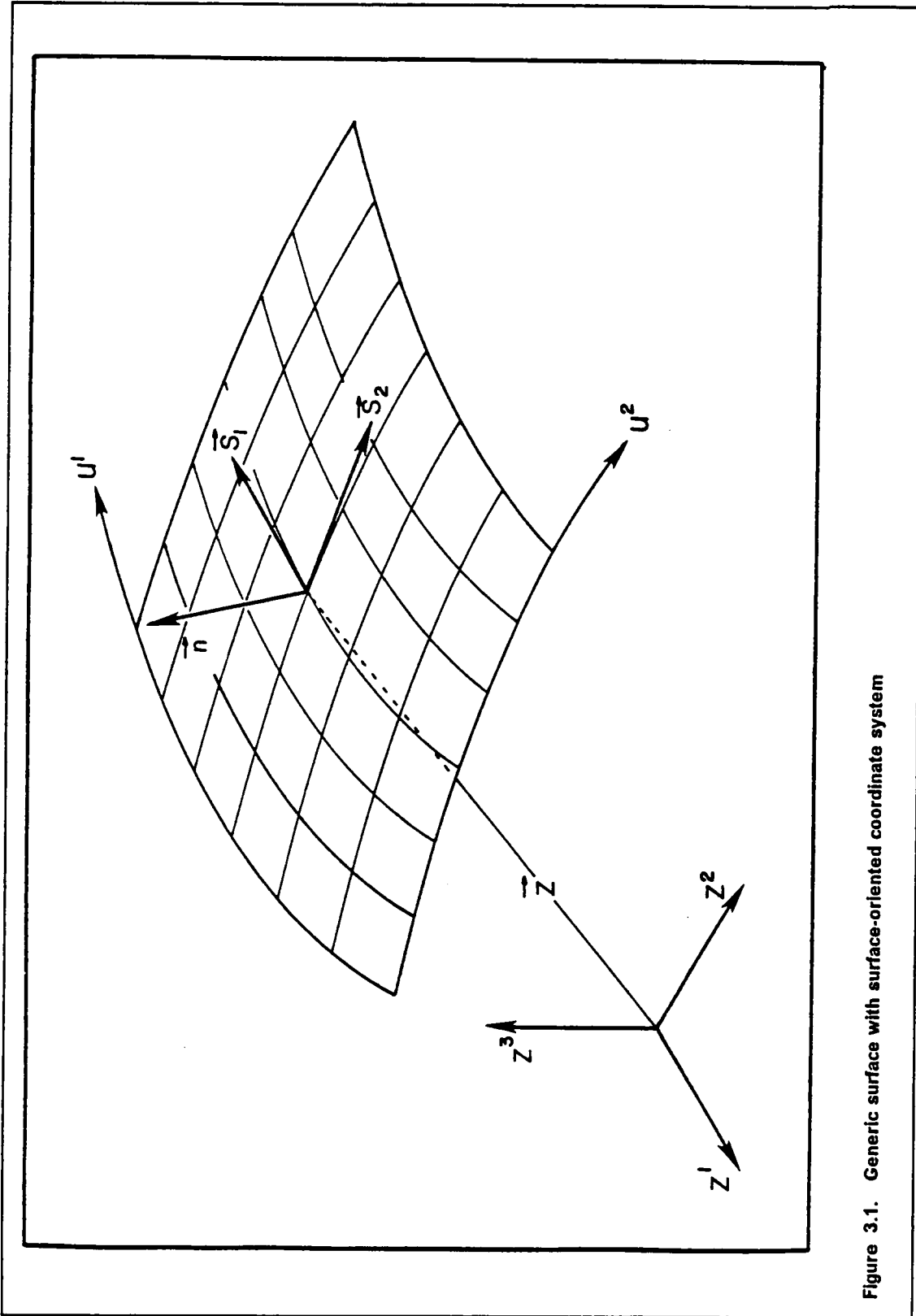


Figure 3.1. Generic surface with surface-oriented coordinate system

If we consider a surface with a metric $a_{\alpha\beta}$, which after deformation becomes $a^*_{\alpha\beta}$, then the strain experienced by a line element on that surface is

$$\varepsilon_{(\alpha)(\beta)} = \frac{\sqrt{a^*_{(\alpha)(\beta)}} - \sqrt{a_{(\alpha)(\beta)}}}{\sqrt{a_{(\alpha)(\beta)}}} \quad (3.10)$$

Another important characteristic of a surface is its principal curvature. The principal curvatures κ of a surface are defined by

$$\det [b_{\alpha\beta} - \kappa a_{\alpha\beta}] = 0 \quad (3.11)$$

3.2 Equations of Motion of Infinitely Long Circular

Cylindrical Shells

Let p be a point on the undeformed shell middle-surface at time t and p^* be the same point on the deformed shell at time t^* (fig. 3.2). The first fundamental forms for the undeformed and deformed middle surface are given, respectively, by

$$(ds)^2 = (a d\theta)^2 \quad (3.12)$$

$$(ds^*)^2 = [r'^2 + (r\phi')^2](d\theta)^2 \quad (3.13)$$

where the prime indicates the derivative with respect to θ . Thus, the strain of the middle-surface is

$$\varepsilon_\theta = \frac{\sqrt{r'^2 + (r\phi')^2} - a}{a} \quad (3.14)$$

The curvature of the undeformed and deformed middle-surface are

$$\kappa_\theta = \text{curvature of the undeformed surface} = \frac{1}{a} \quad (3.15)$$

$$\begin{aligned} \kappa^*_\theta &= \text{curvature of the deformed surface} \\ &= [\phi'(r^2\phi'^2 - rr'' + 2r'^2) + \phi''r'r][r'^2 + r^2\phi'^2]^{-3/2} \end{aligned} \quad (3.16)$$

We introduce the nondimensional displacements w and ψ and nondimensional time τ such that

$$w = \frac{a-r}{a} , \quad \psi = \phi - \theta , \quad \text{and} \quad \tau = [E \rho (1 - \nu^2)]^{1/2} a t \quad (3.17)$$

where E is Young's modulus, ρ is the material's density, and ν is Poisson's ratio. To third order, the strains and principal curvatures are:

ε_θ = strain along the θ -coordinate line

$$= \psi' - w + \frac{1}{2} w'^2 - w\psi' - \frac{1}{2} \psi' w'^2 + \frac{1}{2} w w'^2 \quad (3.18)$$

χ_θ = change in curvature of the middle surface

$$= \frac{1}{a} \left\{ w + w'' + w^2 + 2w w'' + \frac{1}{2} w'^2 - 2\psi' w'' - w'\psi'' + w^3 + 3w^2 w'' - 2w\psi'' w' \right. \\ \left. - 4w\psi' w'' + \frac{3}{2} w w'^2 + 3\psi'' \psi' w' + 3\psi'^2 w'' - \psi' w'^2 - \frac{3}{2} w'' w'^2 \right\} \quad (3.19)$$

The total strain energy functional U is given by Koiter (1960) as

$$U = U_m + U_b \quad (3.20)$$

which for an infinitely long cylindrical shell becomes

$$U_m = \text{membrane strain energy} = a\pi C \int \varepsilon_\theta^2 d\theta \\ = a\pi C \int_0^{2\pi} \left[\psi'^2 - 2\psi' w + w^2 + \psi' w'^2 + 2\psi' w'' - 2w\psi'' - w w'^2 \right. \\ \left. - \psi'^2 w'^2 + w\psi' w'' - w^2 w'' + \frac{1}{4} w'^4 + w^2 \psi'^2 \right] d\theta \quad (3.21)$$

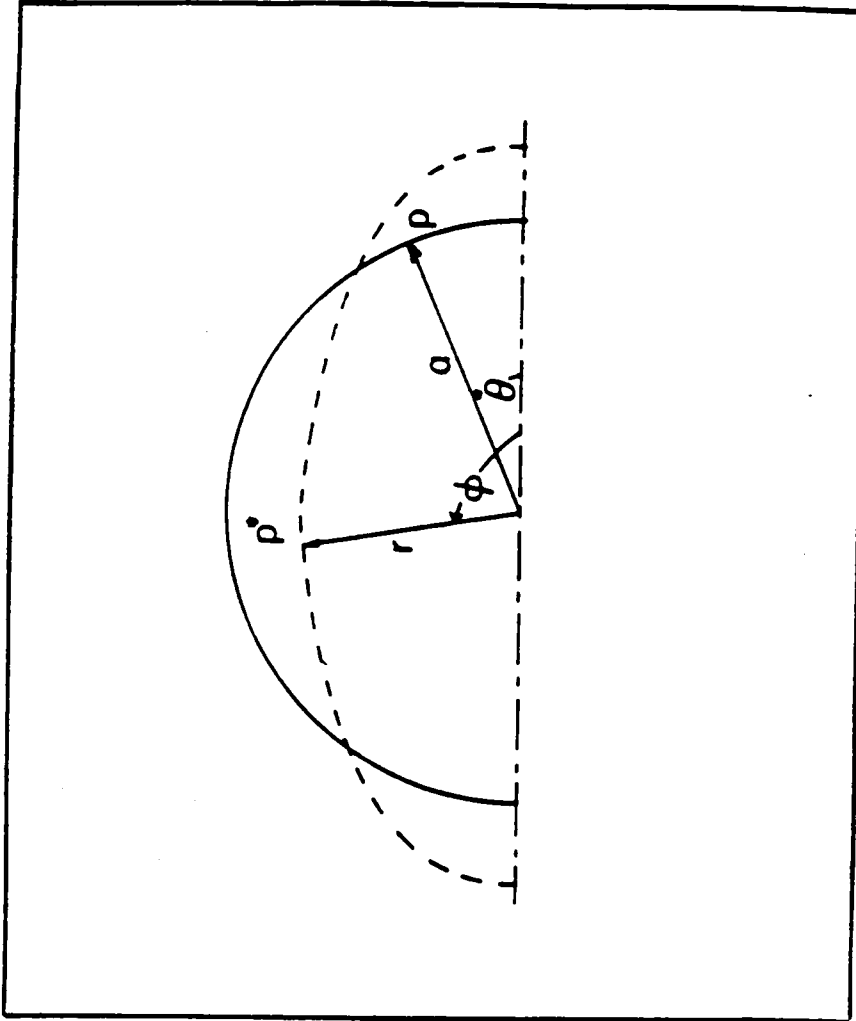


Figure 3.2. Kinematics of deformation for a cylindrical shell: A point (p) at time (t) on the undeformed middle surface and (p') at (t') on the deformed middle surface of the shell

$$\begin{aligned}
U_b = \text{bending strain energy} &= a\pi D \int \chi_\theta^2 d\theta \\
&= a\pi D \int_0^{2\pi} [w''^2 + 2w''w + w^2 + w'^2w - 4\psi'w''w - 2ww'\psi'' + w'^2w'' - 4w''^2\psi' \\
&\quad - 2w'w''\psi'' + 2w^3 + 6w^2w'' + 4ww''^2] d\theta
\end{aligned} \tag{3.22}$$

where

$$\begin{aligned}
C &= \text{extensional stiffness parameter} = Eh/(1 - \nu^2) \\
D &= \text{bending stiffness parameter} = Eh^3/12(1 - \nu^2)
\end{aligned}$$

and h is the thickness of the shell.

The total potential energy V of the loaded shell is

$$V = U + W \tag{3.23}$$

where W is the potential of the applied loads. For radial loads P ,

$$W = -\frac{1}{2} Pa^2 \int_0^{2\pi} [\psi' - 2w - 2w\psi' + w^2] d\theta \tag{3.24}$$

The speed v of p is given by

$$v^2 = \dot{r}^2 + (r\dot{\phi})^2 \tag{3.25}$$

Thus, neglecting rotary inertia, we can write the kinetic energy T as

$$T = \frac{1}{2} \int_V \rho [\dot{r}^2 + (r\dot{\phi})^2] dV = \frac{1}{2} \frac{Eah}{1-\nu^2} \int_0^{2\pi} [\dot{w}^2 + (1-w)^2 \dot{\psi}^2] d\theta \quad (3.26)$$

where the over dot indicates the derivative with respect to τ .

The conservation of the Lagrangian is expressed as

$$\int_{t_1}^{t_2} [\delta T - \delta U_m - \delta U_b - \delta W] dt = 0 \quad (3.27)$$

Substituting equations (3.20)-(3.26) into equation (3.27) and using calculus of variations, we obtain the following equations of motion:

$$\begin{aligned} \ddot{w} + w - \psi' + \alpha^2 \{w^{IV} + 2w'' + w\} = & -\dot{\psi}^2 - \frac{1}{2} w'^2 - 2w\psi' + \psi'^2 + \psi'w'' - ww'' + w'\psi'' \\ & + w\dot{\psi}^2 - 2w'\psi''\psi' + \frac{1}{2} w'^2\psi' - w''\psi'^2 + \frac{3}{2} w''w'^2 - w\psi'^2 + ww'\psi'' - ww'^2 \\ & + ww''\psi' - w^2w'' + \alpha^2 \left\{ -\frac{11}{2} w'^2 + 4w''\psi' + 5w''\psi''' + 4\psi'' w' - 6w''^2 \right. \\ & + 8w'''\psi'' - 8w''w' + 4w^{IV}\psi' + w\psi''' - 11ww'' - 4ww^{IV} - 3w^2 + w'\psi^{IV} \} \\ & + \frac{a(1-\nu^2)}{Eh} P(1 + \psi' - w) \end{aligned} \quad (3.28)$$

$$\begin{aligned} \ddot{\psi} - \psi'' + w' = & 2w\ddot{\psi} + 2\dot{w}\dot{\psi} + w'w'' - 2w'\psi' - 2w\psi'' + 2ww' + ww''w' + w^2\psi'' \\ & - w'^2\psi'' + \frac{1}{2} w'^3 + 2ww'\psi' - 2w''w'\psi' - 2w\dot{w}\dot{\psi} - w^2\ddot{\psi} + \alpha^2 \{w''w' \\ & - w''w''' - ww'''' + w^{IV}w'\} \end{aligned} \quad (3.29)$$

3.3 Equations for the Axisymmetric Motion of Closed Spherical Shells

Let p be a point on the undeformed shell middle-surface at time t (fig. 3.3a) and p^* be the same point on the deformed shell at time t^* (fig. 3.3b). For axisymmetric deformations, $\theta = \eta$ and $\partial(\)/\partial\eta = 0$. The first fundamental forms for the undeformed and deformed middle-surface are given, respectively, by

$$(ds)^2 = (a d\xi)^2 + (a \sin \xi d\theta)^2 \quad (3.30)$$

$$(ds^*)^2 = (r d\phi)^2 + (r \sin \phi d\eta)^2 \quad (3.31)$$

The strains and principal curvatures are given by

$$\varepsilon_\xi = \text{strain along the } \xi\text{-coordinate line} = \frac{[(r\phi')^2 + (r')^2]^{1/2} - a}{a} \quad (3.32)$$

$$\varepsilon_\eta = \text{strain along the } \eta\text{-coordinate line} = \frac{r \sin \phi - a \sin \xi}{a \sin \xi} \quad (3.33)$$

$\chi_\xi =$ change in curvature of the ξ -coordinate line

$$= \frac{rr''\phi' - rr'\phi'' - r^2\phi'^3 - 2r'^2\phi'}{[(r\phi')^2 + r'^2]^{3/2}} - \frac{1}{a} \quad (3.34)$$

$\chi_\eta =$ change in curvature of the η -coordinate line

$$= \frac{\sin(\beta - \phi)}{r \sin \phi} - \frac{1}{a \sin \xi} \quad (3.35)$$

where

$$\beta = \text{rotation of the normal to the middle surface} = \tan^{-1}(r'/r\phi')$$

and the prime indicates the derivative with respect to ξ .

We introduce the nondimensional displacements w and u and nondimensional time τ defined by

$$\varepsilon w = \frac{r}{a} - 1, \quad \varepsilon u = \phi - \xi, \quad \text{and} \quad \tau = [E \rho (1 - \nu^2)]^{1/2} a t \quad (3.36)$$

where $\varepsilon = w_m/a < 1$ is a nondimensional perturbation parameter and w_m is the maximum radial displacement. Substituting equation (3.36) into equations (3.32)-(3.35), we obtain

$$\varepsilon_\xi = \varepsilon(u' + w) + \varepsilon^2\left(\frac{1}{2} w'^2 + w u'\right) + \varepsilon^3\left[-\frac{1}{2} w'^2(u' + w)\right] + O(\varepsilon^4) \quad (3.37)$$

$$\varepsilon_\eta = \varepsilon(u \cot \xi + w) + \varepsilon^2(u w \cot \xi - \frac{1}{2} u^2) + \varepsilon^3\left(-\frac{1}{6} u^3 \cot \xi - \frac{1}{2} u^2 w\right) + O(\varepsilon^4) \quad (3.38)$$

$$\chi_\xi = \frac{1}{a} \left[\varepsilon(w'' + w) + \varepsilon^2\left(-\frac{1}{2} w'^2 - w' u'' - 2w'' u' - 2w'' w - w^2\right) + O(\varepsilon^3) \right] \quad (3.39)$$

$$\chi_\eta = \frac{1}{a} \left[\varepsilon(w' \cot \xi + w) + \varepsilon^2\left(\frac{1}{2} w' u' \cot \xi - 2w' w - w' u \cot \xi\right) + O(\varepsilon^3) \right] \quad (3.40)$$

The total strain energy functional U is given by Kolter (1960) as

$$U = U_m + U_b \quad (3.41)$$

where

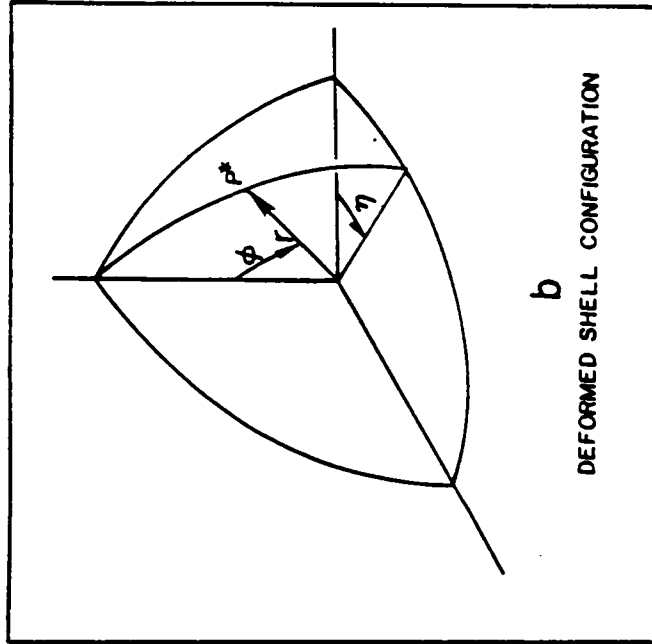
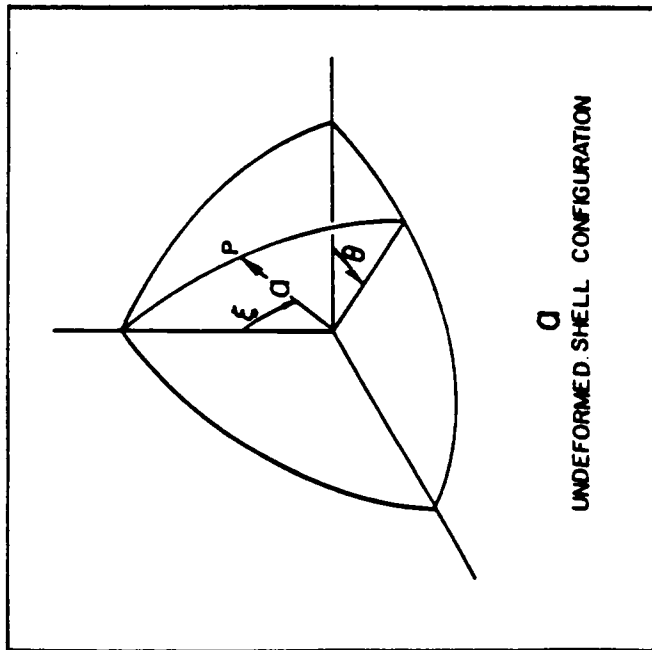


Figure 3.3. Kinematics of deformation for a spherical shell: A point (p) at time (t) on the undeformed middle surface and (p^*) at (t^*) on the deformed middle surface of the shell

$$U_m = \text{membrane strain energy} = \pi C \int \left(\varepsilon_\xi^2 + \varepsilon_\eta^2 + 2\nu\varepsilon_\xi\varepsilon_\eta + \frac{1-\nu}{2} \gamma_{\xi\eta}^2 \right) \sin \xi d\xi \quad (3.42)$$

$$U_b = \text{bending strain energy} = \pi D \int \left(\chi_\xi^2 + \chi_\eta^2 + 2\chi_\eta\chi_\xi + 2(1-\nu) \chi_{\eta\xi}^2 \right) \sin \xi d\xi \quad (3.43)$$

where

$$C = \text{extensional stiffness parameter} = Eh/(1-\nu^2)$$

$$D = \text{bending stiffness parameter} = Eh^3/12(1-\nu^2)$$

Here, h is the thickness of the shell, ε_η , ε_ξ , and $\gamma_{\xi\eta}$ are the mid-surface extensional and shearing strain components, and χ_ξ , χ_η , and $\chi_{\eta\xi}$ are the mid-surface changes in curvature and twist. In the case of axisymmetric deformations, $\gamma_{\xi\eta}$ and $\chi_{\xi\eta}$ are zero.

The total potential energy V of the loaded shell is

$$V = U + W \quad (3.44)$$

where W is the potential of the applied loads. In the case of radial loads p_r ,

$$W = -2\pi \int p_r w \sin \xi d\xi \quad (3.45)$$

Neglecting rotary inertia, we can write the kinetic energy T as

$$T = \frac{1}{2} \int_V \rho \left[(\partial r / \partial t)^2 + r^2 (\partial \phi / \partial t)^2 \right] dV \quad (3.46)$$

Using equations (3.36), we reduce equation (3.46) to

$$T = \frac{\pi a^2 E h}{2(1-\nu^2)} \int_0^{2\pi} [\varepsilon^2(\dot{w}^2 + \dot{u}^2) + \varepsilon^3(2w\dot{u}^2)] \sin \xi d\xi \quad (3.47)$$

Substituting equations (3.41)-(3.47) into the Lagrangian and using the extended Hamiltons principle, we obtain the following equations of motion (McIvor and Sonstegard, 1966):

$$\begin{aligned} \ddot{u} + L_1(w, u) + \varepsilon \left\{ 2w\ddot{u} + 2\dot{w}\dot{u} - 2w'u' - 2wu'' - w'w'' - 2wu' \cot \xi - \frac{(1-\nu)}{2} w'^2 \cot \xi \right. \\ \left. - \frac{(3-\nu)}{2} u^2 \cot \xi - wu(1-\nu - 2 \cot^2 \xi) - 2(1+\nu)ww' - 2\nu w'u \cot \xi \right\} = 0 \end{aligned} \quad (3.48)$$

$$\begin{aligned} \ddot{w} + L_2(w, u) + \varepsilon \left\{ (1+\nu)[2wu' - \frac{1}{2} w'^2 - \frac{1}{2} u^2 + 2wu \cot \xi - ww'' - ww' \cot \xi \right. \\ \left. - w'u' \cot \xi] + u'^2 - w''u' + u^2 \cot^2 \xi - u''w' + 2\nu uu' \cot \xi \right. \\ \left. - \nu w''u \cot \xi + \nu w'u - \dot{u}^2 \right\} = \varepsilon^2 F_r(\xi, \tau) \end{aligned} \quad (3.49)$$

where $\alpha^2 = h^2/12a^2$, $F_r(\xi, \tau)$ is the generalized radial force and L_1 and L_2 are spatial linear differential operators defined as

$$\begin{aligned} L_1(w, u) \equiv -u'' - u' \cot \xi + u(\nu + \cot^2 \xi) - (1+\nu)w' \\ + \alpha^2 \{ (\nu + \cot^2 \xi)(u - w') - u'' - u' \cot \xi + w''' + w'' \cot \xi \} \end{aligned} \quad (3.50)$$

and

$$\begin{aligned}
L_2(w, u) \equiv & (1 + \nu)(u' + u \cot \xi + 2w) \\
& + \alpha^2 \{ -u''' - 2u'' \cot \xi + u'(1 + \nu + \cot^2 \xi) + (\nu - 2 - \cot^2 \xi)u \cot \xi \\
& + w^{iv} + 2w''' \cot \xi - (1 + \nu + \cot^2 \xi)w'' + 2w' \cot \xi + (\cot^2 \xi - \nu)w' \cot \xi \}
\end{aligned}
\tag{3.51}$$

We note that the excitation is ordered as ε^2 since the case to be studied is primary resonance.

CHAPTER 4

CASES INVOLVING TWO-TO-ONE INTERNAL RESONANCE

In this chapter we use the method of multiple-time scales (Nayfeh, 1973, 1981) to study the forced dynamic response of shells in the presence of a two-to-one internal (autoparametric) resonance between the excited mode and another mode. We present three case studies: 1) the breathing mode of an infinitely long circular cylindrical shell is excited by a primary resonance while being involved in a two-to-one internal resonance with a flexural mode, 2) a flexural mode of a spherical shell is excited by a primary resonance and it is involved in a two-to-one internal resonance with a lower flexural mode, and 3) the breathing mode of a cylindrical shell is excited by a subharmonic resonance of order one-half while being involved in a two-to-one internal resonance with a flexural mode.

The method of multiple-time scales results in a set of nonlinear autonomous ordinary-differential equations for the evolution of the amplitudes and phases of the

interacting modes. The resulting modulation equations in the first two case studies have the same general form. We present a numerical example where we study the fixed points and their stability and show that this system exhibits a saturation phenomenon for a level of excitation above a certain threshold. We also show that the response of such systems exhibit supercritical and subcritical Hopf bifurcations as the frequency of the excitation varies. Between the Hopf bifurcation frequencies either closed orbits (limit cycles) or chaotic solutions exists. Stability and bifurcation analysis of the closed orbits show that they go through either symmetry-breaking bifurcations followed by cascades of period-doubling bifurcations culminating in chaos or cyclic-fold bifurcations resulting in chaos.

For the case of subharmonic resonance, we show that the fixed points of the modulation equations exhibit the saturation phenomenon. We also show that as the frequency of excitation varies, the fixed points undergo Hopf bifurcations resulting in orbital (limit-cycle) behavior. Some closed orbits suffer cyclic-fold bifurcations which result in chaos. Period-three motions are also observed.

4.1 Primary Resonance

4.1.1 Primary resonance of the breathing mode of an infinitely long circular cylindrical shell

To capture the modal interaction phenomenon resulting from the two-to-one internal resonance between two modes of the shell, we need to solve up to the

quadratic part of the problem. Retaining the quadratic terms in the equations of motion derived in chapter three, we obtain

$$\ddot{w} + w - \psi' + \alpha^2\{w^{iv} + 2w'' + w\} = -\dot{\psi}^2 - \frac{1}{2}w'^2 - 2w\psi' + \psi'^2 + \psi'w'' - ww'' + w'\psi'' + \frac{a(1-v^2)}{Eh}P(1 + \psi' - w) \quad (4.1)$$

$$\ddot{\psi} - \psi'' + w' = 2w\ddot{\psi} + 2\dot{w}\dot{\psi} + w'w'' - 2w'\psi' - 2w\psi'' + 2ww' \quad (4.2)$$

where the prime indicates the derivative with respect to θ and the overdot indicates the derivative with respect to time τ . These equations can be rewritten in a slightly different form. We note that

$$\ddot{w} = \psi' - w - \alpha^2(w^{iv} + 2w'' + w) + \frac{a(1-v^2)P}{Eh} + \dots \quad (4.3)$$

$$\ddot{\psi} = \psi'' - w' + \dots \quad (4.4)$$

Substituting the above relations into equations (4.1) and (4.2) we obtain

$$\ddot{w} + \alpha^2(w^{iv} + 2w'' + w) - \psi' + w = w''(\psi' - w) - \dot{\psi}^2 + \psi'^2 - 2w\psi' + w'\psi'' - \frac{1}{2}w'^2 + \frac{a(1-v^2)}{Eh}P(1 + \psi' - w) \quad (4.5)$$

$$\ddot{\psi} - \psi'' + w' = w'w'' - 2w'\psi' + 2\dot{w}\dot{\psi} + \frac{a(1-v^2)}{Eh}w'P \quad (4.6)$$

Next, we use the method of multiple-time scales (Nayfeh 1973,1981) to determine a first-order uniformly valid asymptotic expansion of equations (4.5) and (4.6) for small but finite amplitudes when P is given by

$$\frac{a(1-v^2)}{Eh} P = \varepsilon \left[f_0 + \sum_{n=0}^{\infty} f_n \cos n\theta \right] \cos \Omega\tau \quad (4.7)$$

where ε is a small dimensionless perturbation parameter. Moreover, we seek a first-order uniform expansion of the displacement field in the form

$$w(\theta, \tau; \varepsilon) = \varepsilon w_1(\theta, T_0, T_1) + \varepsilon^2 w_2(\theta, T_0, T_1) + \dots \quad (4.8)$$

$$\psi(\theta, \tau; \varepsilon) = \varepsilon \psi_1(\theta, T_0, T_1) + \varepsilon^2 \psi_2(\theta, T_0, T_1) + \dots \quad (4.9)$$

where $T_0 = \tau$ is a fast time scale, characterizing motions with the natural and excitation frequencies, and $T_1 = \varepsilon\tau$ is a slow time scale, characterizing the modulation of the amplitudes and phases of the coupled modes due to the nonlinearities and any other resonances. The time derivatives transform as

$$\frac{\partial}{\partial \tau} = D_0 + \varepsilon D_1 + \dots \quad (4.10)$$

$$\frac{\partial^2}{\partial \tau^2} = D_0^2 + 2\varepsilon D_0 D_1 + \dots \quad (4.11)$$

where $D_n = \partial/\partial T_n$. Substituting equations (4.7)-(4.11) into equations (4.5) and (4.6) and equating coefficients of like powers of ε , we get

Order ε

$$D_0^2 w_1 + \alpha^2 \{ w_1^{iv} + 2w_1'' + w_1 \} - \psi_1' + w_1 = 0 \quad (4.12)$$

$$D_0^2 \psi_1 - \psi_1'' + w_1' = 0 \quad (4.13)$$

Order ε^2

$$D_0^2 w_2 + \alpha^2 \{w_2^{iv} + 2w_2'' + w_2\} - \psi_2' + w_2 = -2D_0 D_1 w_1 + w_1''(\psi_1' - w_1) - (D_0 \psi_1)^2 + \psi_1'^2 \\ - 2w_1 \psi_1' + w_1' \psi_1'' - \frac{1}{2} w_1'^2 + \left[f_0 + \sum_{m=1}^{\infty} f_m \cos m\theta \right] \cos \Omega T_0 \quad (4.14)$$

$$D_0^2 \psi_2 - \psi_2'' + w_2' = -2D_0 D_1 \psi_1 + w_1' w_1'' - 2w_1' \psi_1' + 2(D_0 w_1)(D_0 \psi_1) \quad (4.15)$$

Since the shell is closed, the displacement field must be periodic in θ . Thus, the solution to equations (4.12) and (4.13) is given by

$$w_1 = A_0(T_1) e^{i\omega_0 T_0} + \sum_{m=1}^{\infty} A_m(T_1) e^{i\omega_m T_0} \cos m\theta + \sum_{m=1}^{\infty} B_m(T_1) e^{i\omega_m T_0} \sin m\theta + \text{c.c.} \quad (4.16)$$

$$\psi_1 = - \sum_{m=1}^{\infty} \Gamma_m B_m(T_1) e^{i\omega_m T_0} \cos m\theta + \sum_{m=1}^{\infty} \Gamma_m A_m(T_1) e^{i\omega_m T_0} \sin m\theta + \text{c.c.} \quad (4.17)$$

where c.c. stands for the complex conjugate of the preceding terms, ω_m is the natural frequency of the m^{th} mode and is given by the characteristic equation

$$\omega_m^4 - [m^2 + 1 + \alpha^2(m^2 - 1)^2] \omega_m^2 + \alpha^2 m^2 (m^2 - 1)^2 = 0, \quad m = 0, 1, 2, \dots \quad (4.18)$$

and

$$\Gamma_m = \frac{1}{m} [1 + \alpha^2(m^2 - 1)^2 - \omega_m^2] \quad (4.19)$$

Out of the infinite number of modes present in w_1 and ψ_1 and in the presence of viscous damping, only the externally excited modes and those involved in internal resonance with them are present in the steady-state response (Nayfeh and Mook 1979). In this study, we consider the case in which the frequency of the external excitation is near the natural frequency of the the breathing mode (i.e., $\Omega \approx \omega_0$). Furthermore, we assume that the modal coupling is due to a two-to-one internal resonance between the breathing mode and the n^{th} flexural mode (i.e., $\omega_0 \approx 2\omega_n$). Thus, we express w_1 and ψ_1 as

$$w_1 = A_0(T_1) e^{i\omega_0 T_0} + A_n(T_1) e^{i\omega_n T_0} \cos n\theta + B_n(T_1) e^{i\omega_n T_0} \sin n\theta + \text{c.c.} \quad (4.20)$$

$$\psi_1 = -\Gamma_n B_n(T_1) e^{i\omega_n T_0} \cos n\theta + \Gamma_n A_n(T_1) e^{i\omega_n T_0} \sin n\theta + \text{c.c.} \quad (4.21)$$

We note that A_0 , A_n , and B_n are unknown functions of T_1 at this level of approximation and are determined by imposing the solvability condition at the next level of approximation. To qualitatively express these near resonance conditions, we introduce detuning parameters σ_1 and σ_2 defined by

$$\Omega = \omega_0 + \varepsilon\sigma_1 \quad \text{and} \quad \omega_0 = 2\omega_n + \varepsilon\sigma_2 \quad (4.22)$$

Substituting equations (4.20) and (4.21) into equations (4.14) and (4.15), we obtain

$$\begin{aligned} D_0^2 w_2 + \alpha^2 \{w_2^{iv} + 2w_2'' + w_2\} - \psi_2' + w_2 = & -2i\omega_0 A_0' e^{i\omega_0 T_0} - 2i\omega_n (A_n' \cos n\theta + B_n' \sin n\theta) e^{i\omega_n T_0} \\ & + \left[\frac{1}{4} n^2 + \frac{1}{2} (\omega_n^2 + n^2) \Gamma_n^2 - n\Gamma_n \right] (A_n^2 + B_n^2) e^{i\omega_0 T_0 - i\sigma_2 T_1} \\ & + (n^2 - 2n\Gamma_n) A_0 (\bar{A}_n \cos n\theta + \bar{B}_n \sin n\theta) e^{i\omega_n T_0 + i\sigma_2 T_1} \\ & + \frac{1}{2} (f_0 + f_n \cos n\theta) e^{i\omega_0 T_0 + i\sigma_1 T_1} + \text{c.c.} + \text{NST} \end{aligned}$$

(4.23)

$$D_0^2 \psi_2 - \psi_2'' + w_2' = 2i\omega_n \Gamma_n (B'_n \cos n\theta - A'_n \sin n\theta) e^{i\omega_n T_0} \\ - 2\omega_n \omega_0 \Gamma_n A_0 (\bar{B}_n \cos n\theta - \bar{A}_n \sin n\theta) e^{i\omega_n T_0 + i\sigma_2 T_1} + \text{c.c.} + \text{NST}$$

(4.24)

where *NST* stands for terms that do not produce secular terms.

Equations (4.23) and (4.24) are inhomogeneous differential equations whose homogeneous part has a nontrivial solution. Thus, they have a solution only if their right-hand sides are orthogonal to every solution of the adjoint homogeneous problem. We note that the homogeneous part of equations (4.23) and (4.24) is self-adjoint, thus the solvability condition yields the following modulation equations:

$$2i(A'_0 + \mu_0 A_0) - 4\Lambda_1(A_n^2 + B_n^2)e^{-i\sigma_2 T_1} - fe^{i\sigma_1 T_1} = 0 \quad (4.25)$$

$$2i(A'_n + \mu_n A_n) - 4\Lambda_2 A_0 \bar{A}_n e^{i\sigma_2 T_1} = 0 \quad (4.26)$$

$$2i(B'_n + \mu_n B_n) - 4\Lambda_2 A_0 \bar{B}_n e^{i\sigma_2 T_1} = 0 \quad (4.27)$$

where the prime indicates the derivatives with respect to T_1 , μ_0 is the damping coefficient of the breathing mode, μ_n is the damping coefficient of the n^{th} flexural mode,

$$4\omega_0 \Lambda_1 = \frac{1}{4} n^2 + \frac{1}{2} (\omega_n^2 + n^2) \Gamma_n^2 - n \Gamma_n \quad (4.28)$$

$$4\omega_n (1 + \Gamma_n^2) \Lambda_2 = n^2 - 2n \Gamma_n + 2\omega_0 \omega_n \Gamma_n^2 \quad (4.29)$$

and

$$f_0 = 2\omega_0 f \quad (4.30)$$

To analyze the steady-state solutions of equations (4.25)-(4.27) and determine their stability, we let

$$A_0 = \frac{1}{2} \{ p_1(T_1) - iq_1(T_1) \} e^{iv_1 T_1} \quad (4.31)$$

$$A_n = \frac{1}{2} \{ p_2(T_1) - iq_2(T_1) \} e^{iv_2 T_1} \quad (4.32)$$

$$B_n = \frac{1}{2} \{ p_3(T_1) - iq_3(T_1) \} e^{iv_1 T_1} \quad (4.33)$$

separate real and imaginary parts, and obtain

$$p'_1 = -v_1 q_1 - \mu_0 p_1 - 2\Lambda_1 (p_2 q_2 + p_3 q_3) \quad (4.34)$$

$$q'_1 = v_1 p_1 - \mu_0 q_1 + \Lambda_1 (p_2^2 + p_3^2 - q_2^2 - q_3^2) + f \quad (4.35)$$

$$p'_2 = -v_2 q_2 - \mu_n p_2 - \Lambda_2 (q_1 p_2 - q_2 p_1) \quad (4.36)$$

$$q'_2 = v_2 p_2 - \mu_n q_2 + \Lambda_2 (p_1 p_2 + q_1 q_2) \quad (4.37)$$

$$p'_3 = -v_2 q_3 - \mu_n p_3 - \Lambda_2 (q_1 p_3 - q_3 p_1) \quad (4.38)$$

$$q'_3 = v_2 p_3 - \mu_n q_3 + \Lambda_2 (p_1 p_3 + q_1 q_3) \quad (4.39)$$

where $v_1 = \sigma_1$ and $v_2 = \frac{1}{2}(\sigma_1 + \sigma_2)$.

Next, we consider the case where $p_3 = q_3 = 0$. The resulting set of modulation equations is

$$p'_1 = -v_1 q_1 - \mu_0 p_1 - 2\Lambda_1 p_2 q_2 \quad (4.40)$$

$$q'_1 = v_1 p_1 - \mu_0 q_1 + \Lambda_1 (p_2^2 - q_2^2) + f \quad (4.41)$$

$$p'_2 = -v_2 q_2 - \mu_n p_2 - \Lambda_2 (q_1 p_2 - q_2 p_1) \quad (4.42)$$

$$q'_2 = v_2 p_2 - \mu_n q_2 + \Lambda_2 (p_1 p_2 + q_1 q_2) \quad (4.43)$$

We stop at this point to present the modulation equations for the modal interaction problem in spherical shells and show that they assume the same form as equations (4.40) - (4.43).

4.1.2 Primary resonance of a flexural mode of a closed spherical shell

We present a perturbation solution for the dynamic response of spherical shells subject to a primary-resonant excitation of a flexural mode whose natural frequency is approximately twice that of a lower flexural mode (i.e., a two-to-one internal or autoparametric resonance).

The equations for the axisymmetric oscillations of a closed spherical shell were derived in chapter three and are listed here for convenience:

$$\ddot{u} + L_1(w, u) + \varepsilon \left\{ 2w\ddot{u} + 2\dot{w}\dot{u} - 2w'u' - 2wu'' - w'w'' - 2wu' \cot \xi - \frac{(1-v)}{2} w'^2 \cot \xi - \frac{(3-v)}{2} u^2 \cot \xi - wu(1-v-2\cot^2 \xi) - 2(1+v)ww' - 2vw'u \cot \xi \right\} = 0$$

(4.44)

$$\begin{aligned}
\ddot{w} + L_2(w, u) + \varepsilon\{(1 + \nu) [2wu' - \frac{1}{2} w'^2 - \frac{1}{2} u^2 + 2wu \cot \xi - ww'' - ww' \cot \xi \\
- w'u' \cot \xi] + u'^2 - w''u' + u^2 \cot^2 \xi - u''w' + 2\nu uu' \cot \xi - \nu w''u \cot \xi \\
+ \nu w'u - \dot{u}^2\} = \varepsilon F_r(\xi, \tau)
\end{aligned}
\tag{4.45}$$

where the prime indicates the derivative with respect to ξ , the overdot indicates the derivatives with respect to time τ ,

$$\begin{aligned}
L_1(w, u) \equiv -u'' - u' \cot \xi + u(\nu + \cot^2 \xi) - (1 + \nu)w' + \alpha^2\{(\nu + \cot^2 \xi)(u - w') - u'' \\
- u' \cot \xi + w''' + w'' \cot \xi\}
\end{aligned}
\tag{4.46}$$

and

$$\begin{aligned}
L_2(w, u) \equiv (1 + \nu)(u' + u \cot \xi + 2w) + \alpha^2\{-u''' - 2u'' \cot \xi + u'(1 + \nu + \cot^2 \xi) \\
+ (\nu - 2 - \cot^2 \xi)u \cot \xi + w^{iv} + 2w''' \cot \xi - (1 + \nu + \cot^2 \xi)w'' + 2w' \cot \xi \\
+ (\cot^2 \xi - \nu)w' \cot \xi\}
\end{aligned}
\tag{4.47}$$

Again, we use the method of multiple-time scales and the same procedure outlined in section 4.1.1 to determine a first-order uniformly valid expansion of the solution of equations (4.44) and (4.45) for small but finite amplitudes. We expand the radial excitation $F_r(\xi, \tau)$ in terms of Legendre polynomials as

$$F_r = \sum_{n=0}^{\infty} f_n P_n(\cos \xi) \cos(\Omega\tau)
\tag{4.48}$$

where $P_n(\cos \xi)$ is the Legendre polynomial of the first kind and order n . We consider the case of primary resonance of the m^{th} flexural mode; that is, $\Omega \approx \omega_m$. Moreover, we seek an asymptotic expansion of the displacement field in the form

$$w(\xi, \tau; \varepsilon) = w_1(\xi, T_0, T_1) + \varepsilon w_2(\xi, T_0, T_1) + \dots \quad (4.49)$$

$$u(\xi, \tau; \varepsilon) = u_1(\xi, T_0, T_1) + \varepsilon u_2(\xi, T_0, T_1) + \dots \quad (4.50)$$

Substituting equations (4.48)-(4.50) into equations (4.44) and (4.45) and equating coefficients of like powers of ε , we obtain

Order ε

$$D_0^2 u_1 + L_1(w_1, u_1) = 0 \quad (4.51)$$

$$D_0^2 w_1 + L_2(w_1, u_1) = 0 \quad (4.52)$$

Order ε^2

$$\begin{aligned} D_0^2 u_2 + L_1(w_2, u_2) = & -2D_0 D_1 u_1 + 2w_1' u_1' + 2w_1 u_1'' + w_1' w_1'' + 2w_1 u_1' \cot \xi \\ & + (1 - \nu) \left(\frac{1}{2} w_1'^2 \cot \xi + w_1 u_1 \right) + \frac{1}{2} (3 - \nu) u_1^2 \cot \xi - 2u_1 w_1 \cot^2 \xi \\ & + 2\nu u_1 w_1' \cot \xi + 2(1 + \nu) w_1 w_1' - 2D_0 w_1 D_0 u_1 - 2w_1 D_0^2 u_1 \end{aligned} \quad (4.53)$$

$$\begin{aligned} D_0^2 w_2 + L_2(w_2, u_2) = & -2D_0 D_1 w_1 + (D_0 u_1)^2 - (1 + \nu) \left[2w_1 u_1' - \frac{1}{2} u_1^2 + 2w_1 u_1 \cot \xi \right. \\ & \left. - \frac{1}{2} w_1'^2 - w_1 w_1' \cot \xi - w_1' u_1' \cot \xi - w_1 w_1'' \right] - u_1^2 \cot^2 \xi \\ & + u_1'' w_1' - 2\nu u_1 u_1' \cot \xi + \nu w_1'' u_1 \cot \xi - u_1'^2 + w_1'' u_1' - \nu w_1' u_1 \\ & + \sum_{n=0}^{\infty} f_n P_n \cos(\Omega T_0) \end{aligned}$$

(4.54)

To simplify the algebra, we define the variable ψ_1 such that

$$u_1 = \frac{d\psi_1}{d\xi} \quad (4.55)$$

and the differential operator H as

$$H(\dots) = \frac{d^2(\dots)}{d\xi^2} + \cot \xi \frac{d(\dots)}{d\xi} + 2(\dots) \quad (4.56)$$

Then equation (4.51) becomes

$$\frac{d}{d\xi} [D_0^2 \psi_1 - H(\psi_1) + (1 + \alpha^2)(1 + \nu)(\psi_1 - w_1) - \alpha^2 H(\psi_1 - w_1)] = 0 \quad (4.57)$$

which is integrated into

$$D_0^2 \psi_1 - H(\psi_1) + (1 + \alpha^2)(1 + \nu)(\psi_1 - w_1) - \alpha^2 H(\psi_1 - w_1) = 0 \quad (4.58)$$

The constant of integration is chosen as zero since an additive constant in ψ_1 does not change u_1 . Using equation (4.56), we rewrite equation (4.52) as

$$D_0^2 w_1 + (1 + \nu)H(\psi_1) - 2(1 + \nu)(1 + \alpha^2)(\psi_1 - w_1) - \alpha^2 H H(\psi_1 - w_1) + (\nu + 3)\alpha^2 H(\psi_1 - w_1) = 0 \quad (4.59)$$

The solution of equations (4.58) and (4.59) can be expressed as

$$w_1(\xi, T_0, T_1) = \sum_{n=0}^{\infty} A_n(T_1) P_n(\cos \xi) \exp(i\omega_n T_0) + \text{c.c.} \quad (4.60)$$

$$\psi_1(\xi, T_0, T_1) = \sum_{n=0}^{\infty} B_n(T_1) P_n(\cos \xi) \exp(i\omega_n T_0) + \text{c.c.} \quad (4.61)$$

where c.c. is the complex conjugate of the preceding terms. It follows from equations (55) and (61) that

$$u_1(\xi, T_0, T_1) = \sum_{n=0}^{\infty} B_n(T_1) P'_n(\cos \xi) \exp(i\omega_n T_0) + \text{c.c.} \quad (4.62)$$

The associated Legendre polynomials are not included in w_1 , u_1 , and ψ_1 because they exhibit a singularity at the poles of the shell. Next we substitute equations (4.60) and (4.61) into equations (4.58) and (4.59), use the Legendre differential equation: $\frac{d^2 P_n}{d\xi^2} + \cot \xi \frac{dP_n}{d\xi} + n(n+1)P_n = 0$, and obtain

$$\begin{bmatrix} \beta_n & \gamma_n \\ \rho_n & \delta_n \end{bmatrix} \begin{bmatrix} B_n \\ A_n \end{bmatrix} = \begin{bmatrix} 0 \\ 0 \end{bmatrix} \quad (4.63)$$

where

$$\beta_n = (1 + \alpha^2)(1 + \nu + \lambda_n) - \omega_n^2 \quad (4.64.a)$$

$$\gamma_n = -\alpha^2 \lambda_n - (1 + \alpha^2)(1 + \nu)$$

$$\rho_n = -(1 + \nu)(2 + \lambda_n) - \alpha^2 \{ \lambda_n^2 + (\nu + 3)\lambda_n + 2(1 + \nu) \}$$

$$\delta_n = 2(1 + \alpha^2)(1 + \nu) + \alpha^2 \lambda_n (\lambda_n + \nu + 3) - \omega_n^2$$

$$\text{and} \quad \lambda_n = n(n+1) - 2 \quad (4.64.e)$$

We note that $H(P_n) = -\lambda_n P_n$. Equations (4.63) constitute a system of homogeneous algebraic equations, such a system has a non-trivial solution if and only if the determinant of the coefficient matrix vanishes identically. This produces the characteristic equation

$$\omega_n^4 - \omega_n^2[\alpha^2 \lambda_n \{\lambda_n + \nu + 4\} + \lambda_n + 3(1 + \nu)(1 + \alpha^2)] + \lambda_n[\alpha^2 \{\lambda_n^2 + 2\lambda_n - \nu^2 + 1\} + 1 - \nu^2] = 0 \quad (4.65)$$

Moreover, equation (4.63) yields

$$B_n = -\frac{\gamma_n}{\beta_n} A_n \quad (4.66)$$

Again, we note that out of the infinite number of modes present in w_1 , ψ_1 , and u_1 and in the presence of viscous damping, only the directly excited mode and the modes that are involved in a modal coupling with it will be present in the steady-state response. Thus, to proceed further, we need to define the resonance conditions. In this section, we consider the case of a primary-resonant excitation of the m^{th} flexural mode and introduce the detuning parameter σ_1 defined by

$$\Omega = \omega_m + \varepsilon \sigma_1 \quad (4.67)$$

Moreover, we consider the case of two-to-one internal resonance between the m^{th} and k^{th} flexural modes and introduce the detuning parameter σ_2 defined by

$$\omega_m = 2\omega_k + \varepsilon \sigma_2, \quad m > k \quad (4.68)$$

Thus we can express w_1 and u_1 as

$$w_1(\xi, T_0, T_1) = A_m(T_1)P_m(\cos \xi) \exp(i\omega_m T_0) + A_k(T_1)P_k(\cos \xi) \exp(i\omega_k T_0) + \text{c.c.} \quad (4.69)$$

$$u_1(\xi, T_0, T_1) = -\frac{\gamma_m}{\beta_m} A_m(T_1)P'_m(\cos \xi) \exp(i\omega_m T_0) - \frac{\gamma_k}{\beta_k} A_k(T_1)P'_k(\cos \xi) \exp(i\omega_k T_0) + \text{c.c.} \quad (4.70)$$

Next we substitute equations (4.69) and (4.70) into equations (4.53) and (4.54), seek a particular solution in the form

$$w_2(\xi, T_0, T_1) = Q_1(\xi)e^{i\omega_m T_0} + Q_2(\xi)e^{i\omega_k T_0} + \text{c.c.} \quad (4.71)$$

$$u_2(\xi, T_0, T_1) = R_1(\xi)e^{i\omega_m T_0} + R_2(\xi)e^{i\omega_k T_0} + \text{c.c.} \quad (4.72)$$

separate the the T_0 variations, and obtain

$$-\omega_m^2 R_1 + L_1(Q_1, R_1) = 2i\omega_m \frac{\gamma_m}{\beta_m} \frac{dA_m}{dT_1} P_m' + \Gamma_k A_k^2 e^{-i\sigma_2 T_1} \quad (4.73)$$

$$-\omega_m^2 Q_1 + L_2(Q_1, R_1) = -2i\omega_m \frac{dA_m}{dT_1} P_m + \frac{1}{2} \sum_0^\infty f_n P_n e^{i\sigma_1 T_1} + \Delta_k A_k^2 e^{-i\sigma_2 T_1} \quad (4.74)$$

$$-\omega_k^2 R_2 + L_1(Q_2, R_2) = 2i\omega_k \frac{\gamma_k}{\beta_k} \frac{dA_k}{dT_1} P_k' + \Theta_{mk} A_m \bar{A}_k e^{i\sigma_2 T_1} \quad (4.75)$$

$$-\omega_k^2 Q_2 + L_2(Q_2, R_2) = -2i\omega_k \frac{dA_k}{dT_1} P_k + H_{mk} A_m \bar{A}_k e^{i\sigma_2 T_1} \quad (4.76)$$

where

$$\Gamma_k = \left\{ (v - 4\omega_k^2 + 4k^2 + 4k - 3) \frac{\gamma_k}{\beta_k} + 2v - k^2 - k + 2 \right\} P_k P_k' \\ + \left\{ \frac{3-v}{2} \left(\frac{\gamma_k}{\beta_k} \right)^2 - \frac{1+v}{2} + 2 \frac{\gamma_k}{\beta_k} (1-v) \right\} \cot \xi P_k'^2$$

(4.77)

$$\Theta_{mk} = \left\{ \frac{\gamma_k}{\beta_k} \frac{\gamma_m}{\beta_m} (3-v) - v - 1 + 2(1-v) \left(\frac{\gamma_m}{\beta_m} + \frac{\gamma_k}{\beta_k} \right) \right\} \cot \xi P_k' P_m' \\ + \left\{ \frac{\gamma_k}{\beta_k} (v - 2\omega_k^2 + 2\omega_m \omega_k - 3 + 2k(k+1)) - m^2 - m + 2 \frac{\gamma_m}{\beta_m} m(m+1) + 2(1+v) \right\} P_k' P_m \\ + \left\{ \frac{\gamma_m}{\beta_m} (2m^2 + 2m - 2\omega_m^2 + 2\omega_m \omega_k + v - 3) + (2 \frac{\gamma_k}{\beta_k} - 1)(k^2 + k) + 2(1+v) \right\} P_m' P_k$$

(4.78)

$$\Delta_k = \left\{ -\frac{\gamma_k^2}{\beta_k^2} k(k+1) - \frac{\gamma_k}{\beta_k} [k(k+1) + 2(1+v)] - (1+v) \right\} k(k+1) P_k^2 \\ + 2 \left(\frac{\gamma_k}{\beta_k} + \left(\frac{\gamma_k}{\beta_k} \right)^2 \right) k(k+1)(v-1) \cot \xi P_k' P_k \\ + \left\{ \left(\frac{\gamma_k}{\beta_k} \right)^2 \left[2v \cot^2 \xi + \frac{1}{2} (1+v) - \omega_k^2 - 2 \cot^2 \xi \right] + \frac{\gamma_k}{\beta_k} (k^2 + k + 2v \cot^2 \xi + v \right. \\ \left. - 2 \cot^2 \xi - 1) + \frac{1}{2} (1+v) \right\} P_k'^2$$

(4.79)

$$\begin{aligned}
H_{mk} = & \left\{ -2 \frac{\gamma_m}{\beta_m} \frac{\gamma_k}{\beta_k} (m^2 + m)(k^2 + k) - \frac{\gamma_m}{\beta_m} (k^2 + k + 2 + 2v)(m^2 + m) \right. \\
& \left. - \frac{\gamma_k}{\beta_k} (k^2 + k)(m^2 + m + 2 + 2v) - (1 + v)(m^2 + k^2 + k + m) \right\} P_m P_k \\
& + \left\{ \frac{\gamma_m}{\beta_m} + 2 \frac{\gamma_m}{\beta_m} \frac{\gamma_k}{\beta_k} + \frac{\gamma_k}{\beta_k} \right\} (m^2 + m)(v - 1) \cot \xi P_m P_k' \\
& + \left\{ \frac{\gamma_m}{\beta_m} + 2 \frac{\gamma_m}{\beta_m} \frac{\gamma_k}{\beta_k} + \frac{\gamma_k}{\beta_k} \right\} (k^2 + k)(v - 1) \cot \xi P_m' P_k \\
& + \left\{ \frac{\gamma_m}{\beta_m} (m^2 + m + 2v \cot^2 \xi + v - 2 \cot^2 \xi - 1) + \frac{\gamma_m}{\beta_m} \frac{\gamma_k}{\beta_k} [2\omega_m \omega_k + 4(v - 1) \cot^2 \xi \right. \\
& \left. + v + 1] + \frac{\gamma_k}{\beta_k} (k^2 + k + 2v \cot^2 \xi + v - 2 \cot^2 \xi - 1) + v + 1 \right\} P_m' P_k'
\end{aligned} \tag{4.80}$$

Since the homogeneous parts of equations (4.73)-(4.76) have a non-trivial solution, the inhomogeneous equations have a solution only if a solvability condition is satisfied.

We attack the general form of the problem first and then specialize the results.

Equations (4.73) and (4.74) and equations (4.75) and (4.76) have the general form

$$-\omega^2 u + L_1(w, u) = F_1 \tag{4.81}$$

$$-\omega^2 w + L_2(w, u) = F_2 \tag{4.82}$$

We let $u = d\psi/d\xi$, use the operator H defined in equation (4.56), integrate equation (4.81), multiply both equations by $\sin \xi$, and obtain

$$\sin \xi \left[-\omega^2 \psi - H(\psi) + (1 + v)(1 + \alpha^2)(\psi - w) - \alpha^2 H(\psi - w) = \int_{\xi}^{\xi} F_1 d\xi \right] \tag{4.83}$$

We rewrite equation (4.82) using the operator H , multiply the result by $\sin \xi$, and obtain

$$\sin \xi \left[-\omega^2 w + (1 + \nu)H(\psi) - 2(1 + \nu)(1 + \alpha^2)(\psi - w) - \alpha^2 HH(\psi - w) + (\nu + 3)\alpha^2 H(\psi - w) = F_2 \right] \quad (4.84)$$

We note that the operators $\sin \xi H(\dots)$ and $\sin \xi H H(\dots)$ are self-adjoint operators; that is

$$\int x H(y) \sin \xi d\xi = \int y H(x) \sin \xi d\xi \quad (4.85)$$

$$\int x HH(y) \sin \xi d\xi = \int y HH(x) \sin \xi d\xi \quad (4.86)$$

The problem is now reduced to finding the solvability condition for equations (4.83) and (4.84). Equations (4.83) and (4.84) have a solution if their right-hand sides are orthogonal to each and every solution of the homogeneous adjoint problem. To find the homogeneous adjoint problem, we multiply equations (4.83) and (4.84) by ψ^* and w^* respectively, and integrate the homogeneous form of the equations by parts to obtain the following adjoint problem:

$$\begin{aligned} -\omega^2 \psi^* - H(\psi^*) + (1 + \nu)\psi^* - 2(1 + \nu)w^* + (1 + \nu)H(w^*) + \alpha^2\{(1 + \nu)\psi^* \\ - H(\psi^*) - HH(w^*) + (\nu + 3)H(w^*) - 2(1 + \nu)w^*\} = 0 \end{aligned} \quad (4.87)$$

$$\begin{aligned} -\omega^2 w^* - (1 + \nu)\psi^* + 2(1 + \nu)w^* + \alpha^2\{H(\psi^*) - (1 + \nu)\psi^* + HH(w^*) - (\nu + 3)H(w^*) \\ + 2(1 + \nu)w^*\} = 0 \end{aligned} \quad (4.88)$$

The solutions of equations (4.87) and (4.88) are

$$w^*(\xi) = P_n(\cos \xi) \quad \text{and} \quad \psi^*(\xi) = -\frac{\rho_n}{\beta_n} P_n(\cos \xi) \quad (4.89)$$

for $n = 0, 1, 2, \dots$ where β_n and ρ_n are defined in equations (4.64).

Then the desired solvability conditions are

$$-\frac{\rho_n}{\beta_n} \int_0^{2\pi} \left[P_n(\cos \xi) \sin \xi \int_{\xi} F_1 d\xi \right] d\xi + \int_0^{2\pi} w^* F_2 \sin \xi d\xi = 0 \quad (4.90)$$

Applying condition (4.90) to equations (4.73) and (4.74) and taking $n=m$, we obtain the following modulation equations:

$$2i \left(\frac{dA_m}{dT_1} + \mu_1 A_m \right) - 4\Lambda_1 A_k^2 e^{-i\sigma_2 T_1} + f e^{i\sigma_1 T_1} = 0 \quad (4.91)$$

Similarly, applying condition (4.90) to equations (4.75) and (4.76) and taking $n=k$, we obtain

$$2i \left(\frac{dA_k}{dT_1} + \mu_2 A_k \right) - 4\Lambda_2 A_m \bar{A}_k e^{i\sigma_2 T_1} = 0 \quad (4.92)$$

where

$$\frac{16\omega_m \Lambda_1}{2m+1} \left(\frac{\delta_m}{\beta_m} + 1 \right) = \int_0^{2\pi} P_m \sin \xi \left[-\frac{\rho_m}{\beta_m} \int_{\xi} \Gamma_k d\xi + \Delta_k \right] d\xi \quad (4.94)$$

$$\frac{16\omega_k\Lambda_2}{2k+1} \left(\frac{\delta_k}{\beta_k} + 1 \right) = \int_0^{2\pi} P_k \sin \xi \left[-\frac{\rho_k}{\beta_k} \int_{\xi}^{\oplus} \Theta_{mk} d\xi + H_{mk} \right] d\xi \quad (4.95)$$

$$2\omega_m \left(\frac{\delta_m}{\beta_m} + 1 \right) f = f_m \quad (4.96)$$

and

$$\int_0^{2\pi} \sin \xi P_m P_n d\xi = \begin{cases} \frac{4}{2n+1} & , \text{ if } n = m \\ 0 & , \text{ if } n \neq m \end{cases} \quad (4.97)$$

Modal damping has been added to equations (4.91) and (4.92) with μ_1 and μ_2 being the damping coefficients of the m^{th} and k^{th} modes, respectively.

To analyze the solutions of equations (4.91) and (4.92), we express A_m and A_k in the form

$$A_m = \frac{1}{2} \{p_1(T_1) - iq_1(T_1)\} e^{i\sigma_1 T_1} \quad (4.98)$$

$$A_k = \frac{1}{2} \{p_2(T_1) - iq_2(T_1)\} e^{\frac{1}{2}(\sigma_1 + \sigma_2)T_1} \quad (4.99)$$

Substituting equations (4.98) and (4.99) into equations (4.91) and (4.92) and separating real and imaginary parts, we obtain equations (4.40)-(4.43) again, with $\mu_1 = \mu_0$ and $\mu_2 = \mu_n$.

Equations (4.40)-(4.43) can be reduced further by applying the following transformations of variables: $T_1 = \Lambda_2^{-1/2} \hat{t}$, $p_1 = \Lambda_2^{-1/2} \hat{p}_1$, $q_1 = \Lambda_2^{-1/2} \hat{q}_1$, $p_2 = \Lambda_1^{-1/2} \hat{p}_2$, $q_2 = \Lambda_1^{-1/2} \hat{q}_2$, $\mu_0 = \Lambda_2^{1/2} \hat{\mu}_1$, $\mu_n = \Lambda_2^{1/2} \hat{\mu}_2$, $\sigma_1 = \Lambda_2^{1/2} \hat{\sigma}_1$, $\sigma_2 = \Lambda_2^{1/2} \hat{\sigma}_2$. The resulting modulation equations are

$$\hat{p}'_1 = -\hat{v}_1 \hat{q}_1 - \hat{\mu}_1 \hat{p}_1 - 2\hat{p}_2 \hat{q}_2 \quad (4.100)$$

$$\hat{q}'_1 = \hat{v}_1 \hat{p}_1 - \hat{\mu}_1 \hat{q}_1 + \hat{p}_2^2 - \hat{q}_2^2 + f \quad (4.101)$$

$$\hat{p}'_2 = -\hat{v}_2 \hat{q}_2 - \hat{\mu}_2 \hat{p}_2 - \hat{q}_1 \hat{p}_2 + \hat{q}_2 \hat{p}_1 \quad (4.102)$$

$$\hat{q}'_2 = \hat{v}_2 \hat{p}_2 - \hat{\mu}_2 \hat{q}_2 + \hat{p}_1 \hat{p}_2 + \hat{q}_1 \hat{q}_2 \quad (4.103)$$

where the prime indicates the derivative with respect to \hat{t} , $v_1 = \sigma_1$, and $v_2 = \frac{1}{2}(\sigma_1 + \sigma_2)$.

4.1.3 Numerical results

Next, we give numerical results for the evolution equations (4.100) - (4.103) in the case of a spherical shell. For convenience, we drop the \wedge from all the variables names. We let $\alpha \approx 1.44338 \times 10^{-3}$ or $h/a \approx 1/200$. For this case $\omega_2 \approx 2.722$, $\omega_4 \approx 4.596$, $\Lambda_1 \approx 0.200$, and $\Lambda_2 \approx -0.667$, and hence $\omega_4 \approx 2\omega_2$. Moreover, we let $\mu_{1,2} = 0.01$ and $\sigma_2 = 1.08$.

Equations (4.100) - (4.103) admit two fixed-point solutions; namely,

$$a_1 = f (\mu_1^2 + \sigma_1^2)^{-1/2} \quad \text{and} \quad a_2 = 0 \quad (4.104)$$

and

$$a_1 = a_1^* = \left\{ \mu_2^2 + \frac{1}{4} (\sigma_1 + \sigma_2)^2 \right\}^{1/2} \quad (4.105)$$

$$a_2^2 = \frac{1}{2} \sigma_1(\sigma_1 + \sigma_2) - \mu_1\mu_2 \mp \left[r^2 - \left(\sigma_1\mu_1 + \frac{1}{2} \mu_2(\sigma_1 + \sigma_2)^2 \right)^2 \right]^{1/2} \quad (4.106)$$

where

$$a_1^2 = \text{square of the amplitude of the } 4^{\text{th}} \text{ mode} = p_1^2 + q_1^2$$

$$a_2^2 = \text{square of the amplitude of the } 2^{\text{nd}} \text{ mode} = p_2^2 + q_2^2 \quad (4.107)$$

The stability of the fixed-point solutions to a disturbance proportional to $\exp(\lambda T_1)$ is determined by the roots of the characteristic equation (see section 2.2.1)

$$\begin{vmatrix} \lambda + \mu_1 & v_1 & 2q_2 & 2p_2 \\ -v_1 & \lambda + \mu_1 & -2p_2 & 2q_2 \\ -q_2 & p_2 & \lambda + \mu_2 + q_1 & v_2 - p_1 \\ -p_2 & -q_2 & -v_2 - p_1 & \lambda + \mu_2 - q_1 \end{vmatrix} = 0 \quad (4.108)$$

The solution given by equation (4.104) is essentially the solution to the linear problem. To determine its stability, we let $p_2 = q_2 = 0$ in equation (4.108) and obtain

$$\lambda = -\mu_1 \mp iv_1, \quad -\mu_2 \mp (a_1^2 - v_2^2)^{1/2} \quad (4.109)$$

Consequently the linear solution is stable if and only if

$$a_1^2 \leq v_2^2 + \mu_2^2 \quad (4.110)$$

which, in conjunction with equations (4.104) and (4.105), implies that the linear solution is stable if and only if

$$a_1 \leq a_1^* \text{ or } f \leq a_1^* (\mu_1^2 + \sigma_1^2)^{1/2} \quad (4.111)$$

The solution (4.105) and (4.106) can only be predicted using the nonlinear analysis. In this case the amplitude a_1 of the directly excited mode is independent of the amplitude of the excitation f according to equation (4.105), whereas the amplitude a_2 of the coupled 2nd mode is a function of f according to equation (4.106). In this case the necessary and sufficient conditions for none of the roots of the characteristic equation to have a positive real part are

$$a_2^2 + \mu_1\mu_2 - v_1v_2 > 0 \quad (4.112)$$

$$4\mu_2\mu_1(\mu_1^2 + v_2^2)(4\mu_2^2 + 4\mu_2\mu_1 + \mu_1^2 + v_2^2) + 8(\mu_1 + \mu_2)^2 a_2^2 (\mu_1^2 + 2\mu_1\mu_2 + 2v_1v_2 + v_2^2) > 0 \quad (4.113)$$

Violation of condition (4.113) implies that the real part of a pair of complex conjugate roots of equation (4.108) is positive. The numerical investigation given below shows that when the excitation frequency varies, the modulation equations (4.100)-(4.103) exhibit both subcritical and supercritical Hopf bifurcations (see section 2.2.2).

First we use the amplitude f of the excitation as a bifurcation parameter (in the notation of chapter two; $r = f$) to study the behavior of the fixed-point solutions of equations (4.100)-(4.103). Figure 4.1 shows a representative force-response curve for $\Gamma < 0$ where

$$\Gamma = \frac{1}{2} \sigma_1(\sigma_1 + \sigma_2) - \mu_1\mu_2 \quad (4.114)$$

It shows that if the level of external excitation gradually increases from zero, a_1 increases linearly with f until f reaches the threshold value $f_2 = a_1^* (\mu_1^2 + \sigma_1^2)^{1/2}$. Beyond this threshold, the linear solution becomes unstable. Moreover, the excited 4th

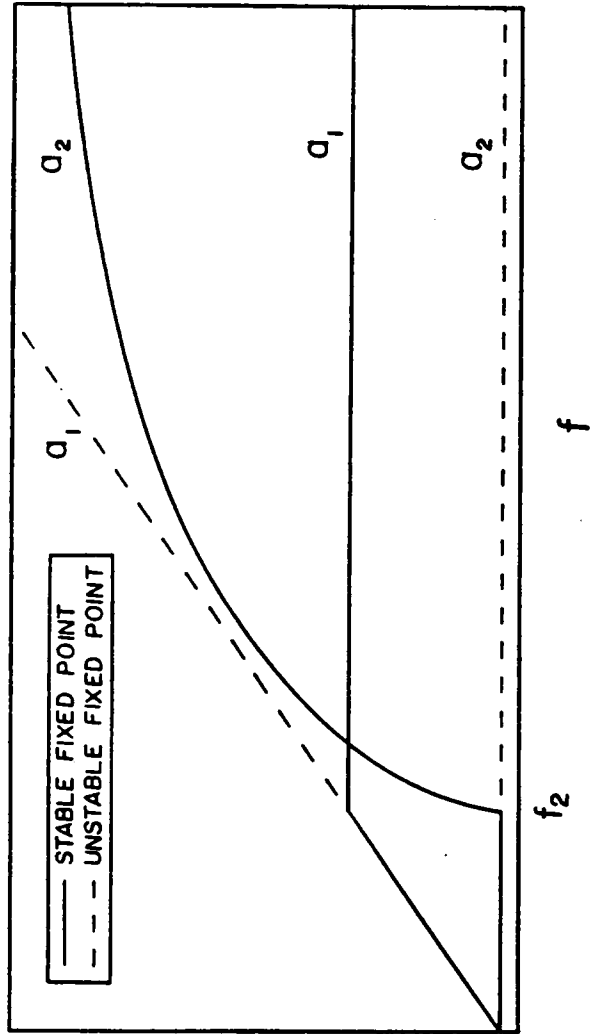


Figure 4.1. A typical force response curve for $\Gamma < 0$.

flexural mode saturates and spills over its extra input energy into the coupled 2nd flexural mode, which starts to grow nonlinearly and eventually dominates the response of the shell.

The damping coefficients and detunings of the system may be such that both the linear and nonlinear solutions coexist over a range of the forcing amplitude f . This occurs when $\Gamma > 0$ and Figure 4.2 shows a representative force-response curve for this case. In addition to the saturation phenomenon, the response exhibits jumps at $f = f_1$ and $f = f_2$. As the forcing amplitude f increases from zero the shell responds linearly (i.e., only the excited 4th flexural mode responds while the other mode is zero). At $f = f_2$, the flow undergoes a subcritical (reversed) pitchfork bifurcation. For $f > f_2$, the linear solution is unstable and the response is nonlinear. Moreover, the excited 4th mode saturates and spills over its extra input energy into the coupled 2nd mode which responds nonlinearly. As f decreases from a value above f_2 , the amplitude of the 2nd mode decreases while that of the 4th mode remains saturated until f_1 is reached. At f_1 , stable and unstable fixed points of the 2nd mode collide and annihilate each other (a saddle-node type bifurcation) and a_2 jumps down to the trivial solution. Below f_1 the response of the shell is linear. For $f_1 < f < f_2$ an unstable fixed point (dashed line) separates two stable fixed points (one trivial and one nontrivial) of the coupled 2nd mode. If f is set equal to a value in this interval, the steady-state response of the shell will depend on the initial conditions.

Next we let $f = 1$ and use σ_1 as the bifurcation parameter to study the solutions of the modulation equations. Figure 4.3 shows typical frequency-response curves, they exhibit a supercritical Hopf bifurcation at $\sigma_1 = -0.5288$ and a subcritical Hopf bifurcation at $\sigma_1 = -0.0002$. Between these frequencies, the fixed-point solutions are unstable and the flow is attracted to either a closed orbit or a chaotic attractor. A limit cycle of the evolution equations corresponds to amplitude- and phase-modulated

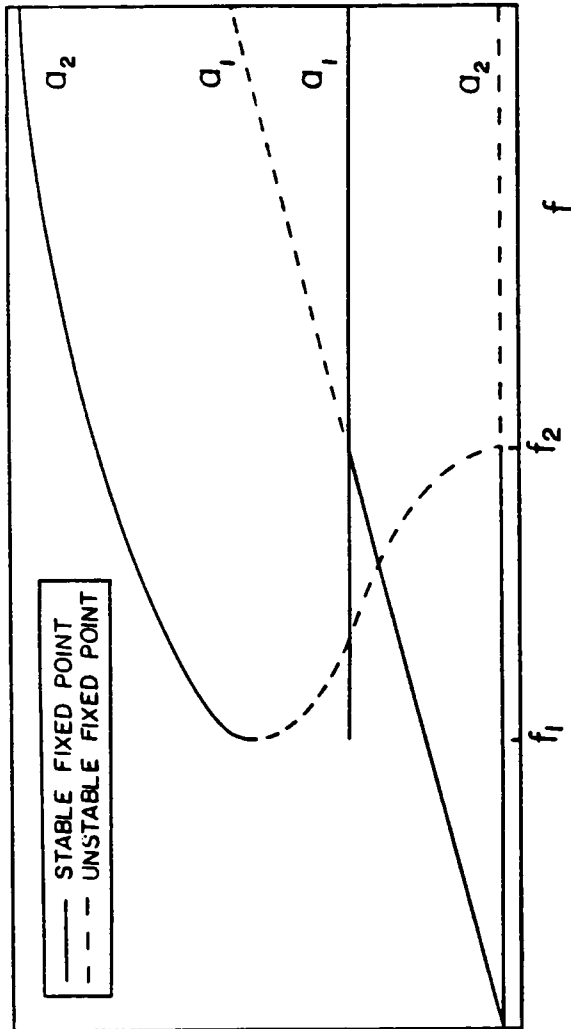


Figure 4.2. A typical force response curve for $\Gamma > 0$.

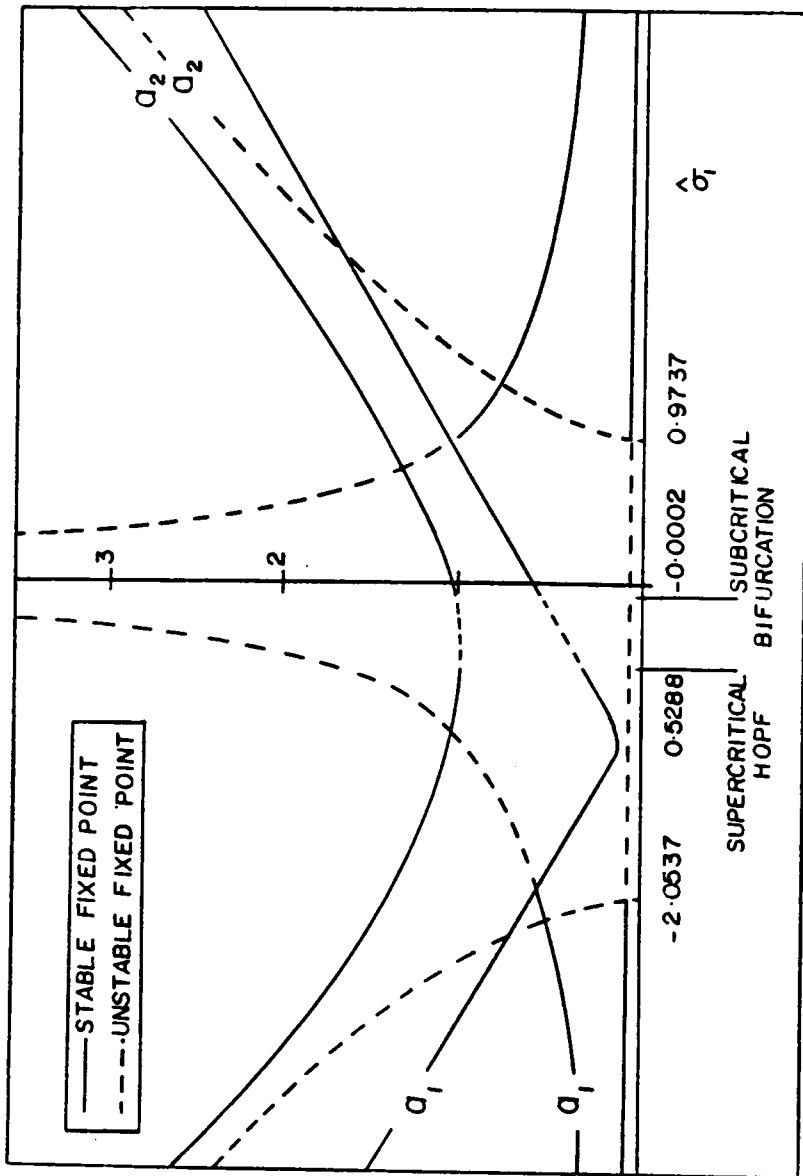


Figure 4.3. Frequency response-curve: solid (dotted) lines indicate a stable (unstable) fixed-point solution.

oscillations of the shell. Inspecting the modulation equations (4.100)-(4.103), we note that they are invariant under the transformation

$$\begin{bmatrix} p_1 \\ q_1 \\ p_2 \\ q_2 \end{bmatrix} \rightarrow \begin{bmatrix} 1 & 0 & 0 & 0 \\ 0 & 1 & 0 & 0 \\ 0 & 0 & -1 & 0 \\ 0 & 0 & 0 & -1 \end{bmatrix} \begin{bmatrix} p_1 \\ q_1 \\ p_2 \\ q_2 \end{bmatrix} \quad (4.115)$$

While the above transformation maps a symmetric limit cycle into itself, it maps an asymmetric limit cycle to its 'reflection'. Thus, we expect asymmetric orbits to exist in pairs, if at all.

Figure 4.4 shows a schematic bifurcation diagram of the modulation equations between and around the Hopf bifurcation points. We used Aprille and Trick's algorithm (see section 2.3.1) to locate the limit cycles and calculate their periods. Floquet analysis is then performed to determine the stability of these limit cycles. We can check the results of the scheme since one of the Floquet multipliers must always be +1 because the modulation equations are autonomous. The circles with the arrows at the top of the figure show how the Floquet multiplier leaves the unit circle in the complex plane at the corresponding bifurcation frequency.

For $\sigma_1 < -0.5288$, a fixed point is the only steady-state solution and the flow approaches it asymptotically as $t \rightarrow \infty$. At $\sigma_1 = -0.5288$, the flow undergoes a Hopf bifurcation and the fixed point loses its hyperbolicity. As σ_1 increases beyond -0.5288, the flow decays along some eigendirections and a symmetric limit cycle with small amplitude is born in the manifold locally normal to these directions indicating a supercritical Hopf bifurcation (Marsden and McCracken, 1976). Figure 4.5a shows such a limit cycle. As σ_1 increases further, the amplitude of the limit cycle increases until it undergoes a pitchfork bifurcation at $\sigma_1 = -0.2320$ and a pair of asymmetric limit

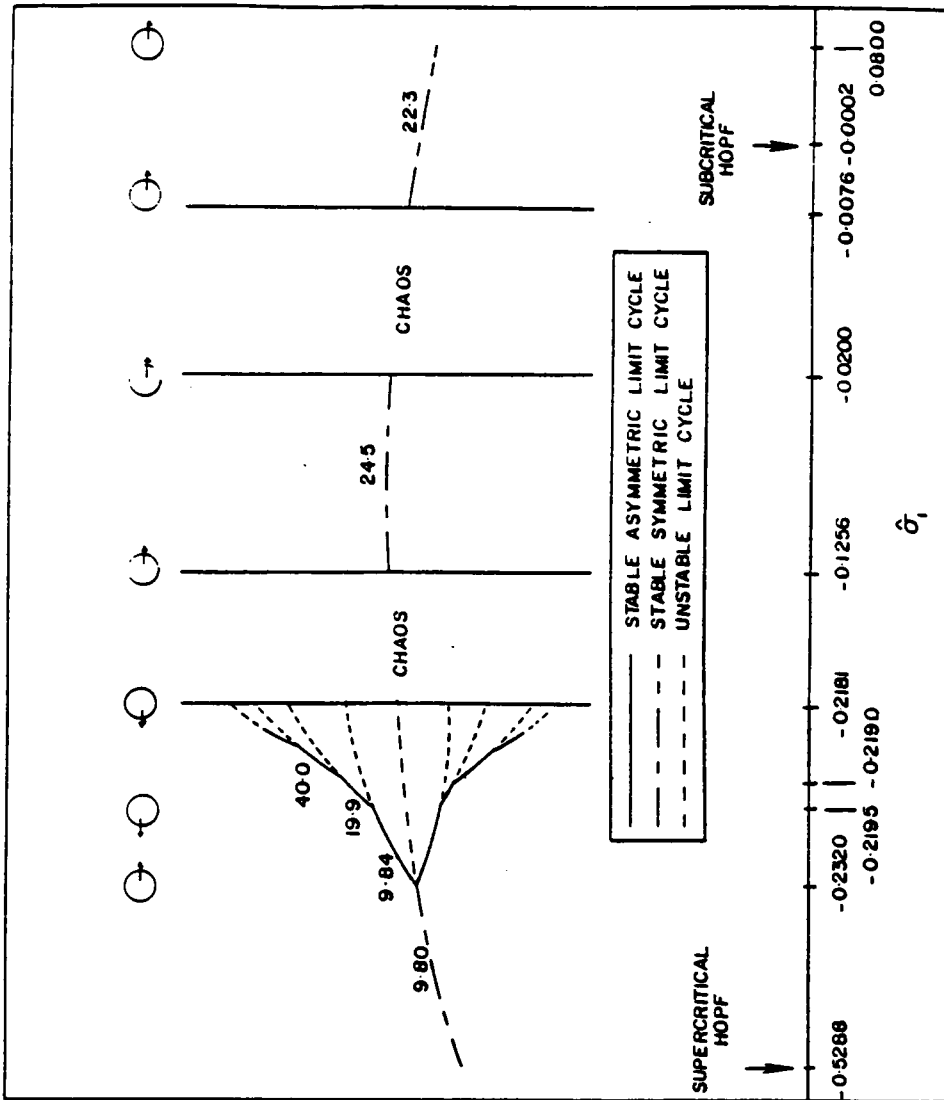
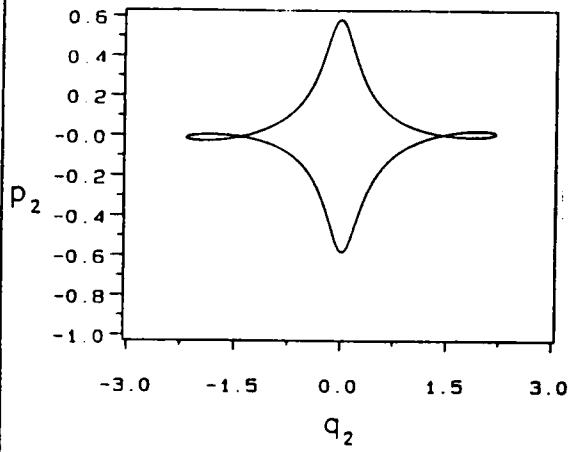
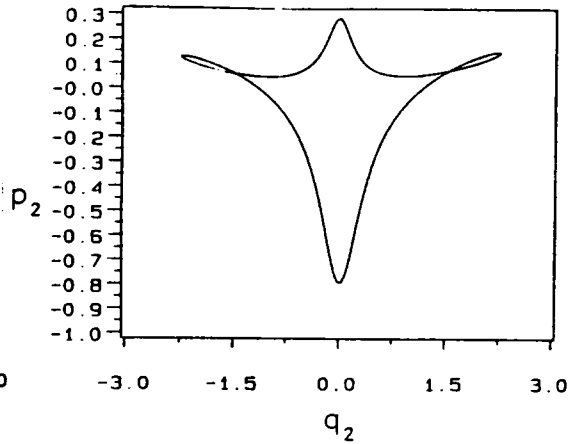


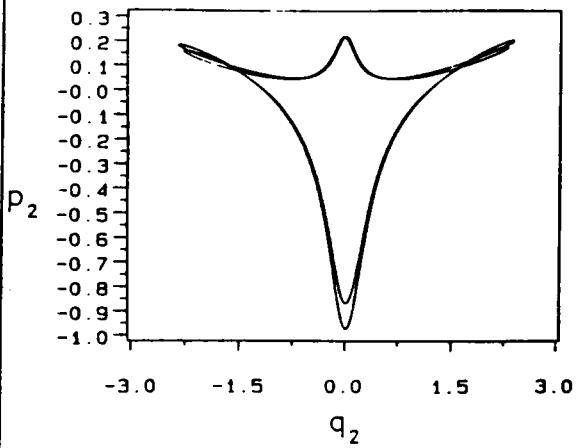
Figure 4.4. : A schematic bifurcation diagram of the modulation equations between and around the Hopf bifurcation excitation frequencies. The numbers indicate the average periods of the orbits, the arrows on the circle show how the Floquet multipliers leave the unit circle in the complex plane.



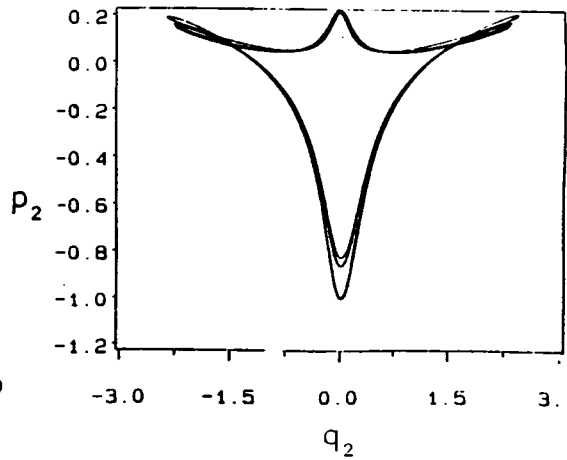
a



b



c



d

Figure 4.5. Symmetry-breaking and first sequence of period-doubling bifurcations.

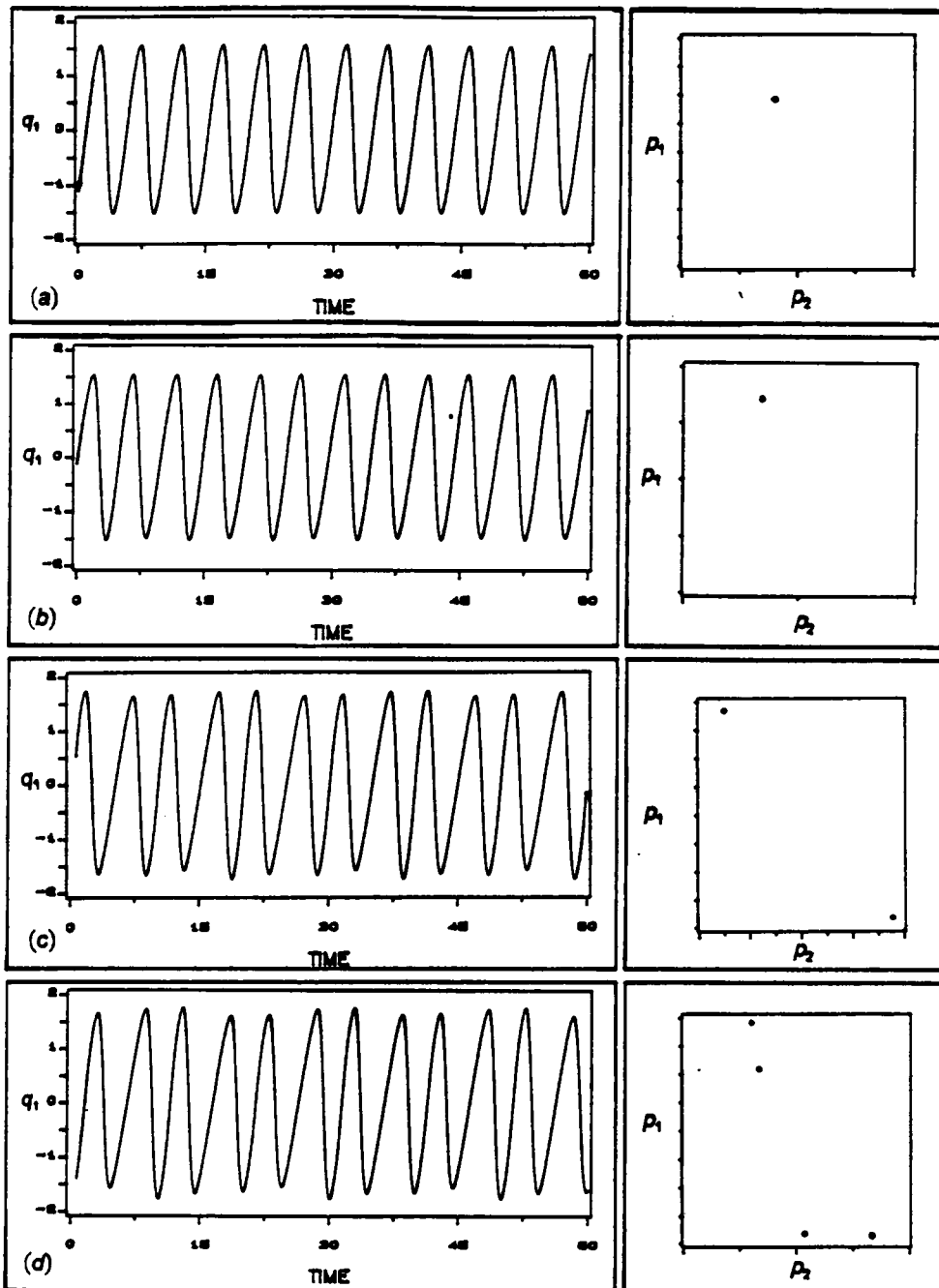


Figure 4.6. Time histories and two-dimensional projections of the Poincaré' section: Poincaré' section is taken at $q_2 = 0$.

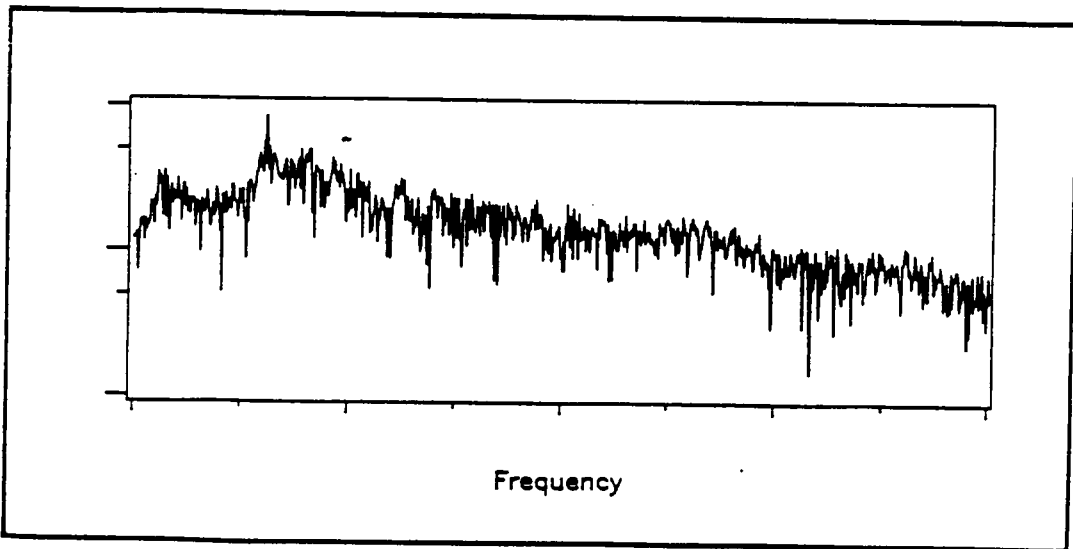
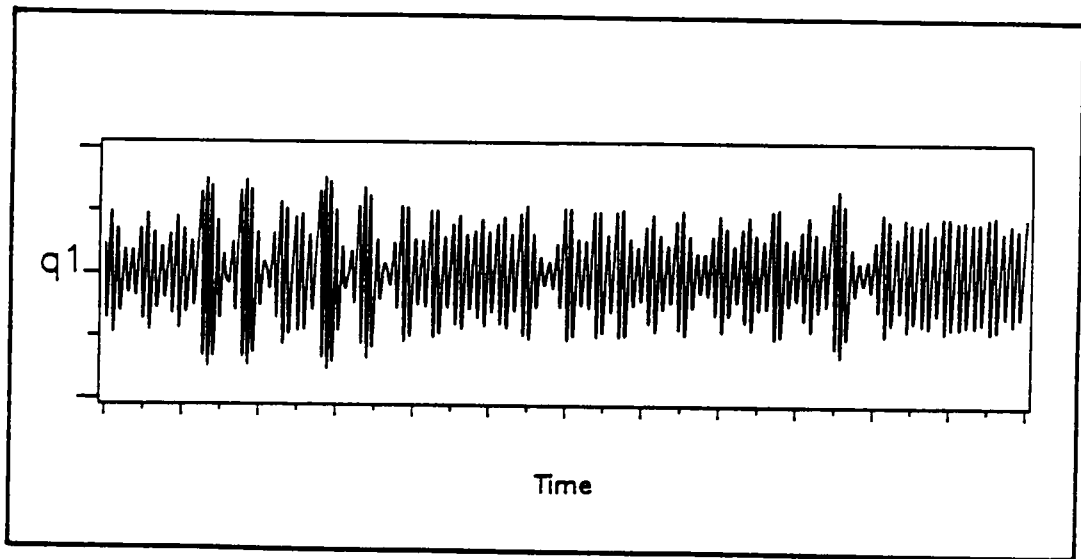


Figure 4.7. Time history and fast Fourier transform of the chaotic attractor at $\sigma_1 = -0.2180$: Both the history and the FFT are for q_1 .

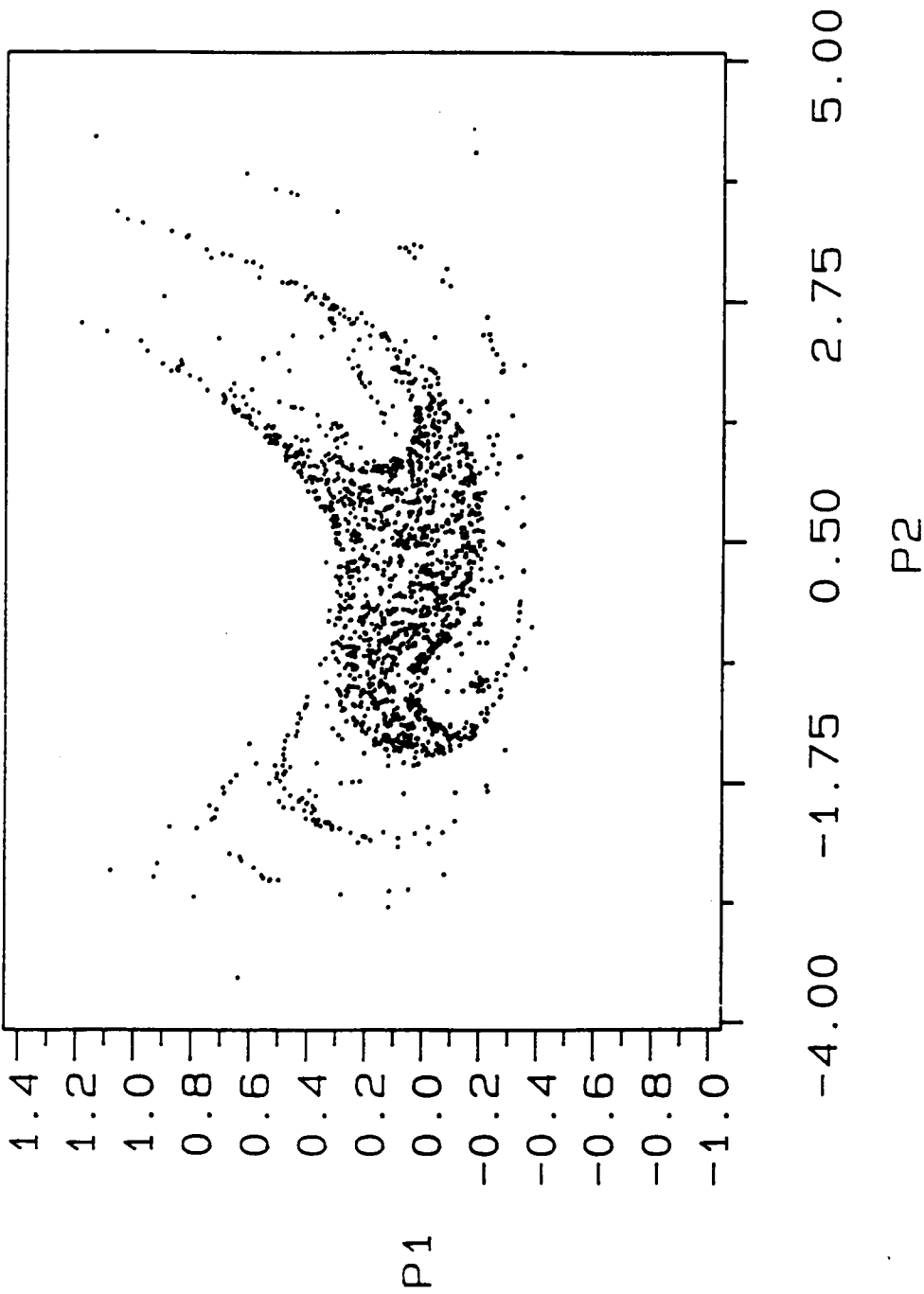


Figure 4.8. Two-dimensional projection of the Poincaré section for the chaotic attractor at $\sigma_1 = -0.2180$: the Poincaré section is taken at $q_3 = 0$.

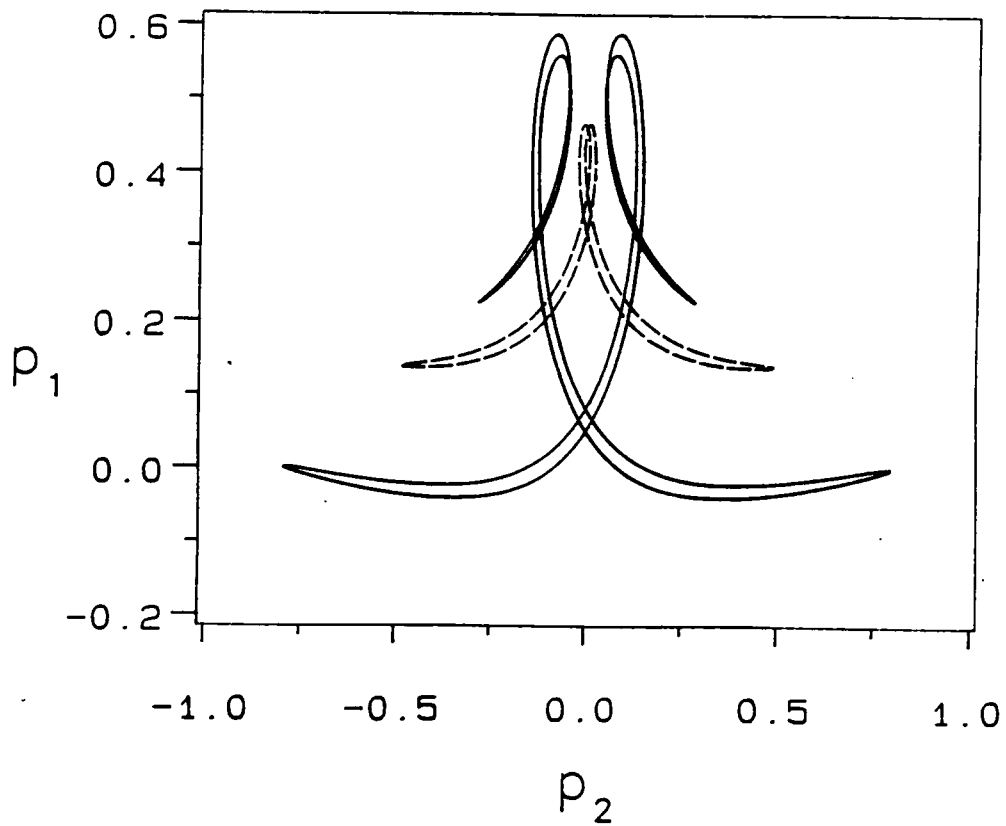


Figure 4.9. An unstable limit cycle separates two stable ones: Two stable symmetric limit cycles (solid line) separated by an unstable orbit (dashed line) for $\hat{\sigma}_1 = -0.22$.

cycles is born (fig. 4.5b). This bifurcation is associated with a Floquet multiplier leaving the unit circle through $+1$. The asymmetric pair of limit cycles undergoes a sequence of period-doubling bifurcations culminating in a chaotic behavior for $\sigma_1 \in (-0.2181, -0.1256)$. The attractor at $\sigma_1 = -0.2180$ has the Lyapunov exponents $= (0.177, 0.000, -0.029, -0.207)$ and a fractal dimension $d_f = 3.718$. The Lyapunov exponents are calculated using the algorithm of Wolf et. al (1985). Each of the period-doubling bifurcations is associated with a Floquet multiplier leaving the unit circle through -1 . The unstable limit cycles continue to exist until the chaotic region is reached. Figures 5c and d show the first two sequences of the cascade of the period-doubling bifurcations. They show only one of the asymmetric attractors, the other reflection is obtained by applying the transformation (4.115). Figure 4.6 shows the time histories and the corresponding two-dimensional projections of the Poincare' map (Poincare section at $q_2 = 0$) corresponding to figure 5. Figure 4.7 shows the time history for q_2 in the chaotic region at $\sigma_1 = -0.2180$ and the fast Fourier transform for this signal. Figure 4.8 shows a two-dimensional projection of the Poincare' section taken in the phase space at $q_2 = 0$ for the same chaotic attractor. All through the above bifurcations, the stable asymmetric limit cycles are separated by an unstable symmetric orbit as shown in figure 9.

For large values of σ_1 , the flow tends towards a fixed point as $t \rightarrow \infty$. However, if we decrease σ_1 , the stable fixed point loses stability through a Hopf bifurcation at $\sigma_1 = -0.0002$. The large amplitude oscillations present around this σ_1 indicate a subcritical Hopf bifurcation. In fact, for $\sigma_1 \in (-0.0002, 0.08)$ a stable fixed point coexists with a stable limit cycle and the flow tends to one or the other depending on their basins of attraction. Figure 4.10a shows a limit cycle coexisting with a fixed point (indicated by a cross). As σ_1 decreases, the limit cycle loses stability through a cyclic-fold bifurcation and the response is chaotic. At $\sigma_1 = -0.01$, its Lyapunov

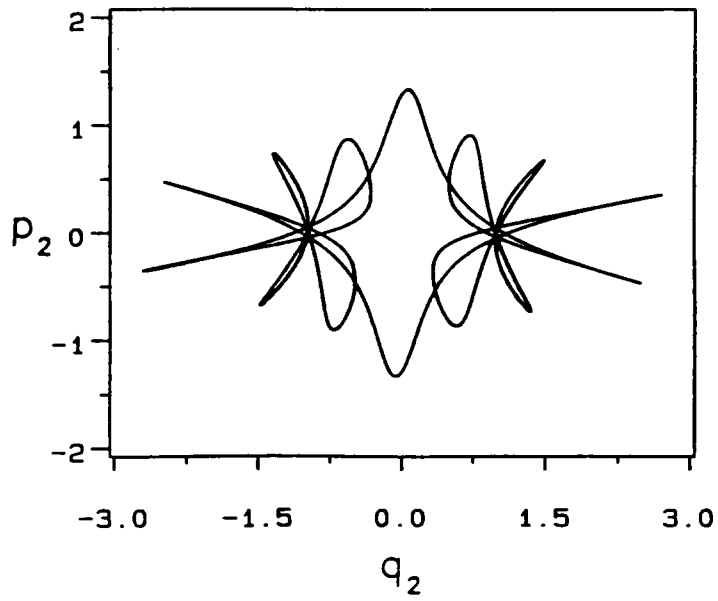
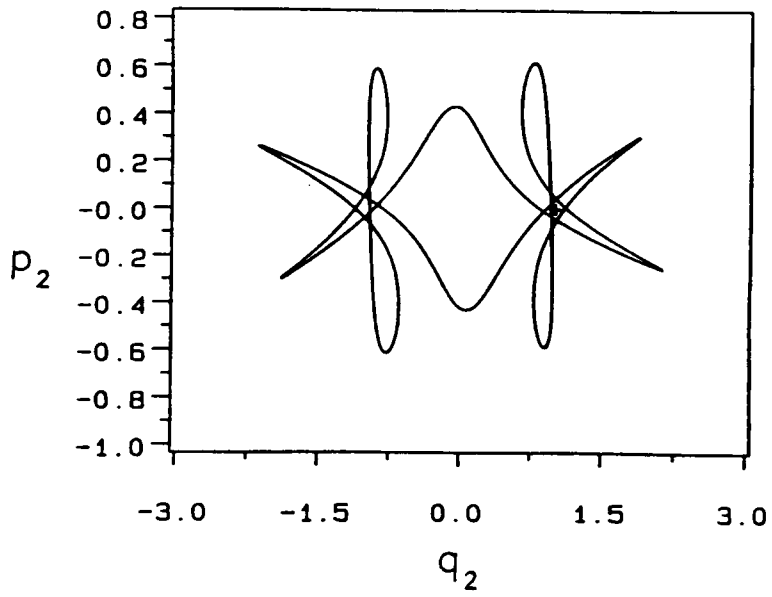


Figure 4.10. : (a) A limit cycle coexisting with a fixed point (indicated by a cross) at $\hat{\sigma}_1 = 0.0001$ and (b) limit cycle at $\hat{\sigma}_1 = -0.03$.

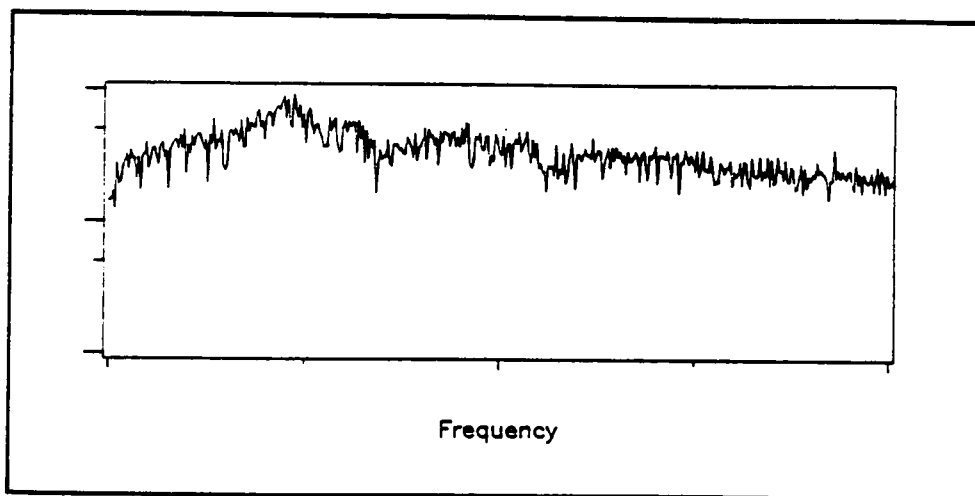
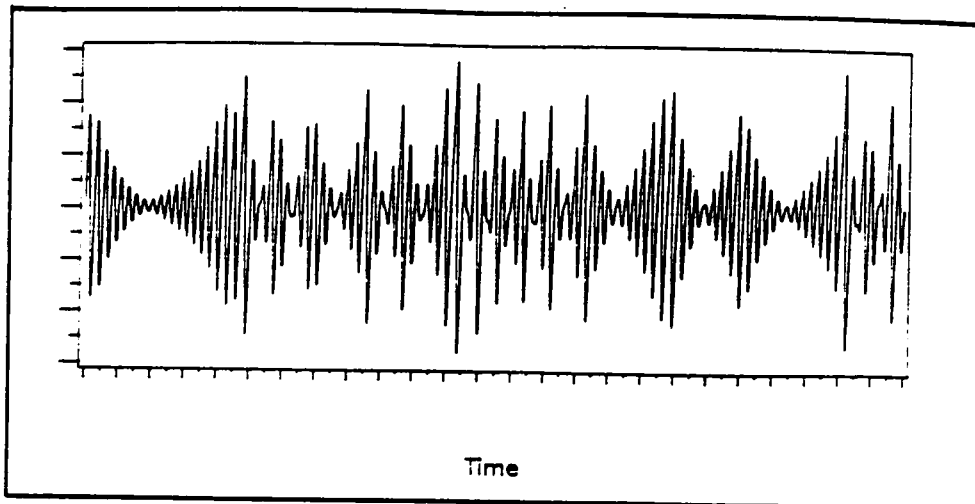


Figure 4.11. Time history and fast Fourier transform of the chaotic attractor at $\hat{\sigma}_1 = -0.01$: Both the history and the FFT are for q_1 .

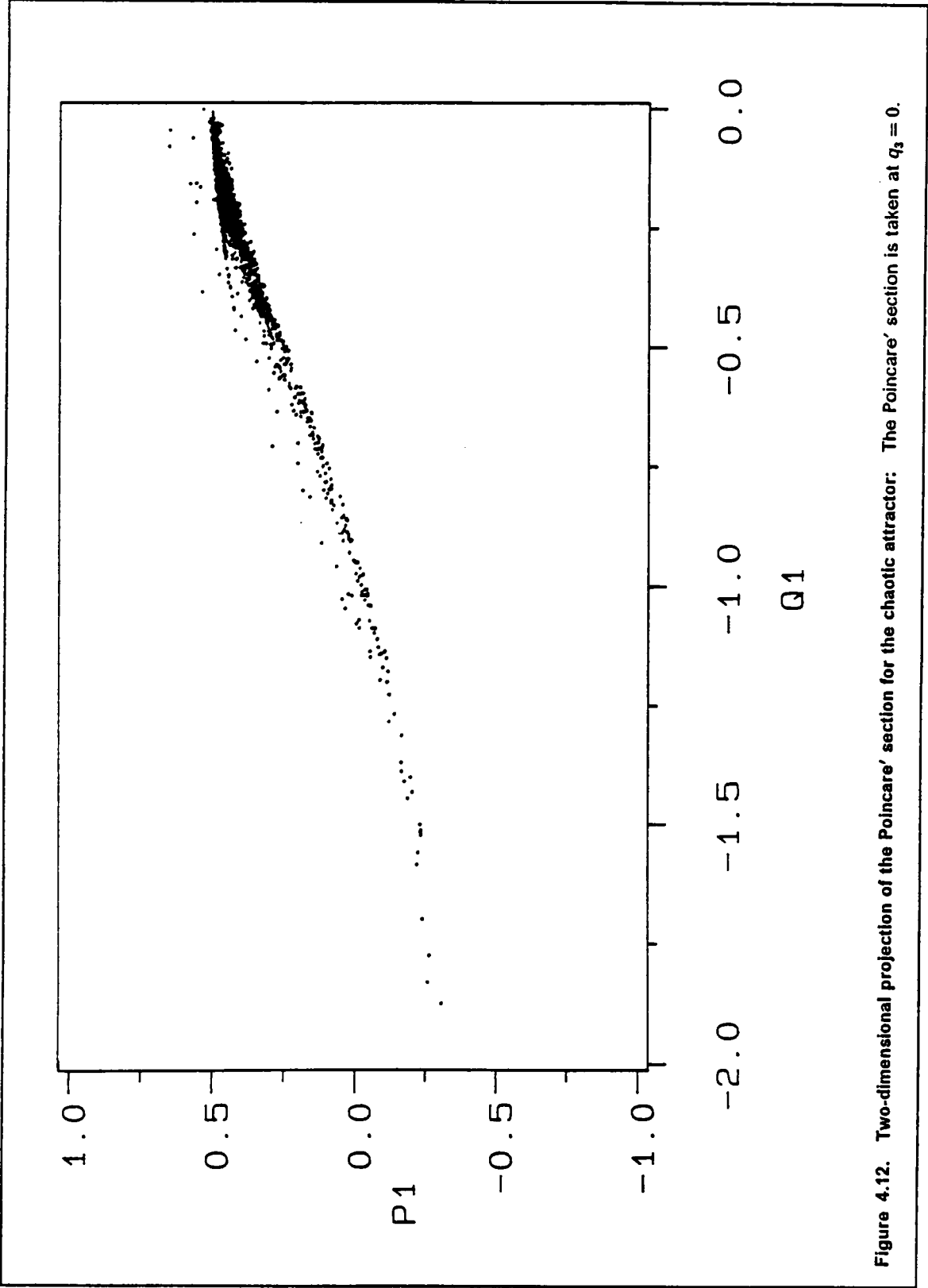


Figure 4.12. Two-dimensional projection of the Poincaré section for the chaotic attractor: The Poincaré section is taken at $q_3 = 0$.

exponents are (0.137, 0.000,-0.029,-0.170) and its dimension is $d_f = 3.651$. Figure 4.11 shows the time history for q_2 in the chaotic region at $\sigma_1 = -0.010$ and the fast Fourier transform for this signal. Figure 4.12 shows a two-dimensional projection of the Poincare' section taken in the phase space at $q_2 = 0$ for the same chaotic attractor. Upon further decreasing σ_1 , the chaotic attractor disappears and a limit cycle appears at $\sigma_1 = -0.02$, see figure 10b. At $\sigma_1 = -0.12566$, this limit cycle undergoes a cyclic-fold bifurcation and the flow jumps into a chaotic motion. This is the same motion obtained earlier through the cascade of period-doubling bifurcations.

4.2 Subharmonic Resonance of the Breathing Mode of Cylindrical Shells

In this last section we use the method of multiple-time scales to determine a first-order uniformly valid expansion of the solutions of equations (4.5) and (4.6) for small but finite amplitudes when P is given by

$$\frac{a(1-v^2)}{Eh} P = \varepsilon F \cos \Omega \tau \quad (4.116)$$

$\Omega \approx 2\omega_0$ and $\omega_0 \approx 2\omega_n$. We seek expansions of the displacement field in the form

$$w(\theta, \tau; \varepsilon) = \varepsilon w_1(\theta, T_0, T_1) + \varepsilon^2 w_2(\theta, T_0, T_1) + \dots \quad (4.117)$$

$$\psi(\theta, \tau; \varepsilon) = \varepsilon \psi_1(\theta, T_0, T_1) + \varepsilon^2 \psi_2(\theta, T_0, T_1) + \dots \quad (4.118)$$

Substituting equations (4.116)-(4.118) into equations (4.5) and (4.6) and equating coefficients of like powers of ε , we obtain

Order ε

$$D_0^2 w_1 + \alpha^2 \{w_1^{IV} + 2w_1'' + w_1\} - \psi_1' + w_1 = F \cos \Omega T_0 \quad (4.119)$$

$$D_0^2 \psi_1 - \psi_1'' + w_1' = 0 \quad (4.120)$$

Order ε^2

$$D_0^2 w_2 + \alpha^2 \{w_2^{IV} + 2w_2'' + w_2\} - \psi_2' + w_2 = -2D_0 D_1 w_1 + w_1''(\psi_1' - w_1) - (D_0 \psi_1)^2 + \psi_1'^2 - 2w_1 \psi_1' + w_1' \psi_1'' - \frac{1}{2} w_1'^2 + F(\psi_1' - w_1) \cos \Omega T_0 \quad (4.121)$$

$$D_0^2 \psi_2 - \psi_2'' + w_2' = -2D_0 D_1 \psi_1 + w_1' w_1'' - 2w_1' \psi_1' + 2(D_0 w_1)(D_0 \psi_1) + F w_1' \cos \Omega T_0 \quad (4.122)$$

Since the coupling occurs between the breathing mode and the n^{th} flexural mode, only these two modes will be present in the steady-state response. Based on the analysis of the previous sections we assume a displacement field of the form

$$w_1 = p_1(T_1) \cos(\omega_0 T_0 + \nu_2 T_1) + q_1(T_1) \sin(\omega_0 T_0 + \nu_2 T_1) + [p_2(T_1) \cos(\omega_n T_0 + \nu_1 T_1) + q_2(T_1) \sin(\omega_n T_0 + \nu_1 T_1)] \cos n\theta + [p_3(T_1) \cos(\omega_n T_0 + \nu_1 T_1) + q_3(T_1) \sin(\omega_n T_0 + \nu_1 T_1)] \sin n\theta + F(1 + \alpha^2 - \Omega^2)^{-1} \cos \Omega T_0 \quad (4.123)$$

$$\psi_1 = \Gamma_n [p_2(T_1) \cos(\omega_n T_0 + \nu_1 T_1) + q_2(T_1) \sin(\omega_n T_0 + \nu_1 T_1)] \sin n\theta - \Gamma_n [p_2(T_1) \cos(\omega_n T_0 + \nu_1 T_1) + q_2(T_1) \sin(\omega_n T_0 + \nu_1 T_1)] \cos n\theta \quad (4.124)$$

where

$$v_1 = \frac{1}{2} \sigma_1 + \frac{1}{4} \sigma_2, \quad v_2 = \frac{1}{2} \sigma_2 \quad (4.125)$$

and σ_1 and σ_2 are detuning parameters defined as

$$\Omega = 2\omega_0 + \varepsilon\sigma_2 \quad \text{and} \quad \omega_0 = 2\omega_n + \varepsilon\sigma_1 \quad (4.126)$$

Substituting equations (4.123) and (4.124) into equations (4.121) and (4.122), using equations (4.126), and imposing the solvability conditions on the resulting inhomogeneous problem, we obtain the following evolution equations:

$$p'_1 = -v_2 q_1 - \mu_0 p_1 - 2\Lambda_1(p_2 q_2 + p_3 q_3) - f q_1 \quad (4.127)$$

$$q'_1 = v_2 p_1 - \mu_0 q_1 + \Lambda_1(p_2^2 + p_3^2 - q_2^2 - q_3^2) - f p_1 \quad (4.128)$$

$$p'_2 = -v_1 q_2 - \mu_n p_2 - \Lambda_2(q_1 p_2 - q_2 p_1) \quad (4.129)$$

$$q'_2 = v_1 p_2 - \mu_n q_2 + \Lambda_2(p_1 p_2 + q_1 q_2) \quad (4.130)$$

$$p'_3 = -v_1 q_3 - \mu_n p_3 - \Lambda_2(q_1 p_3 - q_3 p_1) \quad (4.131)$$

$$q'_3 = v_1 p_3 - \mu_n q_3 + \Lambda_2(p_1 p_3 + q_1 q_3) \quad (4.132)$$

where

$$4\omega_0 \Lambda_1 = \frac{1}{4} n^2 + \frac{1}{2} (\omega_n^2 + n^2) \Gamma_n^2 - n \Gamma_n \quad (4.133)$$

$$4\omega_0 (1 + \Gamma_n^2) \Lambda_2 = n^2 - 2n \Gamma_n + 2\omega_0 \omega_n \Gamma_n^2 \quad (4.134)$$

$$F = 4\omega_0 f \quad (4.135)$$

Modal damping has been incorporated into equations (4.127)-(4.132) with μ_0 being the damping coefficient of the breathing mode and μ_n being the damping coefficient of the n^{th} flexural mode. Equations (4.127)-(4.132) possess two possible fixed-point solutions: either

$$p_i = q_i = 0 \quad \text{for } i = 1, 2 \text{ and } 3 \quad (4.136)$$

or

$$a_0 = \dot{a}_0 = \Lambda_2^{-1} \left\{ \mu_n^2 + \frac{1}{4} \left(\frac{1}{2} \sigma_2 + \sigma_1 \right)^2 \right\}^{1/2} \quad (4.137)$$

$$a_n^2 + b_n^2 = -\chi_1 \mp \left(\frac{f^2 a_0^2}{\Lambda_1^2} - \chi_2^2 \right)^{1/2} \quad (4.138)$$

where

$$a_0^2 = p_1^2 + q_1^2, \quad a_n^2 = p_2^2 + q_2^2, \quad b_n^2 = p_3^2 + q_3^2 \quad (4.139)$$

$$\chi_1 = \frac{4\mu_0\mu_n - \sigma_2 \left(\frac{1}{2} \sigma_2 + \sigma_1 \right)}{4\Lambda_1\Lambda_2} \quad (4.140)$$

$$\chi_2 = \frac{\mu_0(\sigma_2 + 2\sigma_1) + 2\sigma_2\mu_n}{4\Lambda_1\Lambda_2} \quad (4.141)$$

To investigate the stability of the trivial fixed points given by equation (4.136), we calculate the eigenvalues λ of the Jacobi matrix of the right-hand sides of equations (4.127)-(4.132) when $p_n = q_n = 0$. After some algebraic manipulations, we obtain

$$\lambda = -\mu_0 + (f^2 - v_2^2)^{1/2}, \quad -\mu_n \mp iv_1, \quad -\mu_n \mp iv_1 \quad (4.142)$$

Thus, a trivial fixed point is stable if and only if

$$f \leq (\mu_0^2 + v_2^2)^{1/2} \quad (4.143)$$

To analyze the stability of the nontrivial fixed points given by equations (4.137) and (4.138), we consider the case in which $p_3 = q_3 = 0$. Using the above procedure and equations (4.137)-(4.141) we find that $\lambda = 0$, $-2\mu_n$, or

$$\begin{aligned} & \lambda^4 + 2(\mu_0 + \mu_n)\lambda^3 + [\mu_0^2 + 4\mu_0\mu_n + v_2^2 - f^2 + 4\Lambda_1\Lambda_2a_n^2]\lambda^2 \\ & + [2\mu_n\mu_0^2 + 2\mu_nv_2^2 - 2\mu_nf^2 + 4\Lambda_1\Lambda_2(\mu_0 + \mu_n)a_n^2]\lambda + 8\Lambda_1\Lambda_2a_n^2[\Lambda_1\Lambda_2a_n^2 + \mu_0\mu_n - v_1v_2] \end{aligned} \quad (4.144)$$

Consequently, a given fixed point is stable if the real part of each root of equation (4.144) is negative (see section 2.1.1).

4.2.1 Numerical results

Next we present numerical results for the case $\alpha^2 = 2.0918 \times 10^{-4}$ (i.e., $h/a \simeq 1/20$), which yields $\omega_0 \simeq 2\omega_g$. Moreover, we let $\hat{\sigma}_1 = \sigma_1\Lambda_2^{-1/2} = -0.73$ and $\hat{\mu}_{0,g} = \mu_{0,g}\Lambda_2^{-1/2} = 0.02$. For such a high flexural mode number (6), Simmonds (1979) showed that cubic terms have no significant effect. Calculations are performed on the autonomous evolution equations (4.127)-(4.130) rather than on the original equations of motion. A fixed point of the evolution equations corresponds to constant-amplitude sinusoidal oscillations of the shell, whereas closed orbits of the evolution equations correspond to sinusoidally-modulated oscillations of the shell.

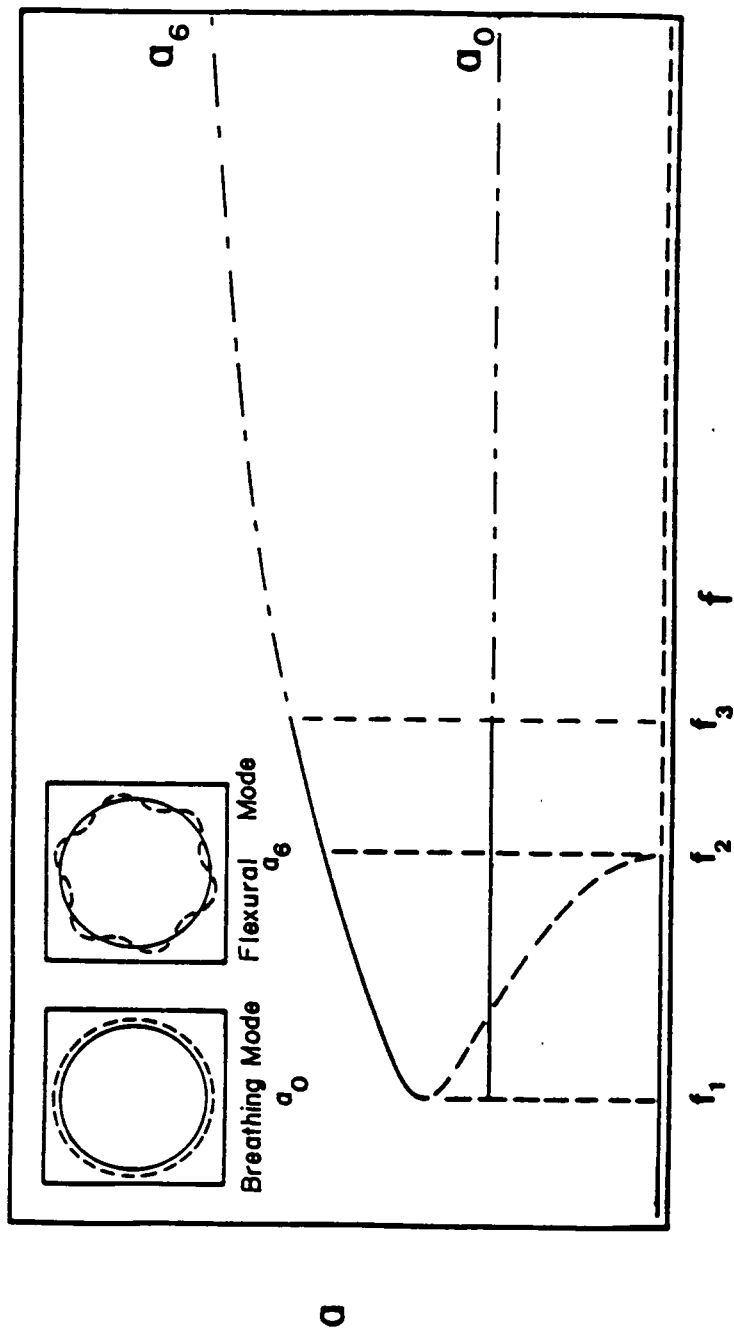


Figure 4.13. A typical Force Response curve for $\chi < 0$: Solid (dashed) lines indicate stable (unstable) fixed points.

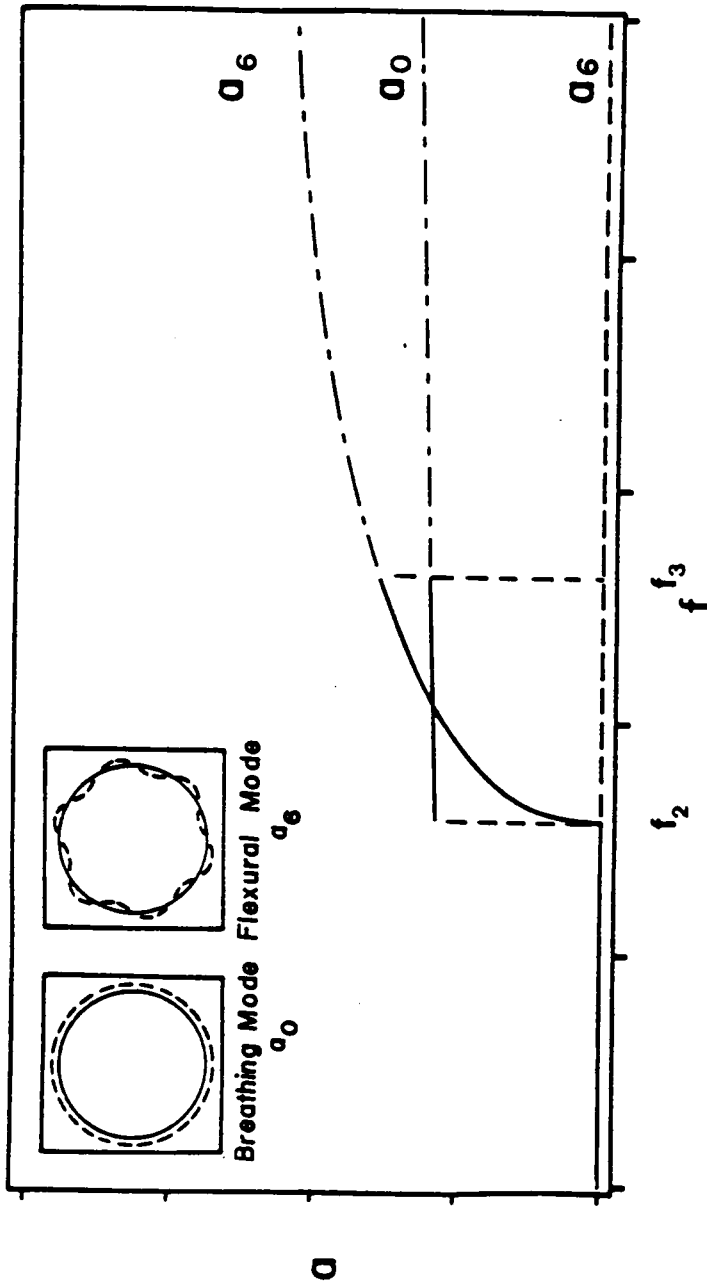


Figure 4.14. A typical Force Response curve for $\chi > 0$: Solid (dashed) lines indicate stable (unstable) fixed points.

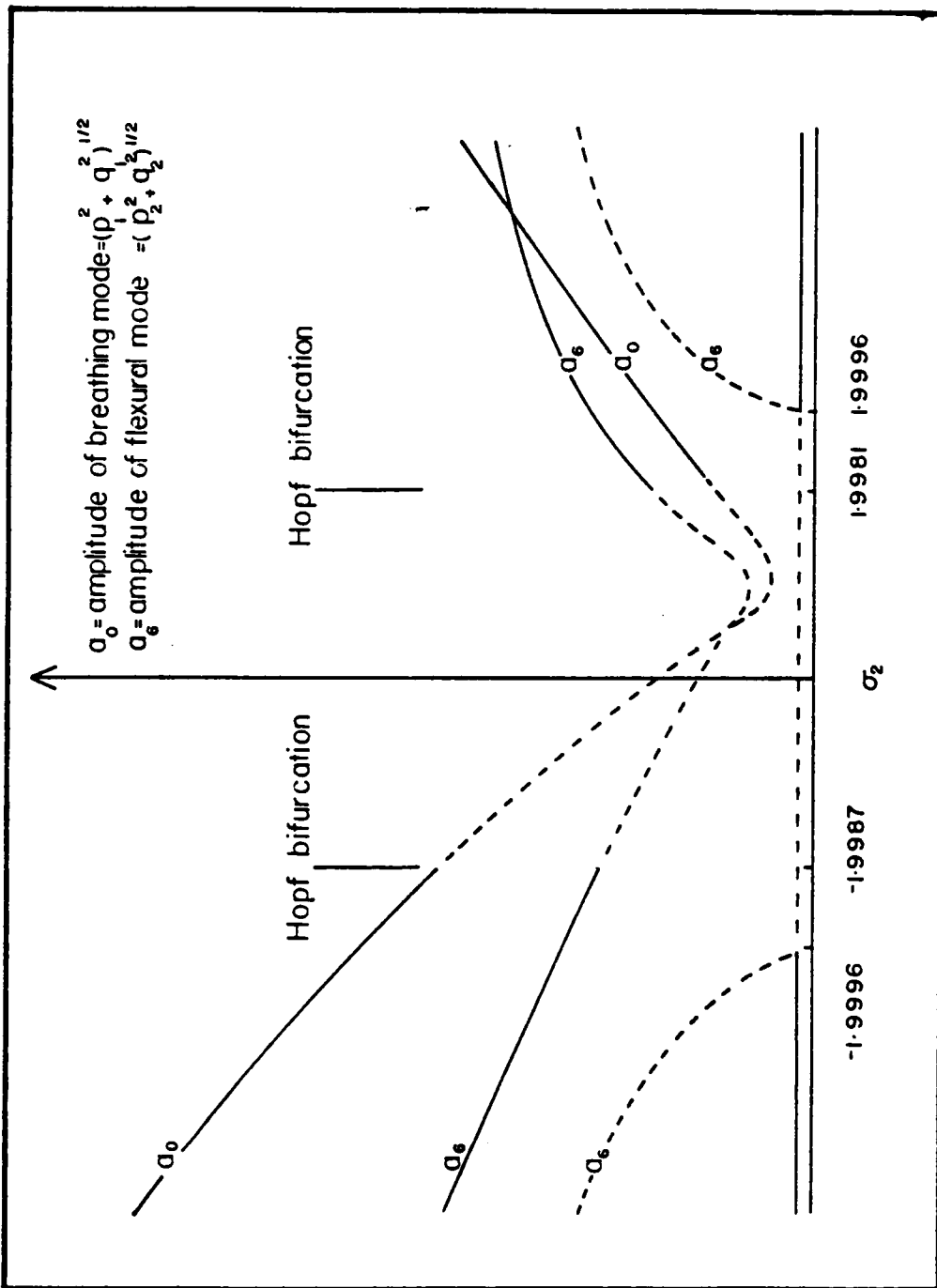


Figure 4.15. Frequency response curve for $f = 1.0$: Solid (dashed) lines indicate stable (unstable) fixed points.

In fig. 4.13, we show the force-response curve for $\chi_1 < 0$. This figure shows the saturation and jump phenomena and it exhibits a Hopf bifurcation. As the forcing amplitude f increases slowly from zero, the trivial fixed point is the only steady-state solution until a threshold is reached at $f = f_2 = 0.1005$. At this value, the trivial fixed point becomes unstable and the flow jumps to a non-trivial solution. As f increases further, the breathing mode saturates, it responds with a constant amplitude and spills over the extra input energy into the coupled flexural mode, which responds nonlinearly, causing a large-amplitude wrinkling of the shell. At $f = f_3 = 0.102$, the nontrivial fixed point undergoes a Hopf bifurcation and amplitude- and phase-modulated oscillations result.

As f decreases beyond f_3 , the shell responds with a constant amplitude of the breathing mode while the amplitude of the flexural mode decreases. At $f = f_2$, the trivial fixed point becomes stable and an unstable fixed point of the flexural mode is born. At $f = f_1 = 0.03$ the nontrivial stable and unstable fixed points of the flexural mode collide in a fold (saddle-node) bifurcation, causing the flow to jump to the stable trivial fixed point. In the region $f_1 < f < f_2$, an unstable fixed point separates two stable fixed points of the flexural mode. If f is set to a value in this interval, the flow tends to one of the stable fixed points depending on their basins of attraction.

Figure 4.14 shows a force-response curve for $\chi_1 > 0$. In this case, no fold bifurcation takes place and the jump occurs only in the breathing mode response.

Figure 4.15 shows a frequency-response curve for $f = 1.0$. It shows a Hopf bifurcation at $\hat{\sigma}_2 = \sigma_2 \Lambda_2^{-1/2} = -1.9987$ and 1.9981 . The non-trivial fixed point becomes unstable as $\hat{\sigma}_2$ increases beyond -1.9987 or decreases below 1.9981 and limit cycles are observed.

In our study of the closed orbit of equations (4.127)-(4.130), we observe cyclic-fold and pitchfork bifurcation associated with a Floquet multiplier leaving the unit circle

through $+1$. The cyclic-fold bifurcations result in cyclic jumps where the flow jumps to another limit cycle or to a chaotic region. To compute the power spectrum, we use the fast Fourier transform algorithm developed by Cooley and Tukey.

For $2.0353 < \hat{\sigma}_2 < -1.9987$, limit cycles do not exist and the flow asymptotically approaches a fixed point as $t \rightarrow \infty$. The behavior of the flow within the above interval is summarized in fig. 4.16. Here we note the following :

1. There always exists an unstable fixed point indicated by a plus sign in the 2-D projections and a cross in the 3-D projections (e.g. fig. 4.17a,b).
2. All periodic limit cycles start and lose stability through either a pitchfork or a cyclic-fold bifurcation.
3. Deformation of limit cycles: all limit cycles undergo deformation as $\hat{\sigma}_2$ changes.

Interesting behaviors are observed in the following:

- a) Limit cycle IV starts at $\hat{\sigma}_2 = -1.8200$ and loses its symmetry just before collision, then the flow jumps onto a chaotic attractor.
 - b) Limit cycles IX and X are born at $\hat{\sigma}_2 = 1.9953$ as symmetric ones, lose symmetry but regain it before their saddle-node bifurcations. Figures 18a-d show the deformation of the limit cycle X.
4. The loss of symmetry is associated with a Floquet multiplier touching $+1$ from within the unit circle. Figure 4.19 shows the behavior of the multipliers for limit cycle X around the symmetry-breaking frequency.
 5. The evolution equations (4.127)-(4.130) exhibit a symmetry apparent in the phase trajectories. The system is invariant under the transformation

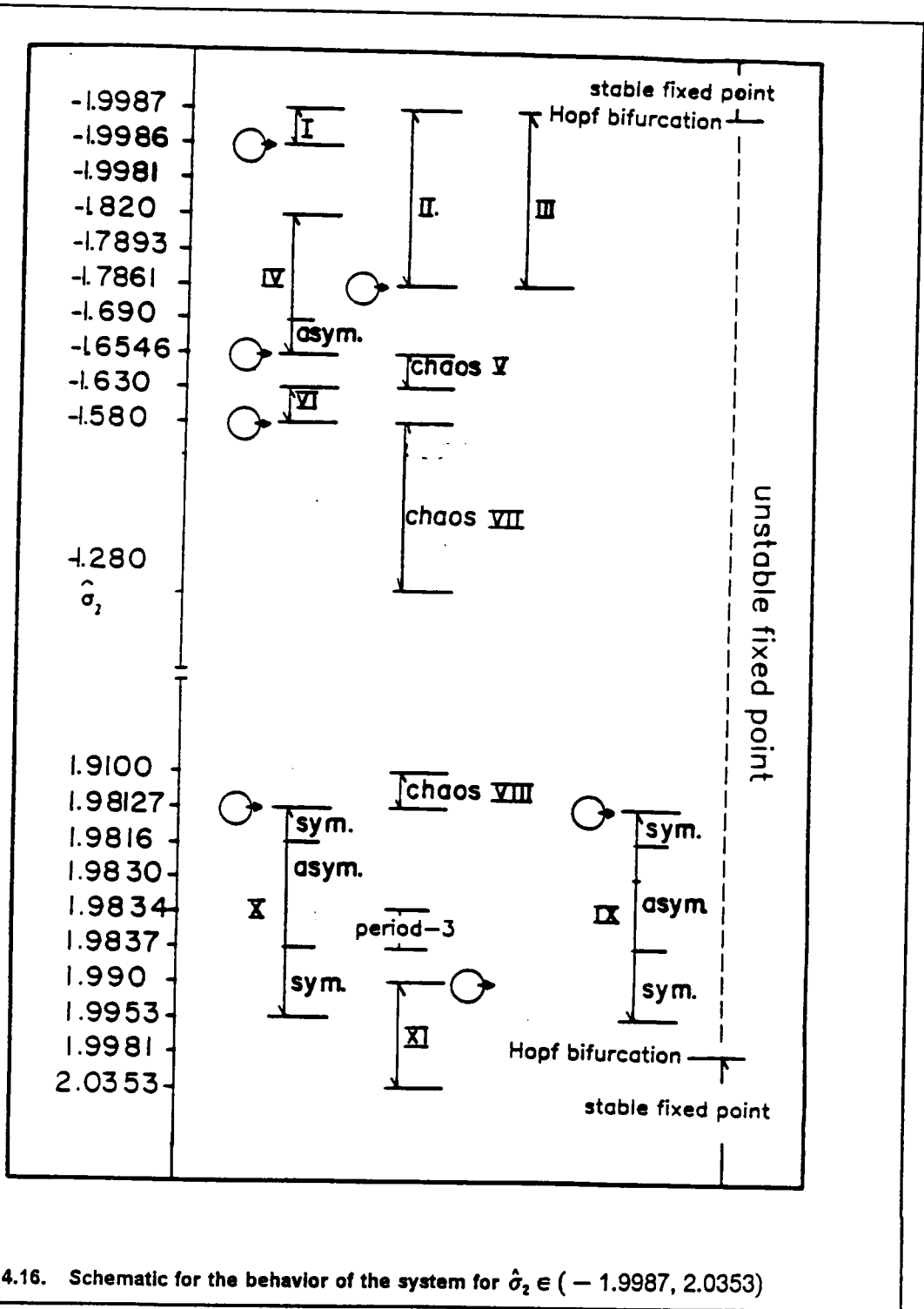


Figure 4.16. Schematic for the behavior of the system for $\hat{\sigma}_2 \in (-1.9987, 2.0353)$

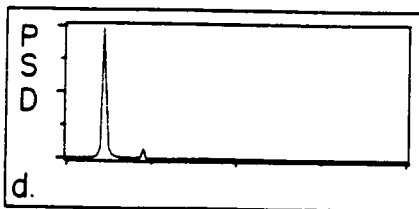
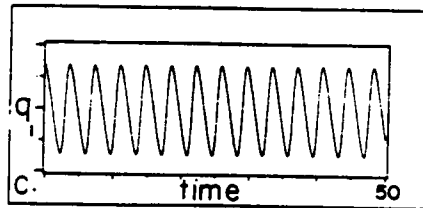
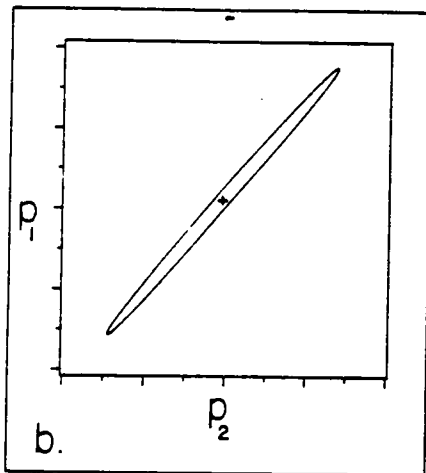
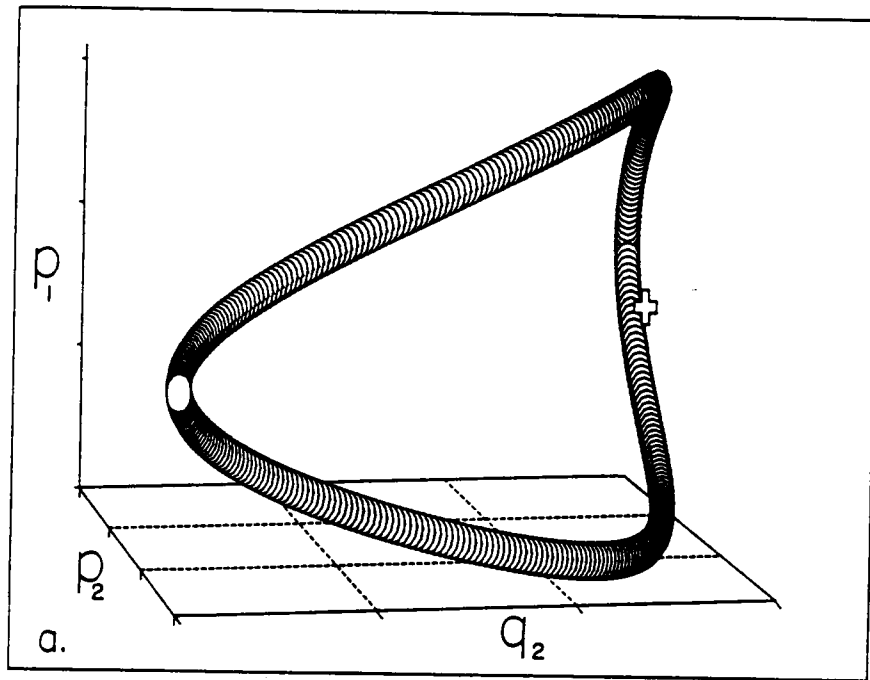


Figure 4.17. Limit cycle I: (a) projection of phase space on the 3-D space spanned by p_1 , p_2 and q_2 ; 'balloons' represent points on the limit cycle, (b) projection of phase space on the 2-D plane spanned by p_1 and p_2 , (c) waveform of q_1 , and (d) power spectral density (PSD) of the q_1 signal.

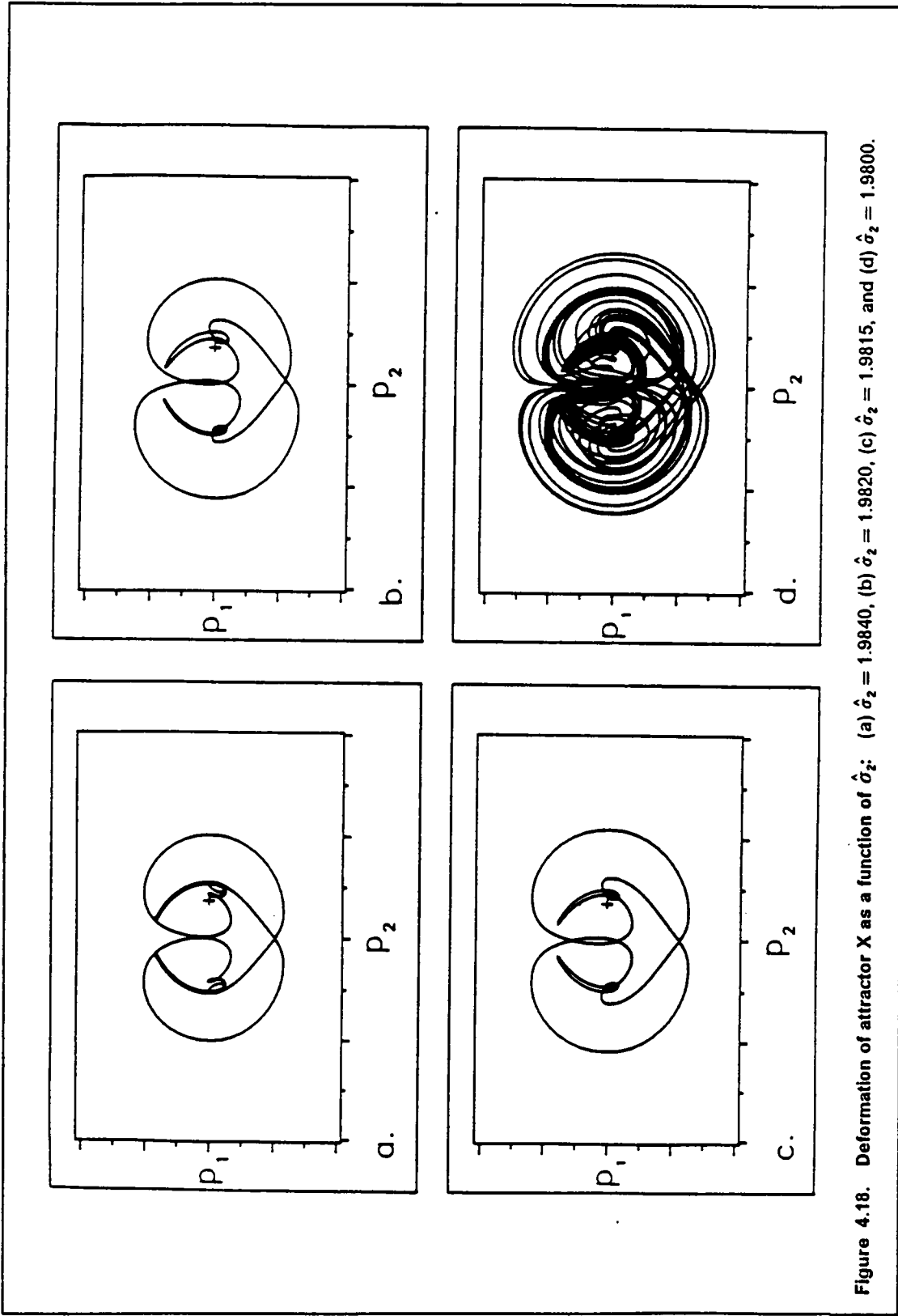


Figure 4.18. Deformation of attractor X as a function of $\hat{\sigma}_2$: (a) $\hat{\sigma}_2 = 1.9840$, (b) $\hat{\sigma}_2 = 1.9815$, (c) $\hat{\sigma}_2 = 1.9820$, and (d) $\hat{\sigma}_2 = 1.9800$.

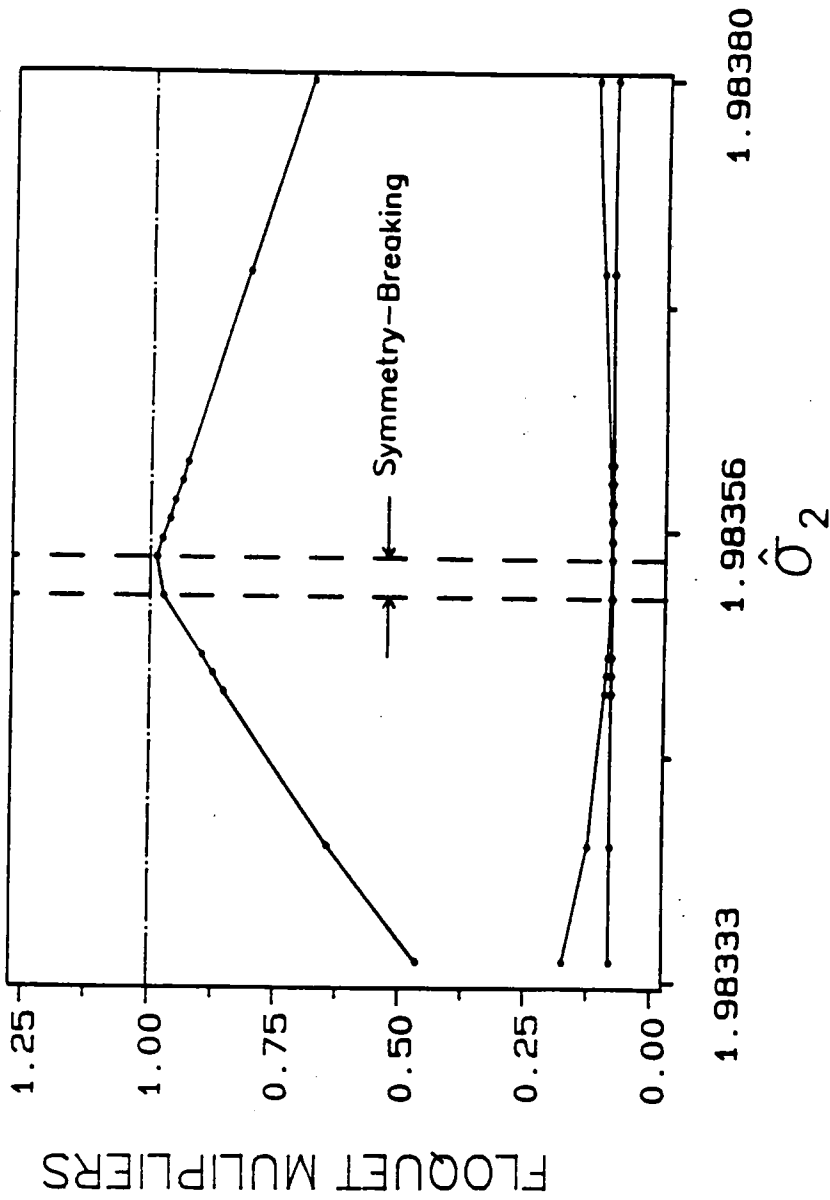


Figure 4.19. Floquet multipliers for limit cycle X around the symmetry-breaking frequency ($\hat{\sigma}_{12} = 1.9837$): The fourth multiplier is +1.

$$T: \begin{bmatrix} p_1 \\ q_1 \\ p_2 \\ q_2 \end{bmatrix} \rightarrow \begin{bmatrix} -1 & 0 & 0 & 0 \\ 0 & -1 & 0 & 0 \\ 0 & 0 & 0 & 1 \\ 0 & 0 & -1 & 0 \end{bmatrix} \begin{bmatrix} p_1 \\ q_1 \\ p_2 \\ q_2 \end{bmatrix} \quad (4.145)$$

Equations (4.145) show the possibility of a mirror image reflection around $p_1 = 0$ and $q_1 = 0$. A rotation of $\frac{1}{2}\pi$ in the $p_2 - q_2$ plane is also possible since the transformation matrix in the $p_2 - q_2$ plane is

$$\begin{bmatrix} 0 & 1 \\ -1 & 0 \end{bmatrix} \quad (4.146)$$

Consider, for example, fig. 4.20, which shows the projection of the limit cycles IX and X onto the $p_2 - q_2$ plane. It is obvious by inspection that there is a rotation of $\frac{1}{2}\pi$ between (a) and (b).

6. For $-1.9987 < \hat{\sigma}_2 < -1.9986$, the unstable limit cycle III separates the stable fixed point from the limit cycle II. Limit cycle I exists for $-1.9987 < \hat{\sigma}_2 < -1.9986$. As $t \rightarrow \infty$, the flow tends to one of the stable states depending on their domain of attraction. The unstable orbit III was achieved by changing the size of the integration step in the Aprile and Trick algorithm and by a short time integration (fig. 4.21). Figure 4.22 shows its accompanying stable orbit II. The two limit cycles collide and annihilate each other at $\hat{\sigma}_2 = -1.7861$.
7. The broadening of the power spectrum of q_1 (fig. 4.23c) compared with the spectra of the limit cycles in figs. 17d, 21d and 22d and the fractal nature of the poincare section (fig. 4.23d) indicate the chaotic nature of the attractor. To confirm the chaotic nature of this attractor, we calculate its Lyapunov exponents and fractal

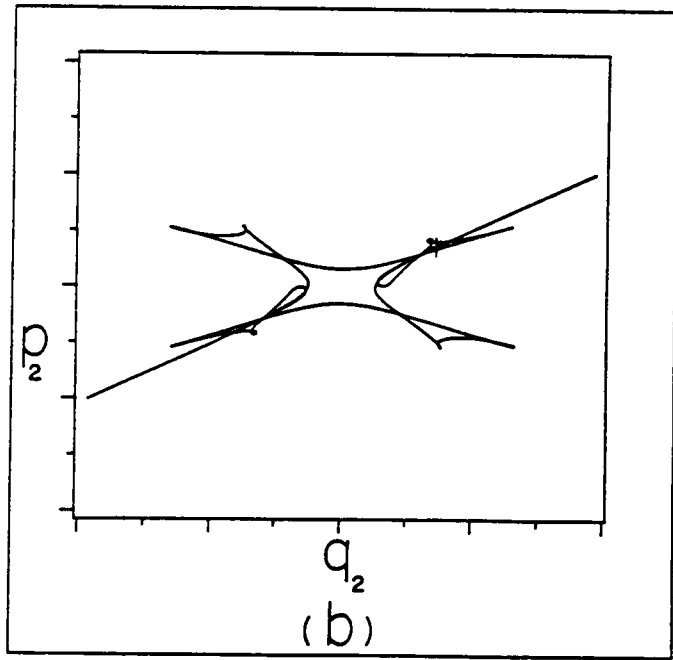
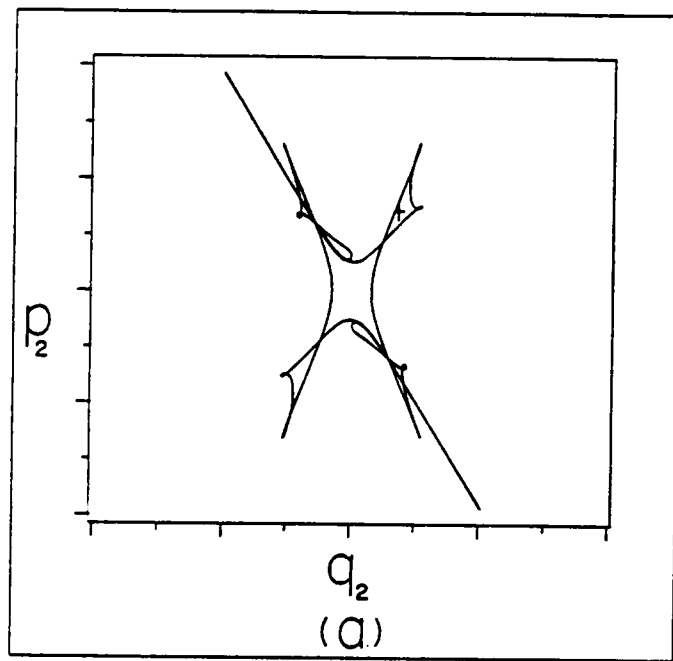


Figure 4.20. Projection of phase space on the $p_2 - q_2$ plane for $\hat{\sigma}_2 = 1.984$: (a) limit cycle IX and (b) limit cycle X.

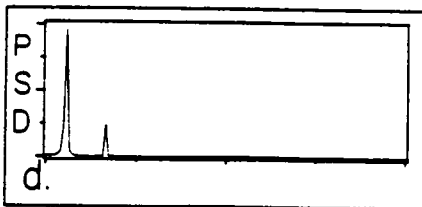
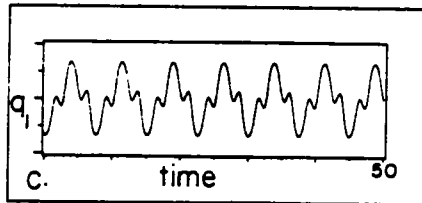
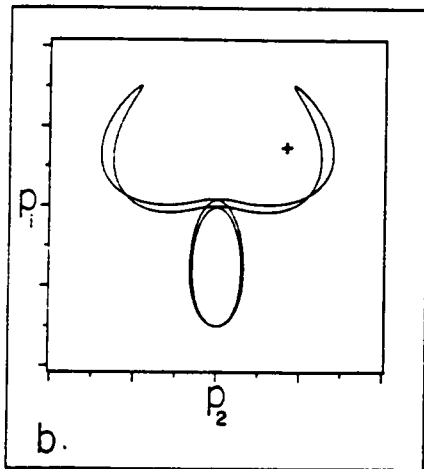
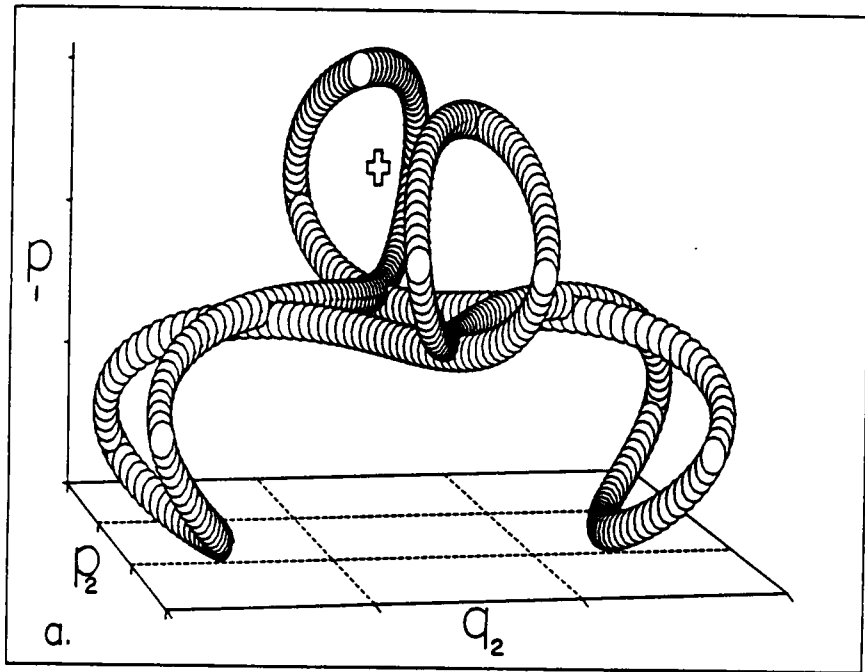


Figure 4.21. Limit cycle III (unstable): (a) projection of phase space on the 3-D space spanned by p_1 , p_2 and q_2 ; 'balloons' represent points on the limit cycle, (b) projection of phase space on the 2-D plane spanned by p_1 and p_2 , (c) waveform of q_1 , and (d) power spectral density (PSD) of the q_1 signal.

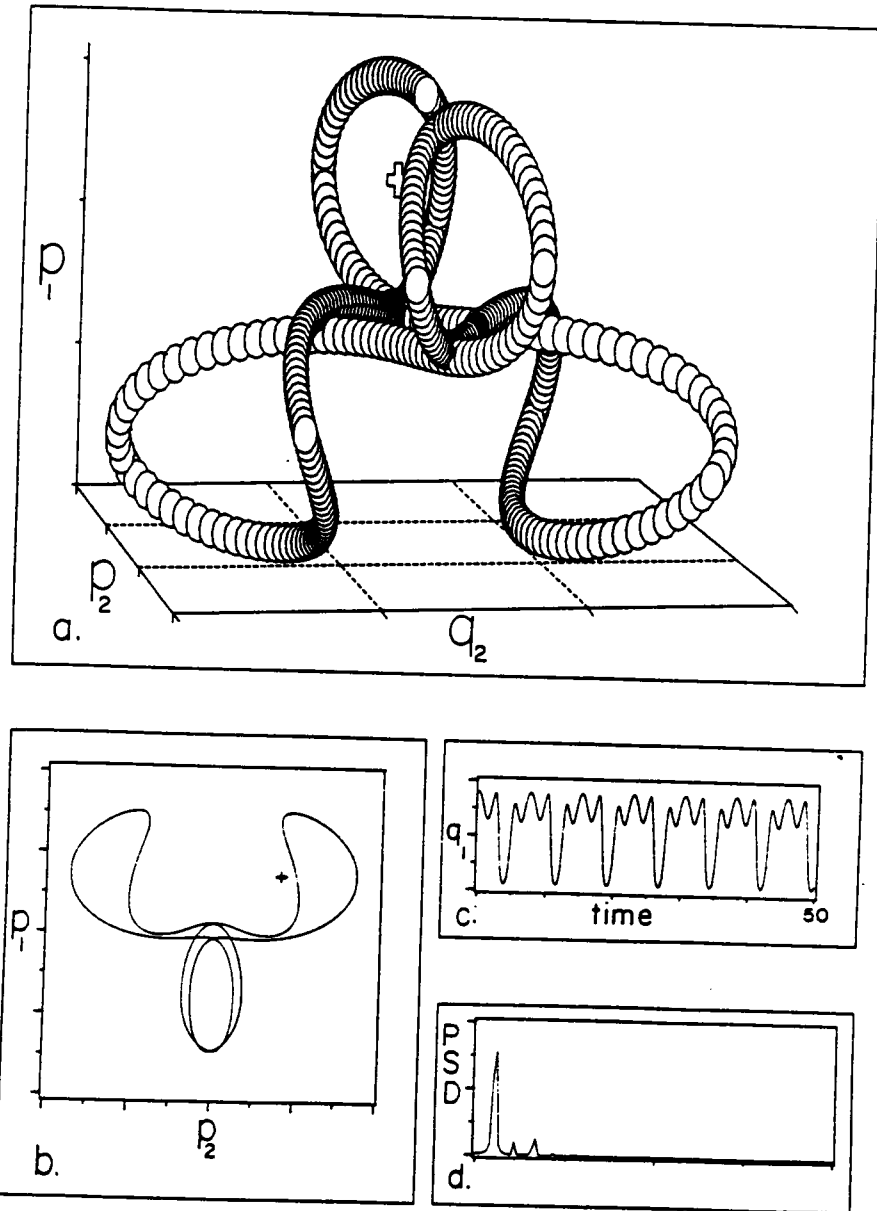


Figure 4.22. Limit cycle II: (a) projection of phase space on the 3-D space spanned by p_1 , p_2 and q_2 ; 'balloons' represent points on the limit cycle, (b) projection of phase space on the 2-D plane spanned by p_1 and p_2 , (c) waveform of q_1 , and (d) power spectral density (PSD) of the q_1 signal.

dimension. At $\hat{\sigma}_2 = -1.55$ (chaotic region VII), the Liapunov exponents are (0.566, 0.000, -0.057, -0.624) and the dimension $d_f \approx 3.8$.

8. Period-three motion is found over a very narrow range of $\hat{\sigma}_2$ (see fig. 4.16). Figure 4.24 shows a projection of this limit cycle.

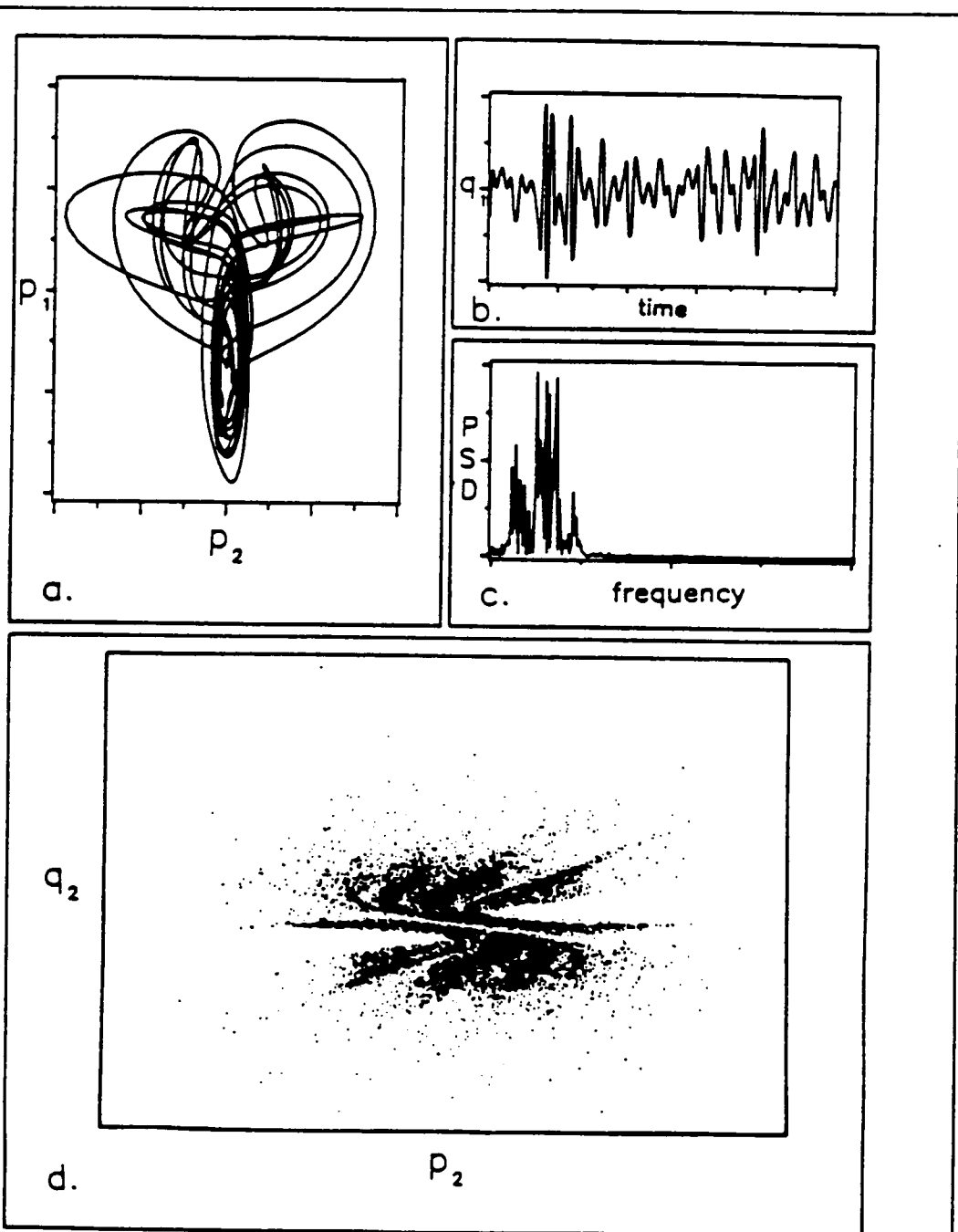


Figure 4.23. Chaotic attractor VII at $\hat{\sigma}_2 = -1.55$: (a) projection of phase space on the 2-D plane spanned by p_1 and p_2 , (b) waveform of q_1 , (c) power spectral density (PSD) of the q_1 signal, and (d) Poincaré section.

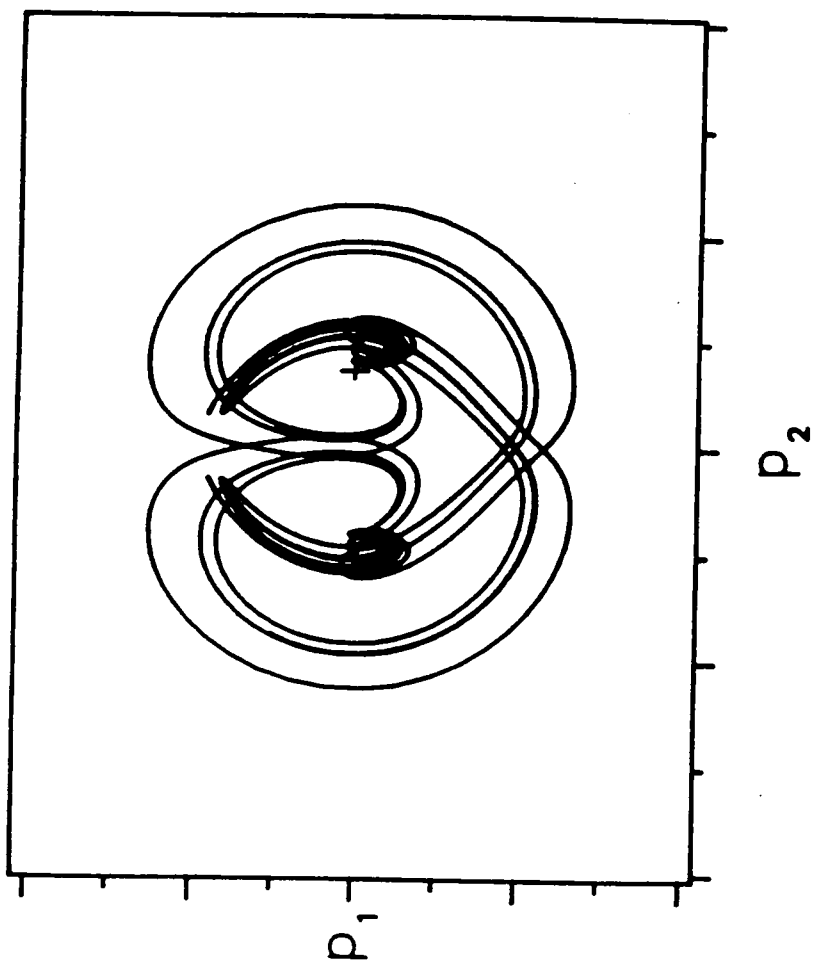


Figure 4.24. Limit cycle XII (period three motion): projection of phase space on the 2-D plane spanned by p_1 and p_2 .

CHAPTER 5

MODAL INTERACTION BETWEEN THE DRIVEN AND COMPANION MODES IN INFINITELY LONG CYLINDRICAL SHELLS

We use a computerized symbolic manipulator to perform a multiple time-scale analysis on the nonlinear equations of motion governing the dynamic response of infinitely long circular cylindrical shells. The equations contain quadratic and cubic nonlinearities. We analyze the case of primary resonance of one of the flexural modes, taking into account its interaction with its companion mode (one-to-one internal or autoparametric resonance). This autoparametric resonance can lead to traveling waves along the circumference of the shell when a standing wave is being excited. Four first-order ordinary differential equations are derived for the modulation of the amplitudes and phases of the interacting modes. The fixed points of the modulation equations provide the frequency-response curves. There are two

possible fixed-point solutions: a single-mode solution consisting of the driven mode only and a two-mode solution consisting of the driven and companion modes. As the excitation frequency varies, the fixed points of the single-mode solution suffer saddle-node collisions resulting in jumps. On the other hand, the fixed points of the two-mode solution go through a Hopf bifurcation. Beyond the Hopf bifurcation frequency, a numerical solution of the modulation equations shows that the fixed points lose stability and limit cycles (closed orbits) occur. For a range of excitation frequencies, the fixed points of the single-mode solution coexist with either fixed points or closed orbits of the two-mode solution, and hence the steady-state response depends on the initial conditions.

The equations of motion for infinitely long cylindrical shells have been derived in Chapter three up to cubic terms, see equations (3.28) and (3.29). These equations differ from those derived earlier by Evensen (1966) and Maewal (1978, 1981, 1986) due to the following:

1. They used the continuum mechanics strain measures, we used engineering strains. Moreover, Evensen (1966) used the Donnell-Mushtari-Vlasov assumptions.
2. They defined the radial and tangential displacements to be along and perpendicular to the undeformed radius. We defined the radial and tangential displacements to be along and perpendicular to the deformed radius.
3. They assumed that the deformations are inextensional, we didn't.
4. They neglected tangential inertia, we didn't.
5. They neglected terms of order $1/n^2$ compared to unity.
6. They retained bending terms only in the linear problem, we kept them up to quadratic terms.

For sake of completeness we list these equations below:

$$\begin{aligned}
\ddot{w} + w - \psi' + \alpha^2\{w^{iv} + 2w'' + w\} = & -\dot{\psi}^2 - \frac{1}{2}w'^2 - 2w\psi' + \psi'^2 + \psi'w'' - ww'' + w'\psi'' \\
& + w\dot{\psi}^2 - 2w'\psi''\psi' + \frac{1}{2}w'^2\psi' - w''\psi'^2 + \frac{3}{2}w''w'^2 - w\psi'^2 + ww'\psi'' - ww'^2 \\
& + ww''\psi' - w^2w'' + \alpha^2\left\{-\frac{11}{2}w'^2 + 4w''\psi' + 5w''\psi''' + 4\psi''w' - 6w''^2\right. \\
& + 8w'''\psi'' - 8w''w' + 4w^{iv}\psi' + w\psi''' - 11ww'' - 4ww^{iv} - 3w^2 + w'\psi^{iv}\} \\
& + \frac{a(1-\nu^2)}{Eh}P(1 + \psi' - w)
\end{aligned} \tag{5.1}$$

$$\begin{aligned}
\ddot{\psi} - \psi'' + w' = & 2w\ddot{\psi} + 2\dot{w}\dot{\psi} + w'w'' - 2w'\psi' - 2w\psi'' + 2ww' + ww''w' + w^2\psi'' \\
& - w'^2\psi'' + \frac{1}{2}w'^3 + 2ww'\psi' - 2w''w'\psi' - 2w\dot{w}\dot{\psi} - w^2\ddot{\psi} + \alpha^2\{w''w' \\
& - w''w''' - ww'''' + w^{iv}w'\}
\end{aligned} \tag{5.2}$$

5.1 Perturbation Solution

As in the previous chapters, we use the method of multiple-time scales to construct a second-order uniformly valid expansion for the solution of equations (5.1) and (5.2) for small but finite oscillations. We seek an asymptotic expansion of the displacement fields in the form

$$w(\tau, \theta) = \varepsilon w_1(T_0, T_1, T_2, \theta) + \varepsilon^2 w_2(T_0, T_1, T_2, \theta) + \varepsilon^3 w_3(T_0, T_1, T_2, \theta) + \dots \tag{5.3}$$

$$\psi(\tau, \theta) = \varepsilon \psi_1(T_0, T_1, T_2, \theta) + \varepsilon^2 \psi_2(T_0, T_1, T_2, \theta) + \varepsilon^3 \psi_3(T_0, T_1, T_2, \theta) + \dots \quad (5.4)$$

where $\varepsilon \ll 1$ is an artificial device introduced to indicate the smallness of the terms and $T_n = \varepsilon^n \tau$. Accordingly, $T_0, T_1,$ and T_2 are, respectively, the fast, slow, and slower time scales. The time derivatives transform as

$$\begin{aligned} \frac{\partial}{\partial \tau} &= D_0 + \varepsilon D_1 + \varepsilon^2 D_2 + \dots \\ \frac{\partial^2}{\partial \tau^2} &= D_0^2 + 2\varepsilon D_0 D_1 + \varepsilon^2 (2D_0 D_2 + D_1^2) + \dots \end{aligned} \quad (5.5)$$

where $D_n = \partial / \partial T_n$.

We consider the case in which the n^{th} mode is excited by a primary resonant pressure of the form

$$\frac{a(1 - \nu^2)}{Eh} P = \frac{1}{2} \varepsilon^3 f \cos n\theta e^{i\Omega T_0} + \text{c.c.} \quad (5.6)$$

where c.c. stands for the complex conjugate of the preceding terms. Later analysis shows that there is no functional dependence on T_1 ; thus we remove the T_1 dependence in the proceeding analysis.

Substituting equations (5.3)-(5.6) into (5.1) and (5.2) and equating coefficients of like powers of ε , we obtain equations governing the w_n and ψ_n , which can be solved in succession. To first order,

$$D_0^2 w_1 + w_1 - \psi_1' + \alpha^2 (w_1^{IV} + 2w_1'' + w_1) = 0 \quad (5.7)$$

$$D_0^2 \psi_1 - \psi_1'' + w_1' = 0 \quad (5.8)$$

whose solution is

$$w_1(\theta, T_0, T_2) = \sum_{m=0}^{\infty} \{ A_m(T_2) \cos m\theta + B_m(T_2) \sin m\theta \} e^{i\omega_m T_0} + \text{c.c.} \quad (5.9)$$

$$\psi_1(\theta, T_0, T_2) = \sum_{m=0}^{\infty} \{ \Gamma_m A_m(T_2) \sin m\theta - \Gamma_m B_m(T_2) \cos m\theta \} e^{i\omega_m T_0} + \text{c.c.} \quad (5.10)$$

where ω_m is the natural frequency of the m^{th} mode, which is given by equation (4.18), and Γ_m is the amplitude ratio given by equation (4.19). The mode $\cos n\theta$ is called the driven mode and the mode $\sin n\theta$ is called the companion mode.

Out of the infinite modes present in w_1 and ψ_1 and in the presence of viscous damping, only the modes which are coupled through resonance conditions will contribute to the steady-state response; Thus to proceed further, we need to identify the resonance conditions. We assume that the n^{th} mode is not coupled with any other mode through an internal resonance. Therefore, the response will consist of the driven and companion modes only and hence, we replace equations (5.9) and (5.10) with

$$w_1(\theta, T_0, T_2) = [A_n(T_2) \cos n\theta + B_n(T_2) \sin n\theta] e^{i\omega_n T_0} + \text{c.c.} \quad (5.11)$$

$$\psi_1(\theta, T_0, T_2) = [\Gamma_n A_n(T_2) \sin n\theta - \Gamma_n B_n(T_2) \cos n\theta] e^{i\omega_n T_0} + \text{c.c.} \quad (5.12)$$

We note that each of w_1 and ψ_1 contains two modes; namely, $\cos n\theta$ and $\sin n\theta$. We call the first one the driven mode because it has the same spatial variation as the excitation. The second mode is called the companion mode. Because A_n is the amplitude of the driven mode and B_n is the amplitude of the companion mode, the linear analysis predicts that $A_n \neq 0$ and $B_n = 0$. However, the nonlinearities make it

possible for the companion mode to participate in the steady-state response. To describe the nearness of Ω to ω_n , we introduce a detuning parameter σ defined according to

$$\Omega = \omega_n + \varepsilon^2 \sigma \quad (5.13)$$

Using the first-order solution, we write the second-order equations as

$$\begin{aligned} D_0^2 w_2 + w_2 - \psi_2 + \alpha^2 \{ w_2^{IV} + 2w_2'' + w_2 \} &= -(D_0 \psi_1)^2 + \psi_1'^2 + w_1' \psi_1'' - \frac{1}{2} w_1'^2 + w_1'' \psi_1' \\ &- 2w_1 \psi_1' - w_1 w_1'' + \alpha^2 \{ -11w_1 w_1'' - 3w_1^2 - 4w_1 w_1^{IV} + w_1 \psi_1''' + 4w_1' \psi_1'' + 4w_1^{IV} \psi_1' \\ &- 8w_1''' w_1 + 8w_1''' \psi_1'' - 6w_1''^2 + 5w_1'' \psi_1''' + 4w_1'' \psi_1' - \frac{11}{2} w_1'^2 + w_1' \psi_1^{IV} \} \\ &= \{ c_1(A_n^2 - B_n^2) \cos 2n\theta + 2c_1 A_n B_n \sin 2n\theta + c_2(A_n^2 + B_n^2) \} \exp(2i\omega_n T_0) \\ &+ \frac{1}{2} c_3(B_n \bar{B}_n - A_n \bar{A}_n) \cos 2n\theta - c_3 \bar{A}_n B_n \sin 2n\theta - c_4(\bar{B}_n B_n + \bar{A}_n A_n) + \text{c.c.} \end{aligned} \quad (5.14)$$

$$\begin{aligned} D_0^2 \psi_2 - \psi_2'' + w_2' &= 2D_0 w_1 D_0 \psi_1 - 2w_1' \psi_1' + w_1'' w_1' + 2w_1 D_0^2 \psi_1 - 2w_1 \psi_1'' \\ &+ 2w_1 w_1' + \alpha^2 \{ w_1'' w_1' + w_1' w_1^{IV} - w_1''' w_1'' - w_1 w_1''' \} \\ &= \{ d_1(A_n^2 - B_n^2) \sin 2n\theta - 2d_1 A_n B_n \cos 2n\theta \} \exp(2i\omega_n T_0) \\ &+ \frac{1}{2} d_2(\bar{B}_n B_n - \bar{A}_n A_n) \sin 2n\theta + d_2 \bar{A}_n B_n \cos 2n\theta \end{aligned} \quad (5.15)$$

where the c_i and d_i are defined in Appendix A. The solution of the second-order problem is

$$\begin{aligned}
w_2(\theta, T_0, T_2) = & \frac{1}{\Delta_n} \{ [4c_1(n^2 - \omega_n^2) + 2nd_1][A_n^2 - B_n^2] \cos 2n\theta + [8(n^2 - \omega_n^2)c_1 + 4nd_1] \\
& \times A_n B_n \sin 2n\theta + \frac{c_2}{1 + \alpha^2 - 4\omega_n^2} (A_n^2 + B_n^2) \} e^{2i\omega_n T_0} \\
& - \frac{c_4}{1 + \alpha^2} (\bar{B}_n B_n + \bar{A}_n A_n) + \frac{1}{\Theta_n} \{ [2n^2 c_3 + nd_2][B_n \bar{B}_n - A_n \bar{A}_n] \cos 2n\theta \\
& - [4n^2 c_3 + 2nd_2] \bar{A}_n B_n \sin 2n\theta \} + \text{c.c.}
\end{aligned} \tag{5.16}$$

$$\begin{aligned}
\psi_2(\theta, T_0, T_2) = & \frac{1}{\Delta_n} \{ [(1 - 4\omega_n^2 + \alpha^2(4n^2 - 1)^2)d_1 + 2nc_1][A_n^2 - B_n^2] \sin 2n\theta \\
& - 2[(1 - 4\omega_n^2 + \alpha^2(4n^2 - 1)^2)d_1 + nc_2] A_n B_n \cos 2n\theta \} e^{2i\omega_n T_0} \\
& + \frac{1}{\Theta_n} [(1 + \alpha^2(4n^2 - 1)^2) \frac{d_2}{2} + nc_4] [\bar{B}_n B_n - \bar{A}_n A_n] \sin 2n\theta \\
& + \frac{1}{\Theta_n} [(1 + \alpha^2(4n^2 - 1)^2)d_2 + 2nc_4] \bar{A}_n B_n \cos 2n\theta + \text{c.c.}
\end{aligned} \tag{5.17}$$

where

$$\Delta_n = 4(n^2 - \omega_n^2)[1 - 4\omega_n^2 + \alpha^2(4n^2 - 1)^2] - 4n^2 \tag{5.18}$$

$$\Theta_n = 4n^2 \alpha^2 (4n^2 - 1)^2 \tag{5.19}$$

Using the first- and second-order solutions, we write the third-order problem as

$$\begin{aligned}
D_0^2 w_3 + w_3 - \psi_3' + \alpha^2 \{ w_3^{IV} + 2w_3'' + w_3 \} = & \{ E_1 B_n A_n \bar{A}_n + E_2 B_n^2 \bar{B}_n + E_3 A_n^2 \bar{B}_n - 2i\omega_n B_n' \} \sin n\theta e^{i\omega_n T_0} \\
& + \left\{ E_1 A_n B_n \bar{B}_n + E_2 A_n^2 \bar{A}_n + E_3 B_n^2 \bar{A}_n - 2i\omega_n A_n' + \frac{1}{2} f e^{i\sigma T_2} \right\} \cos n\theta e^{i\omega_n T_0} \\
& + NST + \text{c.c.}
\end{aligned} \tag{5.20}$$

$$\begin{aligned}
D_0^2 \psi_3 - \psi_3'' + w_3' = & \{G_1 B_n A_n \bar{A}_n + G_2 B_n^2 \bar{B}_n + G_3 A_n^2 \bar{B}_n + 2i\omega_n \Gamma_n B_n'\} \cos n\theta e^{i\omega_n T_0} \\
& - \{G_1 A_n \bar{B}_n B_n + G_2 A_n^2 \bar{A}_n + G_3 B_n^2 \bar{A}_n + 2i\omega_n \Gamma_n A_n'\} \sin n\theta e^{i\omega_n T_0} + NST \\
& + c.c.
\end{aligned} \tag{5.21}$$

where NST stands for terms that do not produce secular terms and the E_j and G_j are constants defined in Appendix B. Equations (5.20) and (5.21) constitute a system of inhomogeneous differential equations whose homogeneous part has a nontrivial solution. Thus, for the inhomogeneous system to have a solution, the right-hand side of these equations must be orthogonal to each solution of the adjoint homogeneous problem. This condition yields the following modulation equations:

$$\begin{aligned}
-2i\omega_n(1 + \Gamma_n^2)A_n' + (E_1 - \Gamma_n G_1)A_n B_n \bar{B}_n + (E_2 - \Gamma_n G_2)A_n^2 \bar{A}_n + (E_3 - \Gamma_n G_3)B_n^2 \bar{A}_n \\
+ \frac{1}{2} f e^{i\sigma T_2} = 0
\end{aligned} \tag{5.22}$$

$$-2i\omega_n(1 + \Gamma_n^2)B_n' + (E_1 - \Gamma_n G_1)B_n A_n \bar{A}_n + (E_2 - \Gamma_n G_2)B_n^2 \bar{B}_n + (E_3 - \Gamma_n G_3)A_n^2 \bar{B}_n = 0 \tag{5.23}$$

Equations (5.22) and (5.23) are a special case of the equations derived by Nayfeh and Pai (1989) for the non-planar parametric responses of inextensional beams. On the other hand, they can be reduced to the form of the equations of Miles (1984 a,b,c) and Maewal (1986) by setting $E_3 = G_3 = 0$.

To analyze the solutions of equations (5.22) and (5.23), we let

$$A_n = \frac{1}{2} \{p_1(T_2) - i q_1(T_2)\} e^{i\sigma T_2}, \quad B_n = \frac{1}{2} \{p_2(T_2) - i q_2(T_2)\} e^{i\sigma T_2} \tag{5.24}$$

Substituting equations (5.24) into equations (5.22) and (5.23) and separating real and imaginary parts, we obtain

$$8\omega_n p'_1 = -8\omega_n \mu_n p_1 - 8\omega_n \sigma q_1 + (\delta_3 - \delta_1) p_2^2 q_1 - (\delta_1 + \delta_3) q_2^2 q_1 - 2\delta_3 p_1 p_2 q_2 - \delta_2 p_1^2 q_1 - \delta_2 q_1^3$$

(5.25)

$$8\omega_n q'_1 = -8\omega_n \mu_n q_1 + 8\omega_n \sigma p_1 + (\delta_1 - \delta_3) q_2^2 p_1 + (\delta_1 + \delta_3) p_2^2 p_1 + 2\delta_3 q_1 p_2 q_2 + \delta_2 q_1^2 p_1 + \delta_2 p_1^3 + F$$

(5.26)

$$8\omega_n p'_2 = -8\omega_n \mu_n p_2 - 8\omega_n \sigma q_2 + (\delta_3 - \delta_1) p_1^2 q_2 - (\delta_1 + \delta_3) q_1^2 q_2 - 2\delta_3 p_1 p_2 q_1 - \delta_2 p_2^2 q_2 - \delta_2 q_2^3$$

(5.27)

$$8\omega_n q'_2 = -8\omega_n \mu_n q_2 + 8\omega_n \sigma p_2 + (\delta_1 - \delta_3) q_1^2 p_2 + (\delta_1 + \delta_3) p_1^2 p_2 + 2\delta_3 q_2 p_1 q_1 + \delta_2 q_2^2 p_2 + \delta_2 p_2^3$$

(5.28)

where $\delta_l = (E_l - \Gamma_n G_l)/(1 + \Gamma_n^2)$ for $l = 1, 2, 3$ and $F = -4f/(1 + \Gamma_n^2)$. Modal damping has been added to equations (5.25)-(5.28) with μ_n being the damping coefficient of the n^{th} flexural mode. These equations are a generalization of the equations derived by Miles (1984a,b), Miles (1984c), and Maewal (1986) for the nonlinear forced response of surface waves, spherical pendulums, and axisymmetric shells, respectively.

5.2 Numerical Simulation

Next we present numerical results for the case $\Omega \simeq \omega_2$, $\mu_2 = 0.05$, $f = 2.0$, and $\alpha^2 \simeq 2.0918 \times 10^{-4}$. In this case $\omega_2 \simeq 0.0388$ and $\delta_1 \simeq -17.61$, $\delta_2 \simeq 2.63$, and $\delta_3 \simeq 20.21$. We

use the detuning parameter σ as the bifurcation parameter and study the behavior of the solution of the modulation equations (5.25) - (5.28) as σ varies, this is tantamount to varying the excitation frequency Ω .

The frequency-response curves are shown in fig. 5.1. There are two possible steady-state solutions: a single-mode solution and a two-mode solution. In the single-mode response, only the driven mode responds with amplitude A_2 while the companion mode has a zero amplitude, $B_2 = 0$. This results in a standing wave along the circumference of the shell. For this solution and for large positive values of σ , the fixed point of the modulation equations is stable, the Jacobi matrix has two complex conjugate eigenvalues with negative real parts and two real negative eigenvalues. As σ decreases, one of the real eigenvalues moves towards the right-half plane and eventually crosses zero along the real axis at $\sigma \simeq 35.63$ (saddle-node bifurcation), this results in a jump to the two-mode response. We note that if we approach the jump point (at $\sigma \simeq 35.63$) along the unstable two-mode solution, a positive and a negative real eigenvalue approach each other along the real axis and eventually collide at zero (linear degeneracy). Starting at a large negative value of σ and with the proper choice of initial conditions, one finds that the steady-state flow is attracted to the lower stable branch of the single-mode response. As σ increases, one of the real eigenvalues of the fixed point approaches zero along the negative real axis and touches the imaginary axis at $\sigma \simeq -29.97$, resulting in a jump to the two-mode response.

We consider the one-to-one mapping y such that

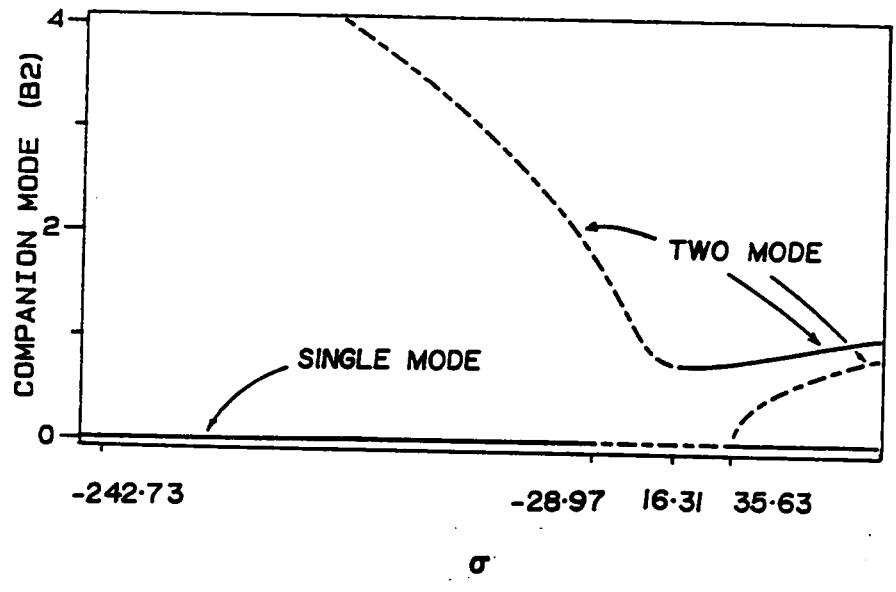
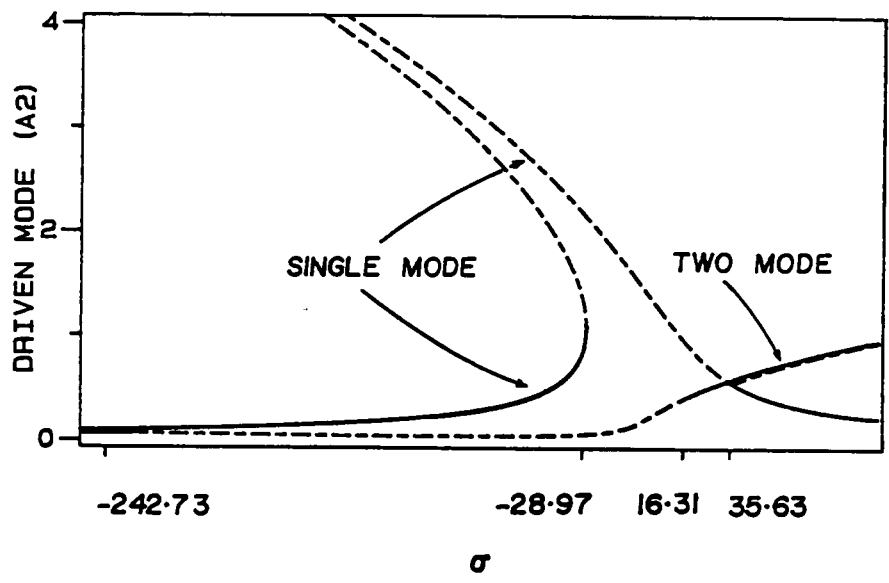


Figure 5.1. Frequency-response curves for $F = -6.4$: Solid (dashed) lines indicate stable (unstable) fixed points.

$$\gamma : \begin{bmatrix} p_1 \\ q_1 \\ p_2 \\ q_2 \end{bmatrix} \rightarrow \begin{bmatrix} p_1 \\ q_1 \\ -p_2 \\ -q_2 \end{bmatrix} \quad (5.29)$$

The system of equations (5.25)-(5.28) is γ -equivariant; that is, γ is a group of symmetries of the modulation equations. We note that the phase space is symmetric with respect to $p_2 = 0$ and $q_2 = 0$. Due to the above symmetry, asymmetric attractors exist in pairs but their stability characteristics are identical. The symmetry group acts on the amplitudes of the companion mode and thus can only be observed in the two-mode response. Figure 5.2 is the frequency-response curves for p_2 and q_2 , the various solutions in each graph are related through the transformation (5.29).

In the two-mode solution, both the driven and companion modes are present in the steady-state response ($A_2 \neq 0, B_2 \neq 0$). This results in a wave traveling along the circumference of the shell. For a large positive value of σ and with the proper choice of initial conditions, the flow may be attracted to the two-mode solution. As σ decreases, the amplitudes of the driven and companion modes (A_2 and B_2) decrease. At $\sigma \simeq 16.31$, the fixed point loses its stability through a Hopf bifurcation.

Figure 5.3 is a schematic bifurcation diagram for the orbits of the system (5.25)-(5.28) between the two Hopf bifurcation frequencies $\sigma = -242.73$ and $\sigma = 16.31$. There are two pairs of asymmetric branches of periodic solutions between the two Hopf bifurcation frequencies. One pair consists of the attractors 1-3-7 and their reflection 2-4-8, they are related through the transformation (5.29). The other pair consists of attractors 5-chaos-9 and its reflection 6-chaos-10, they are also related through the transformation (5.29). Because the stability characteristics for a branch

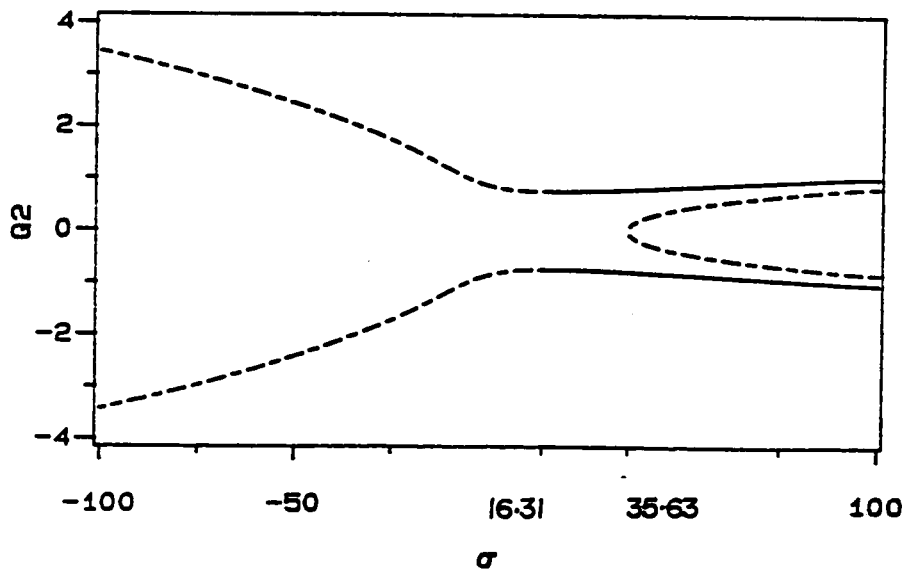
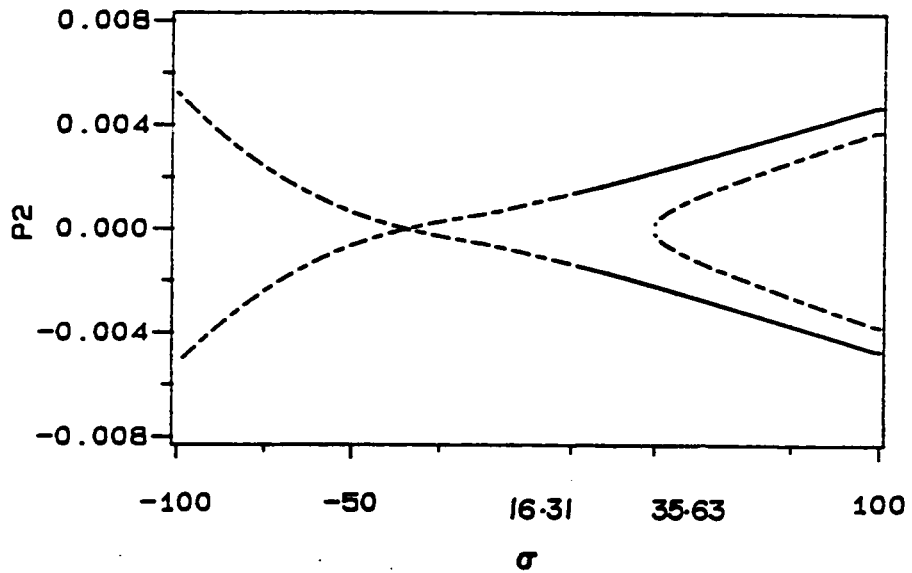


Figure 5.2. Frequency-response curves for the companion mode: The trivial solution is not shown.

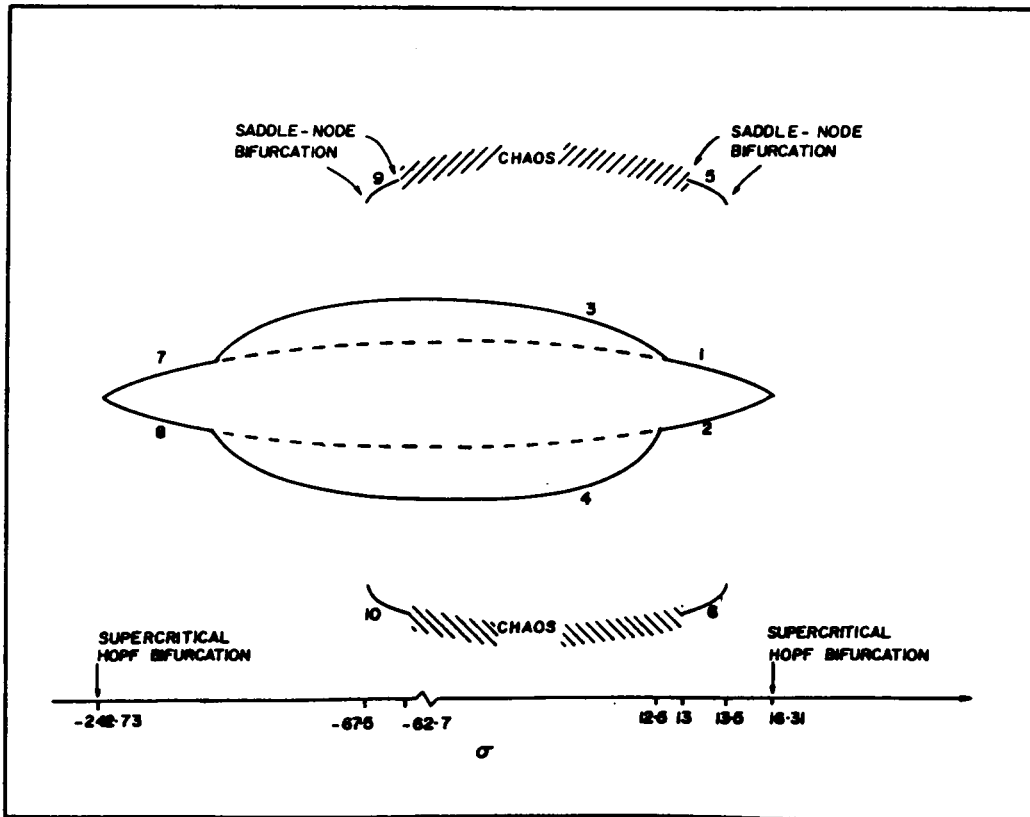


Figure 5.3. A schematic bifurcation diagram for the orbits of the modulation equations: Solid (dashed) lines indicate stable (unstable) orbits. Odd and even-numbered attractors are related through the mapping (5.29).

are the same as those of its reflection, we only follow the upper branch (odd numbered).

We follow the inner branch 1-3-7 as σ decreases. Attractor 1 starts at $\sigma \simeq 16.31$ through a supercritical Hopf bifurcation, its period is approximately 0.3. Figure 5.4 is the two-dimensional projection of this attractor and its reflection on the plane spanned by $q_1 - q_2$. At $\sigma \simeq 12.5$, attractor 1 goes through a period-doubling bifurcation giving birth to attractor 3 with the period $\simeq 0.6$ (fig. 5.5). The original unstable orbit of period 0.3 continues to coexist with the period-doubled one. Eventually, orbit 3 goes through a period-halving bifurcation and attractor 1 reappears as attractor 7.

Next we follow the second branch of periodic orbits (5-chaos-9) by decreasing σ . Attractor 5 is born at $\sigma \simeq 13.5$ through a saddle-node collision (cyclic-fold bifurcation). Figure 5.6 is the two-dimensional projection of this attractor and its reflection on the $q_1 - q_2$ plane. As σ decreases, this attractor deforms and at $\sigma \simeq 13.0$, it suffers another tangent bifurcation. Consequently, the flow jumps to a chaotic attractor. Figure 5.7 is the two-dimensional projection of this chaotic attractor. Figure 5.8 is the power spectral density (PSD) of the q_1 signal, the broad-band spectrum indicates chaos. To confirm the chaotic nature of this attractor, we calculate its Lyapunov exponents. The Lyapunov exponent at $\sigma = 10.0$ are 12.9, 0.0, -0.2, and -13.0, this attractor is also strange because it has a fractal dimension $d_f = 3.9^4$. A Poincare' section of the chaotic attractor at $q_1 = 0.0$ also shows the fractal nature of this attractor. Because the phase space is four-dimensional, the Poincare' section is three-dimensional. Figures 5.9 a-c are the three projections of the Poincare' section and confirm its fractal nature. This chaotic attractor can also be reached from the left in the same

⁴ We use the relation proposed by Frederickson et. al. (1983).

manner; that is, attractor 9 is born through a saddle-node bifurcation at $\sigma \simeq -67.5$ and at $\sigma \simeq -62.7$ it suffers a saddle-node collision which results in a jump to the chaotic attractor. Figure 5.10 is the two-dimensional projection of attractor 9 and its reflection on the $q_1 - q_2$ plane.

The above results agree qualitatively with the results of Miles (1984 b,c), Maewal (1986), and Bajaj and Johnson (1989). Miles (1984 b) and Maewal (1986) integrated the modulation equations for discrete values of the detuning parameter and found fixed points, limit cycles, period-doubled limit cycles, and chaos. However, they did not report multiple solutions and coexisting attractors. Miles (1984 c) found that chaos can be reached through a sequence of period-doubling bifurcations. He did not report coexisting attractors. Bajaj and Johnson (1989) studied the nonlinear dynamics of a string. They note that their averaged equations are similar to Miles' evolution equations and studied their periodic solutions. They reported two branches of periodic solutions. These two branches coexist for certain ranges of the detuning parameters. One branch goes through an incomplete sequence of period-doubling bifurcations followed by period-halving bifurcations and does not become chaotic. This corresponds to branch 1-3-7 (and 2-4-8) in fig. 5.3. The other branch in Bajaj and Johnson's study is created inside the Hopf region through a saddle-node collision and goes through a cascade of period-doubling bifurcations culminating in chaos. Branch 5-chaos-9 (and 6-chaos-8) in fig. 5.3 resemble this branch in that it too is created through saddle-node collisions. However, branch 5-chaos-9 in fig. 5.3 become chaotic through saddle-node collisions and not through period-doubling bifurcations.

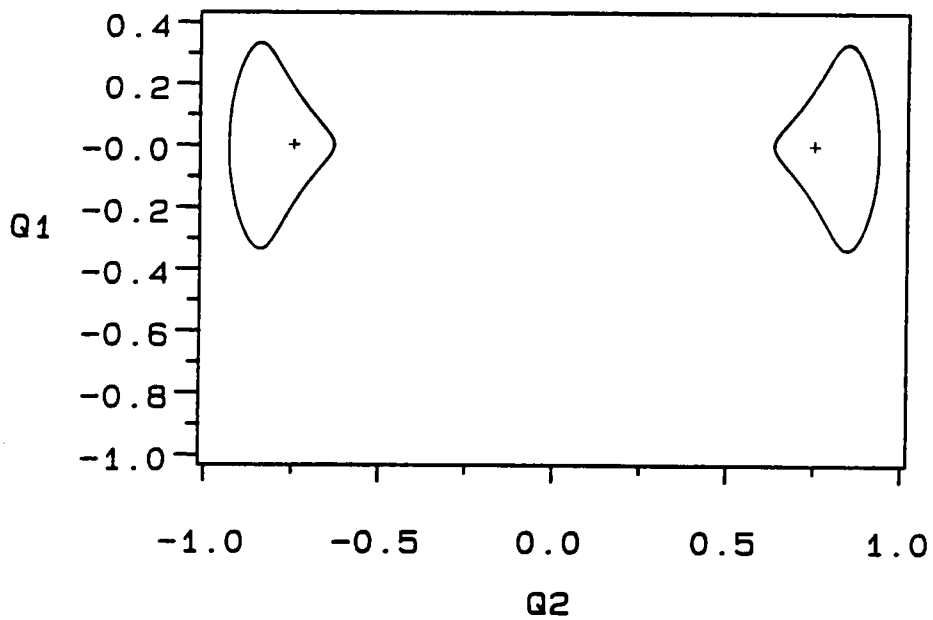


Figure 5.4. A two-dimensional projection of attractors 1 and 2 at $\sigma = 14.0$: The crosses indicate the unstable fixed points.

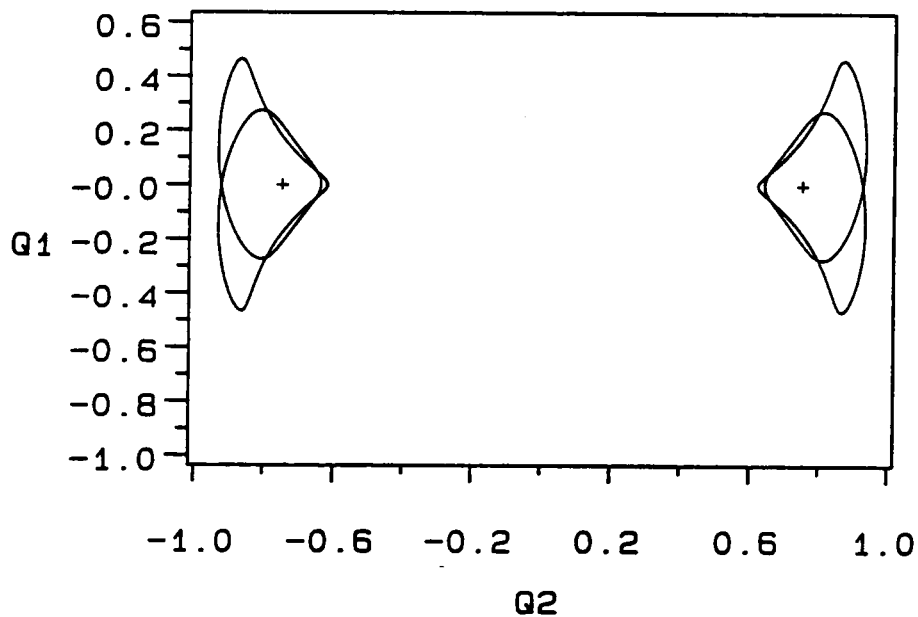


Figure 5.5. A two-dimensional projection of the period-doubled attractors 3 and 4 at $\sigma = 12.40$: The crosses indicate the unstable fixed points.

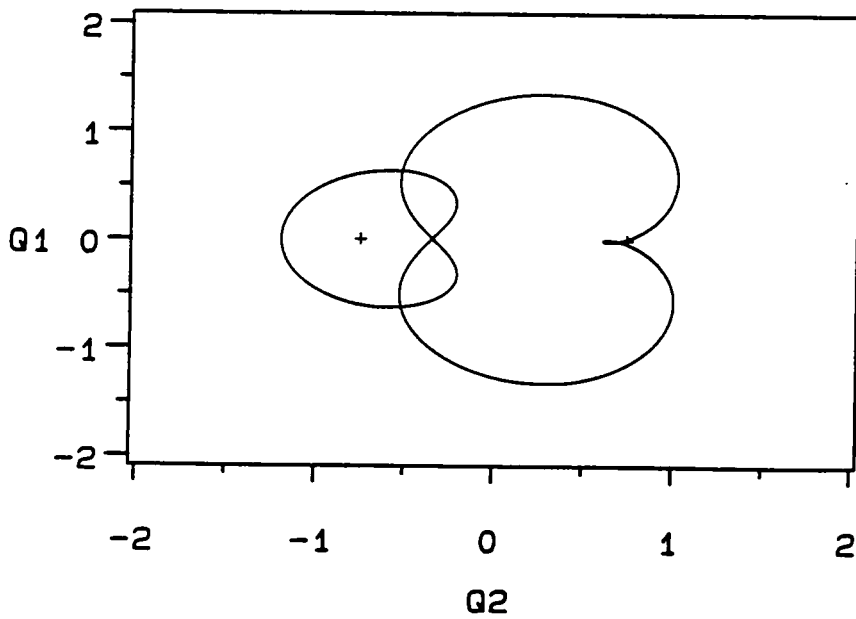
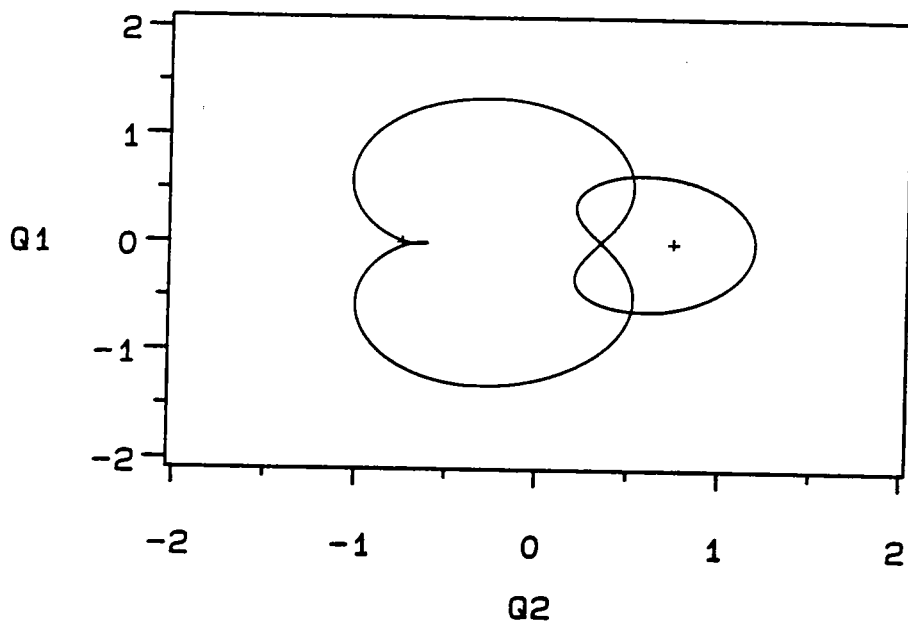


Figure 5.6. A two-dimensional projection of attractors 5 and 6 at $\sigma = 13.3$: The crosses indicate the unstable fixed points.

We note that for some intervals of σ , multiple stable solutions coexist. The steady-state response for a given frequency of excitation in these intervals depends on the initial conditions and basins of attraction of each solution.

5.3 Comparison with Maewal (1981, 1986a)

As we noted earlier, equations (5.22) and (5.23) are a generalized form of those derived by Maewal (1981, 1986a). In this section we consider the kinematic relationships used by Maewal in his study and the ones we use (Chapter three). The main difference between our kinematic relationships and those of Maewal is that his expression for the change in curvature does not contain quadratic terms whereas ours does. In what follows we show that due to the inextensionality assumptions, the form that Maewal used for the change of curvature is a special form of the one we use. To this end, we use the inextensionality condition to eliminate the quadratic terms from our expression for the change in curvature. We start with the kinematic relations derived in Chapter three:

$$\varepsilon_\theta = \text{strain along the } \theta\text{-coordinate line} = \psi' - w + \frac{1}{2} w'^2 - w\psi' \quad (5.30)$$

$$\begin{aligned} \chi_\theta &= \text{change in curvature of the middle surface} \\ &= \frac{1}{a} \left\{ w + w'' + w^2 + 2ww'' + \frac{1}{2} w'^2 - 2\psi'w'' - w'\psi''' \right\} \end{aligned} \quad (5.31)$$

The inextensionality condition dictates that

$$\varepsilon_\theta = 0 \quad (5.32)$$

Then, it follows from equation (5.30) that

$$w = \psi' + \frac{1}{2} w'^2 - w\psi' \quad (5.33)$$

Differentiating equation (5.33) with respect to θ once we obtain

$$w' = \psi'' + w'w'' - w\psi'' - w'\psi' \quad (5.34)$$

Substituting equations (5.33) and (5.34) into equation (5.31) we have

$$\chi_\theta = \psi' + w'' + w'w''\psi'' - w\psi''^2 - w'\psi'\psi'' + \frac{1}{2} w'^2\psi' - w\psi'^2 + w'^2w'' - 2ww''\psi' \quad (5.35)$$

The form of equation (5.35) agrees with the form used by Maewal (1981) in that it contains no quadratic terms. This shows that Maewal's expression for the change in curvature is a special case of ours.

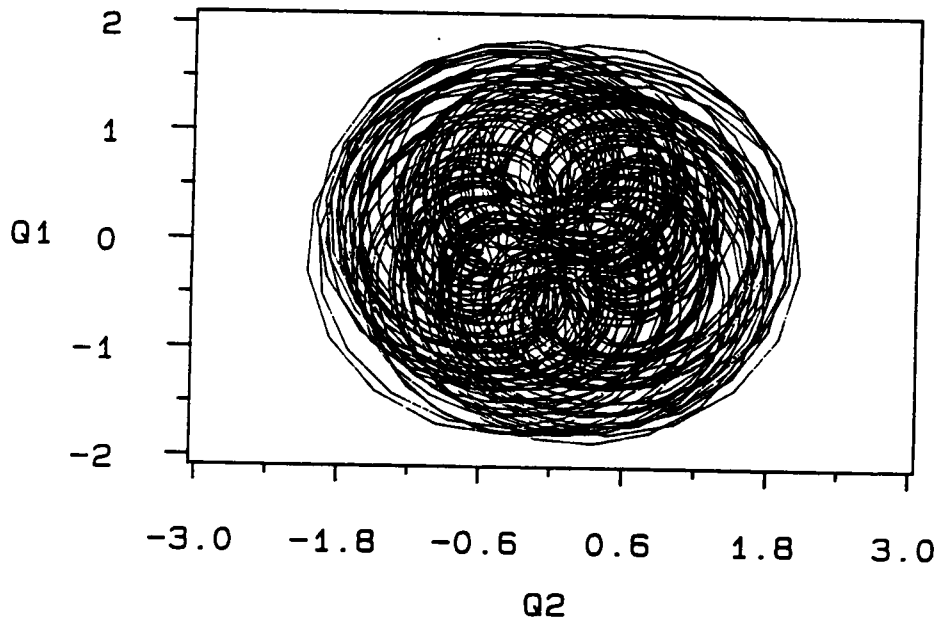
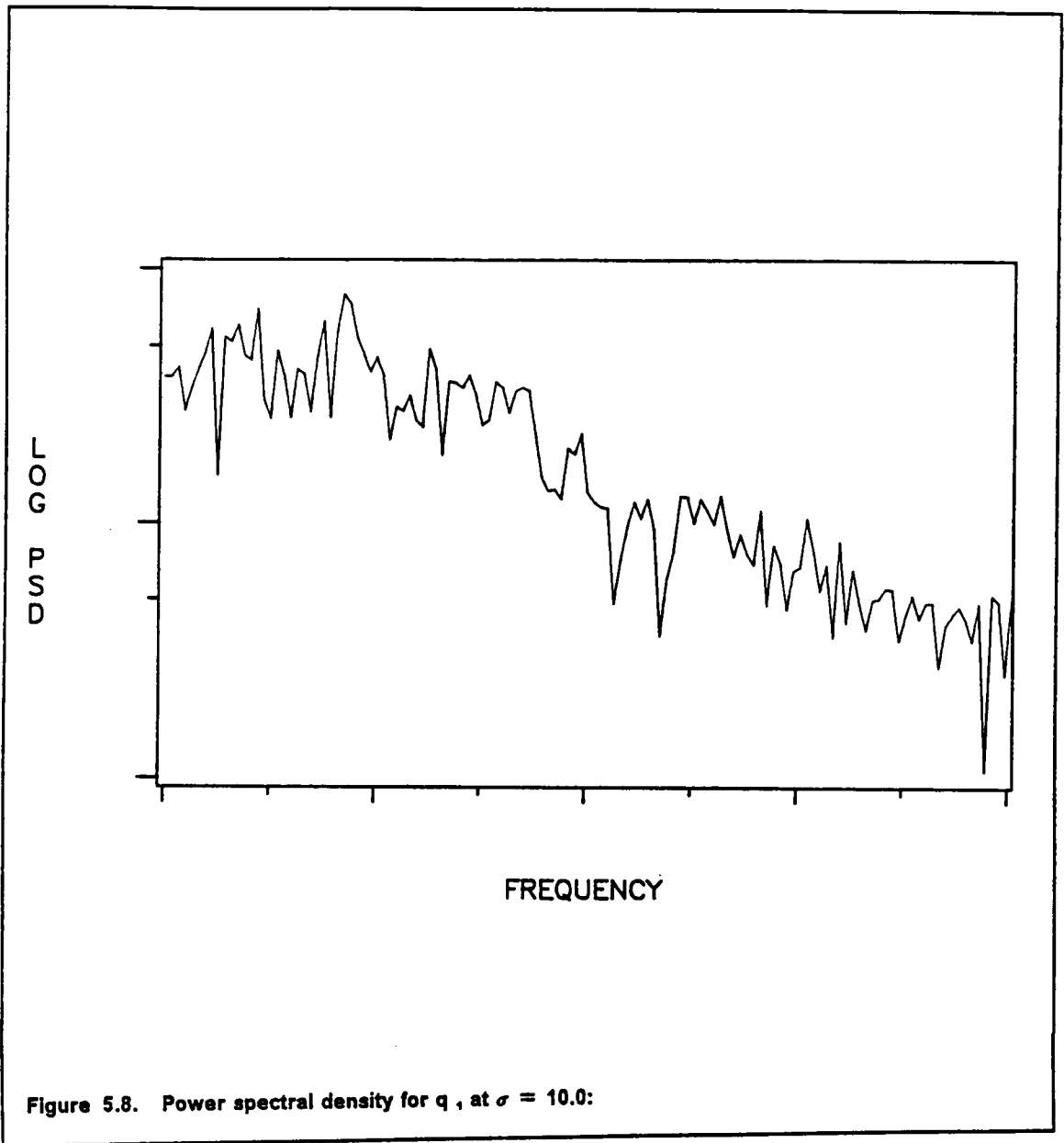


Figure 5.7. A two-dimensional projection of the chaotic attractor at $\sigma = 10.0$:



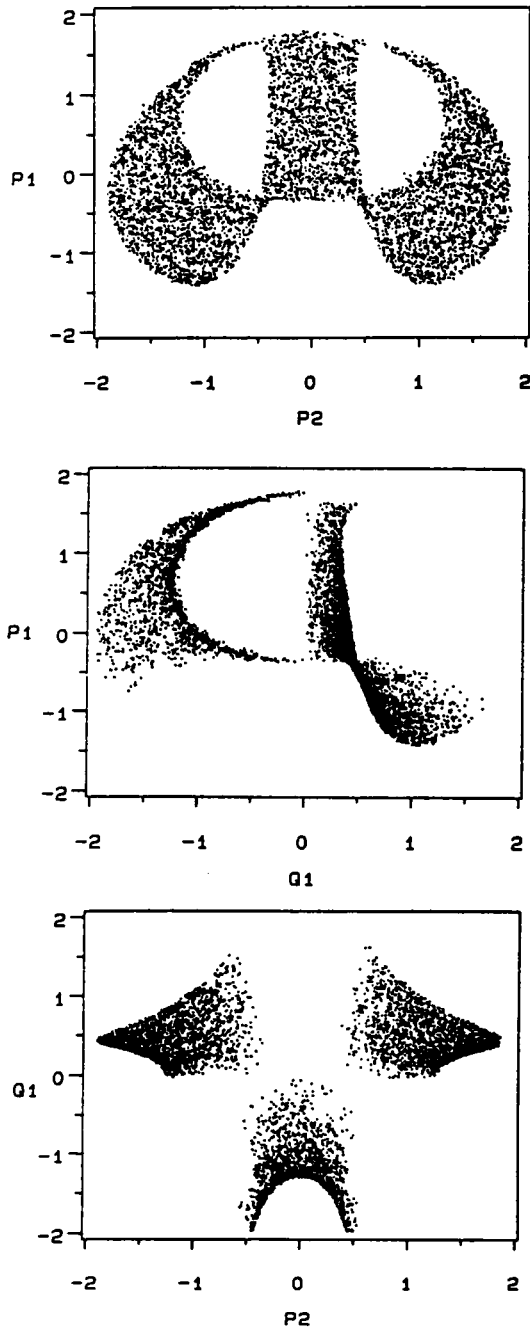


Figure 5.9. Different two-dimensional projections of the Poincaré section of the chaotic attractor: Section taken at $q_1 = 0.0$ and $\sigma = 10.0$.

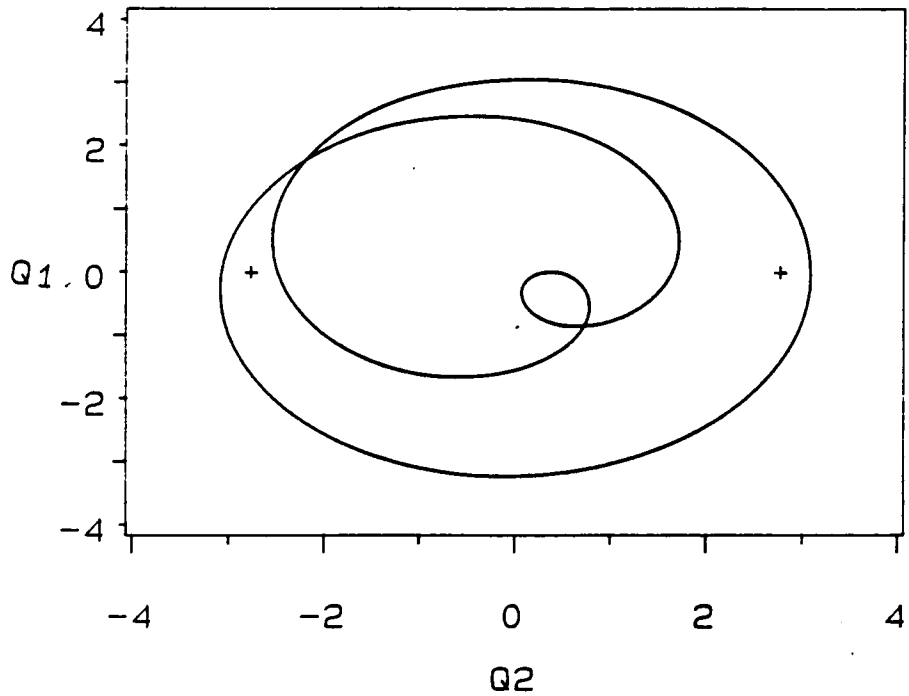
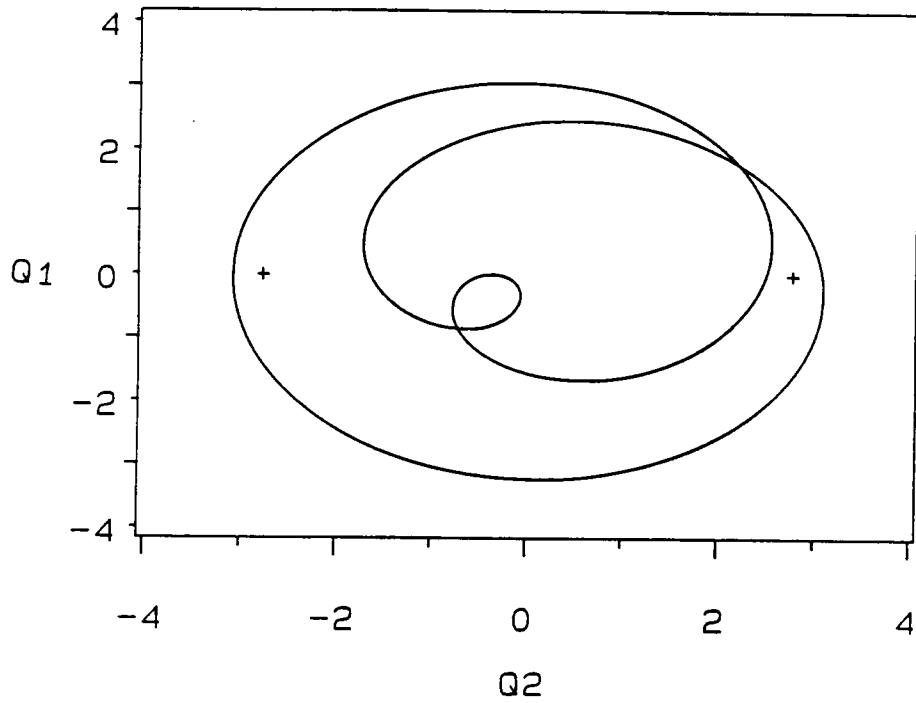


Figure 5.10. A two-dimensional projection of attractors 9 and 10 at $\sigma = -65.0$: The crosses indicate the unstable fixed points.

CHAPTER 6

CONCLUSIONS AND RECOMMENDATIONS

6.1 *Conclusions*

This work presents a numerical-perturbation approach to the study of modal interactions in shells dynamics. The work is divided into four main parts: a survey of related works in nonlinear structural dynamics in general with emphasis on shell dynamics, a review of the basic concepts of modern nonlinear dynamics, derivation of the equations of motion for infinitely long circular cylindrical shells and closed axisymmetric spherical shells, and a multiple-time scale perturbation analysis under different internal and external resonance conditions. The multiple-time scale analysis results in a set of nonlinear-ordinary differential equations describing the modulation of the interacting modes. These equations are referred to as the "modulation equations". The frequency and amplitude of excitation are used as bifurcation

parameters to study the solutions of the modulation equations. The modulation equations possess three possible solutions:

1. Fixed-point solutions corresponding to constant-amplitude harmonic oscillations of the shell.
2. Limit-cycle solutions corresponding to amplitude- and phase-modulated oscillations of the shell.
3. Chaotic solutions corresponding to chaotically modulated motions of the shell.

6.2 Dynamics of Cylindrical and Spherical Shells

A symbolic manipulator is used to derive the nonlinear equations of motion of infinitely long circular cylindrical shells and spherical shells undergoing axisymmetric deformations. The method of multiple-time scales is used to construct a uniformly valid asymptotic expansion for the solutions of the equations of motion under different external and internal resonance conditions. This method results in a set of modulation equations, they are nonlinear autonomous ordinary differential equations which describe the slow-time evolution of the amplitudes and phases of the interacting modes. The level and frequency of excitation are used as bifurcation parameters to study the fixed points, limit-cycle solutions, and chaotic solutions of the modulation equations. A numerical scheme that combines a shooting technique and a Newton-Raphson procedure is used to detect limit cycles of the modulation equations and calculate their periods. The stability of these limit cycles is determined using a Floquet analysis.

6.2.1 Primary-Resonant Excitation of Cylindrical and Spherical Shells with Two-To-One Internal Resonances

A numerical-perturbation approach is used to study modal interactions in the dynamic response of infinitely long circular cylindrical shells to an external harmonic excitation. The excitation frequency is near the linear natural frequency of the breathing mode (i.e., primary resonance of the breathing mode) and the linear natural frequency of the breathing mode is nearly twice that of a flexural mode (i.e., two-to-one internal or autoparametric resonance). The same approach is used to study the axisymmetric dynamic response of spherical shells to a radial harmonic excitation having a frequency near one of the linear natural frequencies of a flexural mode (i.e., primary resonance of a flexural mode) and in the presence of a two-to-one internal resonance between the excited mode and a lower flexural mode. The modulation equations derived for infinitely long circular cylindrical shells and axisymmetric spherical shells are scaled to the same form. The frequency and level of excitation are used as bifurcation parameters in the study of the fixed points, periodic solutions, and chaotic solutions of the modulation equations. As the excitation amplitude f varies, the fixed-point solutions of the modulation equations exhibit the jump and saturation phenomena. Below a certain threshold value of f , the response of the shell is linear; that is, the amplitude of the breathing mode is linearly proportional to f and the amplitudes of all the other modes are zero. Above this threshold, the excited mode responds with a constant amplitude and spills over the extra input energy into the coupled flexural mode which starts to respond nonlinearly and eventually dominates the response of the shell (the saturation phenomenon). As f varies, the fixed points go through supercritical pitchfork, or subcritical pitchfork,

or saddle-node bifurcation, the latter two result in jumps. When the frequency of excitation is used as a bifurcation parameter, the fixed points lose stability through a subcritical pitchfork bifurcation, or supercritical Hopf bifurcation, or subcritical Hopf bifurcation with the frequency of the supercritical Hopf bifurcation being lower than the subcritical one. As the excitation frequency increases above the supercritical Hopf-bifurcation value, the fixed-point solutions become unstable and limit cycles are born. These limit cycles experience symmetry-breaking pitchfork bifurcation followed by a cascade of period-doubling bifurcations culminating in chaos. On the other hand, as the excitation frequency decreases below the subcritical Hopf-bifurcation value, the resulting limit cycle deforms and eventually loses stability through a cyclic-fold bifurcation causing a transition to chaos. In the frequency range between the above two chaotic regions the modulation equations possess limit-cycle solutions.

6.2.2 Subharmonic-Resonant Excitation of Cylindrical Shells with Two-To-One Internal Resonance

The method of multiple-time scales is also used to analyze the nonlinear response of infinitely long circular cylindrical shells to a subharmonic excitation of order one-half of the breathing mode. A two-to-one internal resonance exists between the breathing mode and a flexural mode. Four autonomous modulation equations are derived and their fixed points, limit cycles, and chaotic solutions are studied as the level or frequency of excitation varies. The force-response curves exhibit the saturation phenomenon, supercritical pitchfork, subcritical pitchfork, saddle-node, and Hopf bifurcations. The shell does not respond until a certain

threshold level of excitation is exceeded. Above this threshold, the directly excited mode saturates and spills over its extra input energy into the coupled mode which responds nonlinearly. The frequency-response curves exhibit supercritical pitchfork, subcritical pitchfork, and Hopf bifurcations. For certain parameters and excitation frequencies between the Hopf-bifurcation values, limit-cycle solutions of the modulation equations are found. As the excitation frequency changes, all limit cycles deform and lose stability through either pitchfork or cyclic-fold (saddle-node) bifurcations. Some of these saddle-node bifurcations cause a transition to chaos. The pitchfork bifurcations break the symmetry of the limit cycles. Period-three motions are observed over a narrow range of excitation frequencies.

6.2.3 Primary-Resonant Excitation of Cylindrical Shells with One-To-One Internal Resonance

In the last case study, the numerical-perturbation procedure is used to analyze the nonlinear dynamic response of infinitely long circular cylindrical shells to a primary-resonant excitation of a flexural mode. Due to the complete circular symmetry of the circular cylindrical shell, each linear natural frequency corresponds to two orthogonal mode shapes, the two modes are perfectly tuned (one-to-one internal resonance). The mode with the same spatial variation as that of the excitation is called the driven mode while the other orthogonal mode is called the companion mode. Modal interactions between the driven and companion modes are studied. The steady-state response of the shell can involve either the driven mode alone (single-mode response) or both the driven and excited modes (two-mode response). The single-mode response results in a standing wave along the

circumference of the shell, whereas the two-mode response results in a wave travelling along the circumference of the shell. A symbolic manipulator is used to derive the modulation equations and their fixed points, periodic solutions, and chaotic solutions are studied. The frequency-response curves exhibit jumps and Hopf bifurcations. Between the Hopf-bifurcation frequencies, the modulation equations exhibit multiple limit-cycle solutions. As the excitation frequency varies, these limit cycles go through either cyclic-fold (saddle-node) bifurcations or incomplete sequences of period-doubling bifurcations. Some of the saddle-node bifurcations result in the birth of limit cycles and some result in transition to chaos.

6.2.4 Routes to Chaotic Motions

In all the study cases, the routes to chaos were through either

1. An infinite cascade of period-doubling bifurcations (as in the case of primary-resonant excitation of cylindrical or spherical shells in the presence of two-to-one internal resonances).

or

2. A cyclic-fold (saddle-node) bifurcation in which the flow jumps into a chaotic region (as in the case of a primary- or subharmonic-resonant excitation of a cylindrical shell in the presence of two-to-one internal resonances and the primary-resonant excitation of a cylindrical shell in the presence of one-to-one internal resonances).

6.3 Recommendations for Future Research

This study shows that modal interactions exist in shell dynamics and their effect manifests itself in different phenomena that can not be ignored. Despite the recurring popularity of this topic in the current literature, the following topics still need to be investigated:

1. Derivation of a consistent shell theory based on an asymptotic reduction of the three-dimensional equations of the theory of elasticity.
2. Modal interaction in composite shell structures.
3. Modal interaction taking into account the higher-order shell theories, including shear deformations and rotary inertia.
4. Experimental investigations of the modal interaction phenomenon in shell dynamics.

REFERENCES

Aprille, T. J., Jr., and Trick, T. N., 1972, "A Computer Algorithm to Determine the Steady-State Response of Nonlinear Oscillators," *IEEE Transactions on Circuit Theory*, Vol. CT-19, pp . 354-366.

Aron, H., 1874, " Das Gleichgewicht und die Bewegung einer unendlich dunnen, beliebig gekrummten Elastischen Schale," *J. Mathematik (Crelle)*, Vol. 78.

Atluri, S., 1972, "A Perturbation Analysis of Non-Linear Free Flexural Vibrations of a Circular Cylindrical Shell," *International Journal of Solids and Structures*, Vol. 8, pp . 549-569.

Bajaj, A. K., and Johnson, J. M., 1989, "Asymptotic Techniques and Complex Dynamics in Weakly Nonlinear Forced Mechanical Systems," *International Journal of Non-Linear Mechanics*, to appear.

Bedford, T., and Swift, J., *New Directions in Dynamical Systems* , Cambridge University Press, Cambridge.

Berge', P., Pomeau, Y., and Vidal, C., 1984, *Order Within Chaos, Towards a Deterministic Approach to Turbulence* , Wiley-Interscience, New York.

Bieniek, M. P., Fan, T. C., and Lackman, L. M., 1966, "Dynamic Stability of Cylindrical Shells," *AIAA Journal*, Vol. 4, pp. 495-500.

Budiansky, B., 1968, "Notes on Nonlinear Shell Theory," *ASME JOURNAL OF APPLIED MECHANICS*, Vol. 35, pp. 392-401.

Budiansky, B., 1974, "Theory of Buckling and Post-Buckling Behavior of Elastic Structures," in *Advances in Applied Mechanics* , Vol.14, ed. Chia-Shun Yih.

Chen, J. C., and Babcock, C. D., 1975, "Nonlinear Vibrations of Cylindrical Shells," *AIAA Journal*, Vol. 13, pp . 868-876.

Chow, S.N., and Hale, J. K., 1982, *Methods of Bifurcation Theory* , Springer-Verlag New York Inc..

Chua, L. O., and Lin, P. M., 1975, *Computer Aided Analysis of Electronic Circuits: Algorithms and Computational Techniques* , Printice-Hall, Inc., Englewood Cliffs, New Jersey.

Ciliberto, S., and Gollub, J. P., 1985, "Chaotic Mode Competition in Parametrically Forced Surface Waves," *Journal of Fluid Mechanics*, Vol. 158, pp. 381-398.

Croquette, V., and Pointou, C., 1981, "Cascade of Period Doubling Bifurcations and Large Stochasticity in the Motion of a Compass," *J. Physique-Letters*, Vol. 42, pp. L537-L539.

Donnell, L. H., 1933, "Stability of Thin Walled Tubes Under Torsion," NACA Report No. 479.

Donnell, L. H., 1938, "A Discussion of Thin Shell Theory," Proceedings of the 5 th International Congress of Applied Mechanics.

Dowell, E. H., and Pezeshki, C., 1986, "On the Understanding of Chaos in Duffings Equation Including a Comparison with Experiment," ASME JOURNAL OF APPLIED MECHANICS, Vol. 53, pp. 5-9.

Euler, L., 1766, "Tentamen de Sono Campanarum," Novi Commentarii, St. Petersburg Academy, St. Petersburg.

Evensen, D. A., 1966, "Nonlinear Flexural Vibrations of Thin Circular Rings," ASME JOURNAL OF APPLIED MECHANICS, Vol. 33, pp. 553-560.

Feng, Z. C., and Sethna, P. R., 1989, "Symmetry-Breaking Bifurcations in Resonant Surface Waves," Journal of Fluid Mechanics, Vol. 199, pp. 495-518.

Flügge, W., 1960, *Stresses in Shells*, Springer-Verlag, Berlin.

Forsberg, K., 1964, "Influence of Boundary Conditions on the Modal Characteristics of Thin Cylindrical Shells," AIAA Journal, Vol. 2, pp. 2150-2167.

Frederickson, P., Kaplan, J. L., York, E. D., and Yorke, J. A., 1983, "The Liapunov Dimension of Strange Attractors," Journal of Differential Equations, Vol. 49, pp. 185-207.

Germaine, S., 1821, "Recherches Sur La Theorie Des Surfaces Elastiques," Paris.

Goodier, J. N., and McIvor, I. K., 1964, "The Elastic Cylindrical Shell Under Nearly Uniform Radial Impulse," ASME JOURNAL OF APPLIED MECHANICS, Vol. 31, pp. 259-266.

Grebogi, C., Ott, E., Pelikan, S. and Yorke, J. A., 1984, "Strange Attractors that are not Chaotic," Physica D, Vol. 13, pp. 261-268.

Gu, X. M., and Sethna, P. R., 1987, "Resonant Surface waves and Chaotic Phenomena," Journal of Fluid Mechanics, Vol. 183, pp. 543-565.

Guckenheimer, J., and Holmes, P. J., 1983, *Nonlinear Oscillations, Dynamical Systems and Bifurcation of Vector Fields*, Springer-Verlag New York Inc..

Haddow, A. G., Barr, A. D. S., and Mook, D. T., 1984, "Theoretical and Experimental Study of Modal Interaction in a Two-Degree-of-Freedom Structure," Journal of Sound and Vibration, Vol. 97, pp. 451-473.

Haken, H. 1983, *Advanced Synergetics, Instability Hierarchies of Self-Organizing Systems and Devices*, Springer-Verlag New York Inc..

Hale, J. K., 1963, *Oscillations in Nonlinear Systems*, McGraw-Hill Book Co., Inc.

Hassard, B. D., Kazarinoff, N. D., and Wan, Y. H., 1981, *Theory and Application of Hopf Bifurcation*, Cambridge University Press, Cambridge.

Hatwal, H., Mallik, A. K., and Ghosh, A., 1983a, "Forced Nonlinear Oscillations of an Autoparametric System-Part 1: Periodic Responses," ASME JOURNAL OF APPLIED MECHANICS, Vol. 50, pp. 657-662.

Hatwal, H., Mallik, A. K., and Ghosh, A., 1983b, "Forced Nonlinear Oscillations of an Autoparametric System-Part 2: Chaotic Responses," ASME JOURNAL OF APPLIED MECHANICS, Vol. 50, pp. 663-668.

Hirsch, M. W., and Smale, S., 1974, *Differential Equations, Dynamical Systems and Linear Algebra* , Academic Press, Inc., New York and London.

Holmes, P. J., and Moon, F. C., 1983, "Strange Attractors and Chaos in Nonlinear Mechanics," ASME JOURNAL OF APPLIED MECHANICS, Vol. 50, pp. 1021-1032.

Holmes, P. J., 1986, " Chaotic Motion in a Weakly Nonlinear Model for Surface Waves," Journal of Fluid Mechanics, Vol. 162, pp. 365-388.

Iooss, G., and Joseph, D. D., 1980, *Elementary Stability and Bifurcation Theory*, Springer-Verlag New York Inc..

Johnson, J. M., and Bajaj, A. K., 1989, "Amplitude Modulated and Chaotic Dynamics in Resonant Motion of Strings," Journal of Sound and Vibration, Vol. 128, pp. 87-107.

Jordan, D. W., and Smith, P., 1987, *Nonlinear Ordinary Differential Equations* , Clarendon Press, Oxford.

Koiter, W. T., 1960, "A Consistent First Approximation in the General Theory of Thin Elastic Shells," in *The Theory of Thin Elastic Shells*, North-Holland, Amsterdam, pp . 12-33.

Koiter, W. T., 1966, "On the Nonlinear Theory of Thin Elastic Shells," Proc. K. Ned. Akad. Wet., ser. B69.

Koiter, W. T., and Simmonds, J. G., 1972, "Foundations of Shell Theory," WTHD 40, Delft University of Technology.

Leonard, R. W., 1961, *Nonlinear First Approximation Thin Shell and Membrane Theory*, M.Sc. Thesis, Virginia Polytechnic Institute and State University, Blacksburg, VA.

Libai, A. and Simmonds, J. G., 1988, *The Nonlinear Theory of Elastic Shells, One Spatial dimension*, Academic Press, Inc..

Lichtenberg, A. J., and Lieberman, M. A., 1983, *Regular and Stochastic Motion*, Springer-Verlag New York Inc..

Love, A. E. H., 1888, "On the Small Free Vibrations and deformations of Thin Elastic Shells," Phil. Transactions Royal Society (London), Vol. 179A.

Maewal, A., 1978, "Nonlinear Flexural Vibration of an Elastic Ring," ASME JOURNAL OF APPLIED MECHANICS, Vol. 45, pp. 428-428.

Maewal, A., 1981, "Nonlinear Harmonic Oscillations of Gyroscopic Structural Systems and the Case Of a Rotating Ring,", ASME JOURNAL OF APPLIED MECHANICS, Vol. 48, pp. 627-633.

Maewal, A., 1986a, "Miles' Evolution Equations for Axisymmetric Shells: Simple Strange Attractors in Structural Dynamics," International Journal of Non-Linear Mechanics, Vol. 21, pp. 433-438.

Maewal, A., 1986b, "Chaos in a Harmonically Excited Elastic Beam," ASME JOURNAL OF APPLIED MECHANICS, Vol. 53, pp. 625-632.

Maewal, A., 1986c, "Finite Element Analysis of Steady Nonlinear Harmonic Oscillations of Axisymmetric Shells," Computer Methods in Applied Mechanics and Engineering, Vol. 68, pp. 37-50.

Maganty, S. P., and Bickford, W. B., 1987, "Large Amplitude Oscillations of Thin Circular Rings," ASME JOURNAL OF APPLIED MECHANICS, Vol. 54, pp . 315-322.

Maganty, S. P., and Bickford, W. B., 1988, "Influence of Internal Resonance on the Non-Linear Oscillations of a Circular Ring Under Primary Resonance Conditions," Journal of Sound and Vibration, Vol. 122, pp . 547-521.

Marlowe, M. B., and Flugge, W., 1968, *Some New Developments in the Foundations of Shell Theory* , Thesis, Stanford University, Stanford, CA.

Marsden, J. E., and McCracken, M. , 1976, *The Hopf Bifurcation and its Applications*, Springer-Verlag New York Inc..

Mclvor, I. K., 1962, "Dynamic Stability and Nonlinear Oscillations of Cylindrical Shells (Plane Strain) Subjected to Impulsive Pressure," A Ph.D. Dissertation, Stanford University, Stanford, CA.

Mclvor, I. K., 1966, "The Elastic Cylindrical Shell Under Radial Impulse," ASME JOURNAL OF APPLIED MECHANICS, Vol. 33, pp. 831-837.

Mclvor, I. K., and Sonstegard, D. A., 1966, "Axisymmetric Response of a Closed Spherical Shell to a Nearly Uniform Radial Impulse," The Journal of the Acoustical Society of America, Vol. 40, pp. 1540-1547.

Mclvor, I. K. and Lovell, E. G., 1968, "Dynamic Response of Finite- Length Cylindrical Shells to Nearly Uniform Radial Impulse," AIAA Journal, Vol. 6, pp. 2346-2351.

Mees, A. I., 1981, *Dynamics of Feedback Systems*, Wiley-Interscience, New York.

Mente, L. J., 1973, "Dynamic Nonlinear Response of Cylindrical Shells to Axisymmetric Pressure Loading," AIAA Journal, Vol. 11, pp. 793-800.

Miles, J. W., 1984a, "Internally Resonant Surface Waves in a Circular Cylinder," Journal of Fluid Mechanics, Vol. 149, pp. 1-14.

Miles, J. W., 1984b, "Resonantly forced Surface Waves in a Circular Cylinder," Journal of Fluid Mechanics, Vol. 149, pp. 15-31.

Miles, J. W., 1984c, "Nonlinear Faraday Resonance," Journal of Fluid Mechanics, Vol. 146, pp. 285-302.

Miles, J. W., 1984d, "Resonant Motion of a Spherical Pendulum," *Physica D*, Vol. 11, pp. 309-323.

Miles, J. W., 1984e, "Resonant, Nonplanar Motion of a Stretched String," *Journal of the Acoustical Society of America*, Vol. 75, pp. 1505-1510.

Miles, J. W., 1985, "Parametric Excitation of an Internally Resonant Double Pendulum," *Journal of Applied Mathematics and Physics (ZAMP)*, Vol. 36, pp. 337-345.

Mook, D. T., Marshall, L. R., and Nayfeh A. H., 1974, "Subharmonic and Superharmonic Resonances in the Pitch and Roll Modes of Ship Motions," *Journal of Hydrodynamics*, Vol. 8, pp. 32-40.

Moon, F. C., 1980, "Experiments on Chaotic Motions of a Forced Nonlinear Oscillator: Strange Attractors," *ASME JOURNAL OF APPLIED MECHANICS*, Vol. 47, pp. 638-644.

Moon, F. C., 1987, *Chaotic Vibrations, An Introduction for Applied Scientists and Engineers*, Wiley-Interscience.

Mushtari, K. M., 1938, "Certain Generalizations of the Theory of Thin Shells," *Izv. Fiz. Mat. ob-va. pri Kaz. un-te.*, Vol. 11.

Naghdi, P. M., and Nordgren, R. P., 1963, "Nonlinear Theory of elastic Shells," *Quarterly Applied Mathematics*, Vol. 21, pp. 19-59.

Naghdi, P. M., 1963, "Foundations of Elastic Shell Theory," in *Progress in Solid Mechanics*, Vol. 4, Wiley-Interscience, New York.

Nayfeh A. H. H., 1973, *Perturbation Methods*, Wiley-Interscience, New York.

Nayfeh A. H., Mook, D. T., and Marshall, L. R., 1973, "Nonlinear Coupling of Pitch and Roll Modes in Ship Motion," *Journal of Hydronautics*, Vol. 7, pp. 145-152.

Nayfeh, A. H. and Mook, D. T., 1979, *Nonlinear Oscillations*, Wiley-Interscience, New York.

Nayfeh A. H., 1981, *Introduction to Perturbation Techniques*, Wiley-Interscience, New York.

Nayfeh A. H., and Khdeir, A. A., 1986a, "Nonlinear Rolling of Ships in Regular Beam Seas," *International Shipbuilding Progress*, Vol. 33, pp. 40-49.

Nayfeh A. H., and Khdeir, A. A., 1986b, "Nonlinear Rolling of Biased Ships in Regular Beam Waves," *International Shipbuilding Progress*, Vol. 33, pp. 84-93.

Nayfeh A. H., and Zavodney, L. D., 1986, "The Response of Two-Degree-of-Freedom Systems with Quadratic Non-linearities to a Combination Parametric Resonance," *Journal of Sound and Vibration*, Vol. 107, pp. 329-350.

Nayfeh A. H., 1987a, "Parametric Excitation of Two Internally Resonant Oscillators," *Journal of Sound and Vibration*, Vol. 119, pp. 95-109.

Nayfeh A. H., 1987b, "Surface Waves in Closed Basins Under Parametric and Internal Resonances," *Physics of Fluids*, Vol. 30, pp. 2976-2983.

Nayfeh A. H., and Raouf, R. A., 1987, "Non-Linear Oscillations of Circular Cylindrical Shells," *International Journal of Solids and Structures*, Vol. 23, pp. 1625-1638.

Nayfeh A. H., 1988a, "Numerical-Perturbation Methods in Mechanics," *Computers and Structures*, Vol. 30, pp. 185-204.

Nayfeh A. H., 1988b, "On the Undesirable Roll Characteristics of Ships in Regular Seas," *Journal of Ship Research*, Vol. 32, pp. 92-100.

Nayfeh A. H., and Zavodney, L. D., 1988, "Experimental Observation of Amplitude- and Phase-Modulated Responses of Two Internally Coupled Oscillators to a Harmonic Excitation," *ASME JOURNAL OF APPLIED MECHANICS*, Vol. 55, pp. 706-711.

Nayfeh A. H., Balachandran, B., Colbert, M., and Nayfeh, M. A., 1988, "An Experimental Investigation of Complicated Responses of a Two-Degree-of-Freedom Structure," *ASME JOURNAL OF APPLIED MECHANICS*, submitted for publication.

Nayfeh A. H., and Pai, P. F., 1989, "Non-linear Non-planar Parametric Responses of an Inextensional Beam," *International Journal of Non-Linear Mechanics*, Vol. 24, pp. 139-158.

Novozhilov, V. V., 1953, *Foundations of the Nonlinear Theory of Elasticity*, Greylock Press, Rochester, New York.

Pietraszkiewicz, W., and Szwabowicz, M. L., 1981, "Entirely Lagrangian Non-Linear Theory of Thin Shells," *Arch. Mech.*, Vol. 33, pp. 273-288.

Raouf, R. A., 1986, *Nonlinear Forced Response of Circular Cylindrical Shells*, M.Sc. Thesis, Virginia Polytechnic Institute and State University, Blacksburg, VA.

Rayleigh, J. W. S., 1882, "On the Infinitesimal Bending of Surfaces of Revolution," *London Mathematical Society Proceeding*, Vol. 13.

Reissner, E., 1950, "An Axisymmetric Deformation Theory of Thin Shells of Revolution," *Proc. Symp. Appl. Math.*, Vol. 3, pp. 27-52.

Reissner, E., 1963, "On the Equations for Finite Symmetrical Deflections of Thin Shells of Revolution," in *Progress in Applied Mechanics, Prager Anniversary Volume*.

Robbins, K. A., 1977, "A new Approach to Subcritical Instability and Turbulent Transitions in a Simple Dynamo," *Math. Proc. Camb. Phil. Soc.*, Vol. 82, pp. 309-325.

Rossler, O. E., 1976, "Chemical Turbulance: Chaos in a Small Reaction-Diffusion System," *Z. Naturforsch*, Vol. 31a, pp. 1168-1172.

Sanders, J. L., 1959, "An Improved First Approximation Theory of Thin Shells," NASA TR-24.

Sanders, J. L., 1963, "Nonlinear Theories of Thin Shells," *Quarterly Applied Mathematics*, Vol. 21, pp. 21-36.

Schmidt, R., 1984, "Thin Elastic Shells Undergoing Small Strains and Large Rotations - a Simple Consistent Theory and Variational Principle," in *Numerical Methods for Nonlinear Problems*, Vol. 2, eds. C. Taylor, E. Hinton and D. Owen, Pineridge Press, Swansea, Great Britain.

Schmidt, R., 1985, "On the Entirely Lagrangian First Approximation Theory of Thin Elastic Shells Undergoing Small Strains and Arbitrary Rotations," *ZAMM*. Vol. 65, pp. 119-121.

Sethna, P. R., 1965, "Vibrations of Dynamical Systems with Quadratic Nonlinearities," *ASME JOURNAL OF APPLIED MECHANICS*, Vol. 32, pp. 576-582.

Simmonds, J. G., 1979, "Accurate Nonlinear Equations and a Perturbation Solution for the Free Vibrations of Circular Elastic Rings," *ASME JOURNAL OF APPLIED MECHANICS*, Vol. 46, pp. 156-160.

Simmonds, J. G., and Danielson, D. A., 1972, "Nonlinear Shell Theory with Finite Rotation and Stress-Function Vectors," *ASME JOURNAL OF APPLIED MECHANICS*, Vol. 39, pp. 1085-1090.

Simonelli, F., and Gollub, J. P., 1989, "Surface Wave Mode Interactions: Effects of Symmetry and Degeneracy," *Journal of Fluid Mechanics*, Vol. 199, pp. 471-494.

Soedel, W., 1981, *Vibrations of Shells and Plates*, Marcel Dekker, Inc., New York and Basel.

Streit, D. A., Bajaj, A. K., and Krousgrill, C. M., 1988, "Combination Parametric Resonance Leading to Periodic and Chaotic Response in Two-Degree-Of-Freedom Systems with Quadratic Non-Linearities," *Journal of Sound and Vibration*, Vol. 124, pp. 297-314.

Stricklin, J. A., Martinez, J. E., Tillerson, J. R., Hong, J. H., and Haisler, W. E., 1971, "Nonlinear Dynamic Analysis of Shells of Revolution by Matrix Displacement Method," *AIAA Journal*, Vol. 9, pp. 629-636.

Thompson, J. M. T., and Stewart, H. B., 1986, *Nonlinear Dynamics and Chaos, Geometric Methods for Engineers and Scientists*, John Wiley and Sons Ltd., Great Britain.

Ueda, Y., 1979, "Randomly Transitional Phenomena in the System Governed by Duffing's Equation." *Journal of Statistical Physics*, Vol. 20, pp. 181-196.

Urabe, M., 1967, *Nonlinear Autonomous Oscillations*, Academic Press, Inc, New York and London.

Vanderbauwhede, A., 1982, *Local Bifurcations and Symmetry*, Pitman Books Ltd., Great Britain.

Vlasov, V. Z., 1951, "Basic Differential Equations in the General Theory of Elastic Shells," NACA TM 1241 (Translated from 1944 Russian version).

Wolf, A., Swift, J. B., Swinney, H. L., and Vastano, J. A., 1985, "Determining Lyapunov Exponents from a Time Series," *Physica-D*, Vol. 16, pp. 285-317.

Yasuda, K., and Kushida, G., 1984, "Nonlinear Forced Oscillations of a Shallow Spherical Shell." Bulletin JSME, Vol. 27, pp. 2233-2240.

Zavodney, L. D., and Nayfeh A. H., 1988, "The Response of a Single-Degree-of-Freedom System with Quadratic and Cubic Non-Linearities to a Fundamental Parametric Resonance," Journal of Sound and Vibration, Vol. 120, pp. 63-93.

Appendix A

CONSTANTS FOR EQUATIONS (5.13) AND (5.14)

$$c_1 = -\frac{1}{2}(\omega_n^2 - n^2)\Gamma_n^2 - \Gamma_n n(n^2 + 1) + \frac{3}{4}n^2 + \alpha^2\left\{-\frac{3}{2} + \frac{33}{4}n^2 - 9n^4 - \frac{9}{2}\Gamma_n n^3 + 9\Gamma_n n^5\right\} \quad (\text{A.1})$$

$$c_2 = -n\Gamma_n + \frac{1}{4}n^2 + \frac{1}{2}\Gamma_n^2(\omega_n^2 + n^2) + \alpha^2\left\{-\frac{1}{2}\Gamma_n n^3 - n^4 + \frac{11}{4}n^2 - \frac{3}{2}\right\} \quad (\text{A.2})$$

$$c_3 = -\Gamma_n^2(n^2 + \omega_n^2) + \Gamma_n(2n^3 + 2n) - \frac{3}{2}n^2 - \alpha^2\{18\Gamma_n n^5 - 9\Gamma_n n^3 - 18n^4 + \frac{33}{2}n^2 - 3\} \quad (\text{A.3})$$

$$c_4 = \frac{1}{2}\Gamma_n^2(\omega_n^2 - n^2) + \Gamma_n n - \frac{1}{4}n^2 + \alpha^2\left\{n^4 + \frac{1}{2}\Gamma_n n^3 - \frac{11}{4}n^2 + \frac{3}{2}\right\} \quad (\text{A.4})$$

$$d_1 = -\Gamma_n(\omega_n^2 - 2n^2) + \frac{1}{2}n^3 - n \quad (\text{A.5})$$

$$d_2 = -4\Gamma_n n^2 + n(2 - n^2) \quad (\text{A.6})$$

Appendix B

CONSTANTS FOR EQUATIONS (5.19) AND (5.20)

$$\begin{aligned} E_1 = & \frac{3}{2} \Gamma_n^2 \omega_n^2 + \frac{1}{2} \Gamma_n^2 n^4 - \frac{3}{2} \Gamma_n^2 n^2 - \frac{3}{4} \Gamma_n n^3 - \frac{3}{4} n^4 + n^2 + \frac{1}{\Delta_n} \{ 36 \Gamma_n \alpha^2 \omega_n^2 n^3 c_1 \\ & - 64 \Gamma_n \alpha^2 \omega_n^2 n^4 d_1 + 32 \Gamma_n \alpha^2 \omega_n^2 n^2 d_1 - 4 \Gamma_n \alpha^2 \omega_n^2 d_1 - 50 \Gamma_n \alpha^2 n^4 d_1 + 4 \Gamma_n \alpha^2 n^2 d_1 \\ & + 16 \Gamma_n \omega_n^4 d_1 + 8 \Gamma_n \omega_n^2 n^3 c_1 - 4 \Gamma_n \omega_n^2 d_1 - 4 \Gamma_n n^4 d_1 + 144 \alpha^2 \omega_n^2 n^4 c_1 + 24 \alpha^2 \omega_n^2 c_1 \\ & - 24 \alpha^2 n^2 c_1 - 16 \alpha^2 n d_1 - 8 \omega_n^2 n^3 d_1 - 12 \omega_n^2 n^2 c_1 + 16 \omega_n^2 n d_1 + 16 n^4 c_1 - 8 n^2 c_1 \\ & + 100 \alpha^2 n^3 d_1 - 132 \alpha^2 \omega_n^2 n^2 c_1 - 4 n d_1 - 16 \Gamma_n \omega_n^2 n^2 d_1 + 132 \alpha^2 n^4 c_1 + 8 n^3 d_1 \} \\ & + \frac{c_4}{1 + \alpha^2} \{ 2 \Gamma_n \alpha^2 n^3 + 4 \Gamma_n n + 8 \alpha^2 n^4 - 22 \alpha^2 n^2 12 \alpha^2 - 2 n^2 \} \end{aligned}$$

(B.1)

$$\begin{aligned}
E_2 = & \frac{1}{4} \Gamma_n^2 \omega_n^2 + \frac{3}{4} \Gamma_n^2 n^4 - \frac{9}{4} \Gamma_n^2 n^2 - \frac{9}{8} n^4 + \frac{3}{2} n^2 - \frac{9}{8} \Gamma_n n^3 + \frac{1}{\Delta_n} \{2 \Gamma_n \alpha^2 n^2 d_1 \\
& - 32 \Gamma_n \alpha^2 \omega_n^2 n^4 d_1 + 18 \Gamma_n \alpha^2 \omega_n^2 n^3 c_1 + 16 \Gamma_n \alpha^2 \omega_n^2 n^2 d_1 - 2 \Gamma_n \alpha^2 \omega_n^2 d_1 - 2n d_1 \\
& - 25 \Gamma_n \alpha^2 n^4 d_1 + 8 \Gamma_n \omega_n^4 d_1 + 4 \Gamma_n \omega_n^2 n^3 c_1 - 8 \Gamma_n \omega_n^2 n^2 d_1 + 4n^3 d_1 - 4n^2 c_1 \\
& - 2 \Gamma_n \omega_n^2 d_1 - 2 \Gamma_n n^4 d_1 + 72 \alpha^2 \omega_n^2 n^4 c_1 - 66 \alpha^2 \omega_n^2 n^2 c_1 + 12 \alpha^2 \omega_n^2 c_1 + 66 \alpha^2 n^4 c_1 \\
& + 50 \alpha^2 n^3 d_1 - 12 \alpha^2 n^2 c_1 - 8 \alpha^2 n d_1 - 4 \omega_n^2 n^3 d_1 - 6 \omega_n^2 n^2 c_1 + 8 \omega_n^2 n d_1 + 8n^4 c_1\} \\
& + \frac{1}{\Theta_n} \{25 \Gamma_n \alpha^2 n^4 d_2 + 12 \alpha^2 n^2 c_3 - 50 \alpha^2 n^3 d_2 - 2 \Gamma_n \alpha^2 n^2 d_2 - 8n^4 c_3 + 4n^2 c_3 \\
& - 4n^3 d_2 + 2 \Gamma_n n^4 d_2 - 66 \alpha^2 n^4 c_3 + 8 \alpha^2 n d_2 + 2n d_2\} + \frac{c_4}{1 + \alpha^2} \{2 \Gamma_n \alpha^2 n^3 \\
& - 2n^2 + 4 \Gamma_n n + 8 \alpha^2 n^4 - 22 \alpha^2 n^2 + 12 \alpha^2\} + \frac{c_2}{1 - 4\omega_n^2 + \alpha^2} \{- \Gamma_n \alpha^2 n^3 + n^2 \\
& - 2 \Gamma_n n - 4 \alpha^2 n^4 + 11 \alpha^2 n^2 - 6 \alpha^2\}
\end{aligned}
\tag{B.2}$$

$$\begin{aligned}
E_3 = & -\frac{5}{4} \Gamma_n^2 \omega_n^2 + \frac{1}{4} \Gamma_n^2 n^4 - \frac{3}{4} \Gamma_n^2 n^2 - \frac{3}{8} \Gamma_n n^3 - \frac{3}{8} n^4 + \frac{1}{2} n^2 + \frac{1}{\Delta_n} \{32 \Gamma_n \alpha^2 \omega_n^2 n^4 d_1 \\
& - 18 \Gamma_n \alpha^2 \omega_n^2 n^3 c_1 - 16 \Gamma_n \alpha^2 \omega_n^2 n^2 d_1 + 2 \Gamma_n \alpha^2 \omega_n^2 d_1 + 25 \Gamma_n \alpha^2 n^4 d_1 - 2 \Gamma_n \alpha^2 n^2 d_1 \\
& - 8 \Gamma_n \omega_n^4 d_1 - 4 \Gamma_n \omega_n^2 n^3 c_1 + 8 \Gamma_n \omega_n^2 n^2 d_1 + 2 \Gamma_n \omega_n^2 d_1 + 2 \Gamma_n n^4 d_1 - 72 \alpha^2 \omega_n^2 n^4 c_1 \\
& + 66 \alpha^2 \omega_n^2 n^2 c_1 - 12 \alpha^2 \omega_n^2 c_1 - 66 \alpha^2 n^4 c_1 - 50 \alpha^2 n^3 d_1 + 8 \alpha^2 n d_1 + 4 \omega_n^2 n^3 d_1 + 2n d_1 \\
& + 6 \omega_n^2 n^2 c_1 - 8 \omega_n^2 n d_1 - 8n^4 c_1 - 4n^3 d_1 + 4n^2 c_1 + 12 \alpha^2 n^2 c_1\} + \frac{1}{\Theta_n} \{4n^2 c_3 \\
& + 25 \Gamma_n \alpha^2 n^4 d_2 - 2 \Gamma_n \alpha^2 n^2 d_2 + 2 \Gamma_n n^4 d_2 - 66 \alpha^2 n^4 c_3 - 50 \alpha^2 n^3 d_2 + 2n d_2 \\
& + 12 \alpha^2 n^2 c_3 + 8 \alpha^2 n d_2 - 8n^4 c_3 - 4n^3 d_2\} + \frac{c_2}{1 - 4\omega_n^2 + \alpha^2} \{11 \alpha^2 n^2 - 6 \alpha^2 \\
& - \Gamma_n \alpha^2 n^3 - 2 \Gamma_n n - 4 \alpha^2 n^4 + n^2\}
\end{aligned}
\tag{B.3}$$

$$\begin{aligned}
G_1 = & \frac{3}{2} \Gamma_n n^2 + \frac{1}{4} n^3 - \frac{3}{2} \Gamma_n \omega_n^2 - \frac{1}{2} \Gamma_n n^4 + \frac{1}{\Delta_n} \{ 8 \Gamma_n \omega_n^4 c_1 - 4 \Gamma_n \omega_n^2 n d_1 - 8 \Gamma_n n^4 c_1 \\
& - 4 \Gamma_n n^3 d_1 + 64 \alpha^2 \omega_n^2 n^4 d_1 - 36 \alpha^2 \omega_n^2 n^3 c_1 - 32 \alpha^2 \omega_n^2 n^2 d_1 + 4 \alpha^2 \omega_n^2 d_1 - 8 \omega_n^2 n^3 c_1 \\
& + 50 \alpha^2 n^4 d_1 - 4 \alpha^2 n^2 d_1 - 16 \omega_n^4 d_1 + 16 \omega_n^2 n^2 d_1 + 4 \omega_n^2 d_1 + 4 n^4 d_1 \} + \frac{c_4}{1 + \alpha^2} \\
& \times \{ 4 \Gamma_n n^2 - 4 \Gamma_n \omega_n^2 - 2 \alpha^2 n^3 - 4 n \}
\end{aligned} \tag{B.4}$$

$$\begin{aligned}
G_2 = & -\frac{1}{4} \Gamma_n \omega_n^2 - \frac{3}{4} \Gamma_n n^4 + \frac{9}{4} \Gamma_n n^2 + \frac{3}{8} n^3 + \frac{1}{\Delta_n} \{ 4 \Gamma_n \omega_n^4 c_1 - 2 \Gamma_n \omega_n^2 n d_1 - 4 \Gamma_n n^4 c_1 \\
& - 2 \Gamma_n n^3 d_1 + 32 \alpha^2 \omega_n^2 n^4 d_1 - 4 \omega_n^2 n^3 c_1 - 18 \alpha^2 \omega_n^2 n^3 c_1 - 16 \alpha^2 \omega_n^2 n^2 d_1 + 2 \alpha^2 \omega_n^2 d_1 \\
& + 25 \alpha^2 n^4 d_1 - 2 \alpha^2 n^2 d_1 - 8 \omega_n^4 d_1 + 8 \omega_n^2 n^2 d_1 + 2 \omega_n^2 d_1 + 2 n^4 d_1 \} + \frac{1}{\Theta_n} \{ -2 n^4 d_2 \\
& + 4 \Gamma_n \omega_n^2 n^2 c_3 + 2 \Gamma_n \omega_n^2 n d_2 + 4 \Gamma_n n^4 c_3 + 2 \Gamma_n n^3 d_2 - 25 \alpha^2 n^4 d_2 + 2 \alpha^2 n^2 d_2 \} \\
& + \frac{c_2}{1 - 4 \omega_n^2 + \alpha^2} \{ 2 \Gamma_n \omega_n^2 - 2 \Gamma_n n^2 + \alpha^2 n^3 + 2 n \} + \frac{c_4}{1 + \alpha^2} \{ 4 \Gamma_n n^2 \\
& - 4 \Gamma_n \omega_n^2 - 2 \alpha^2 n^3 - 4 n \}
\end{aligned} \tag{B.5}$$

$$\begin{aligned}
G_3 = & \frac{5}{4} \Gamma_n \omega_n^2 - \frac{1}{4} \Gamma_n n^4 + \frac{3}{4} \Gamma_n n^2 + \frac{1}{8} n^3 + \frac{1}{\Delta_n} \{ 2 \Gamma_n \omega_n^2 n d_1 - 4 \Gamma_n \omega_n^4 c_1 \\
& + 4 \Gamma_n n^4 c_1 + 2 \Gamma_n n^3 d_1 - 32 \alpha^2 \omega_n^2 n^4 d_1 + 16 \alpha^2 \omega_n^2 n^2 d_1 - 2 \alpha^2 \omega_n^2 d_1 - 25 \alpha^2 n^4 d_1 \\
& + 2 \alpha^2 n^2 d_1 + 8 \omega_n^4 d_1 + 4 \omega_n^2 n^3 c_1 + 18 \alpha^2 \omega_n^2 n^3 c_1 - 8 \omega_n^2 n^2 d_1 - 2 \omega_n^2 d_1 - 2 n^4 d_1 \} \\
& + \frac{1}{\Theta_n} \{ 4 \Gamma_n \omega_n^2 n^2 c_3 + 2 \Gamma_n \omega_n^2 n d_2 + 4 \Gamma_n n^4 c_3 + 2 \Gamma_n n^3 d_2 - 25 \alpha^2 n^4 d_2 - 2 n^4 d_2 \\
& + 2 \alpha^2 n^2 d_2 \} + \frac{c_2}{1 - 4 \omega_n^2 + \alpha^2} \{ 2 \Gamma_n \omega_n^2 - 2 \Gamma_n n^2 + \alpha^2 n^3 + 2 n \}
\end{aligned} \tag{B.6}$$

**The vita has been removed from
the scanned document**